Flow Physics for Control

Summary of the research performed in year 3 (Amitay, Taira and Theofilis)

In year 2, the effect of sweep angle and taper ratio on the formation of separated flows over finite span cantilevered wings with $sAR = 2$ at $Re_c = O(10^2)$ and $O(10^5)$ were investigated experimentally in water and wind tunnels, respectively, Direct Numerical Simulation and TriGlobal stability analysis. Most of the numerical simulations and the stability analysis were performed at a low Reynolds number $O(10^2)$. Therefore, a key comparison was first needed to be established: the experimental results for $Re_c = 247, 500$ were compared with results obtained at $Re_c = 600$. The comparison of the spanwise distributions of the reversed flow area for geometrically identical wings at the above-mentioned Reynolds numbers are shown in Fig. 1 (left). Even at these vastly different Reynolds numbers, the trend of shifting the peak reversed flow region towards wingtip and towards root for sweptback and swept forward models were captured.

We also showed that the trends between the low Reynolds number experiments and the low Reynolds number DNS were verified to share the same features. The spanwise distributions of the normalized reversed flow area from the DNS and the SPIV are presented in Fig. 1 (right). The DNS revealed analogous behavior as the peak reversed flow area shifted outboard with increasing sweptback angle. The overall conclusion drawn from the features studied with DNS and stability analysis have provided a *fundamental basis to study large-scale separated flow structures over wings at much higher Reynolds numbers*. Year 3 was dedicated to controlling the separation over the various wing geometries. The three thrusts are discussed below.

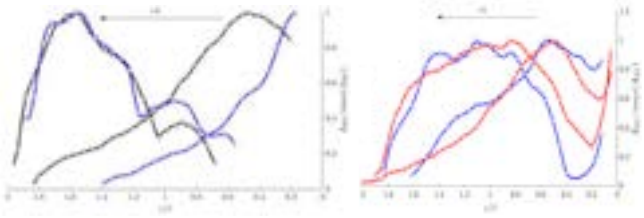

Fig. 1 *Comparison of spanwise distribution of the normalized reversed flow area at $Re_c = 600$ (blue) and $Re_c = 247, 500$ (black) for selected cases (left), and comparison of DNS (red) and SPIV (black), at $Re_c = 600$ (right).*

Theoretically-founded Flow Control (low-Re): High-angle of attack flows over swept three-dimensional wings based on the NACA0015 profile were studied theoretically at low Reynolds numbers. Linear stability analysis was initially used to compute instability and receptivity of the flow via the respective three-dimensional (TriGlobal) direct and adjoint eigenmodes. The magnitude of the (3D global) adjoint eigenvectors was then used to identify regions of maximum flow receptivity to momentum forcing. It was found that such regions are located above the primary three-dimensional separation line, their spanwise position varying with wing sweep. The wavemaker region corresponding to the leading global eigenmode was then computed and found to lie inside the laminar separation bubble (LSB) at the spanwise location of peak recirculation. Increasing the Reynolds number led to the wavemaker becoming more compact in the spanwise direction and concentrated in the vicinity of the upper and lower shear layers of the LSB. As sweep was introduced, the wavemaker was found to move towards the wing tip, following the spanwise displacement of maximum recirculation. Flow modifications resulting from actuation using different types of forcing were subsequently studied by direct numerical simulation initialized with insights gained from stability analysis. Periodic forcing at the regions of maximum receptivity to momentum forcing was found result in greater departure from the baseline case compared to same (low, linear) amplitude forcing applied elsewhere, underlining the potential of linear stability analysis to identify optimal regions for actuator positioning. Information gained from these analyses was constantly interchanged with the experimental and large-scale computations groups, in

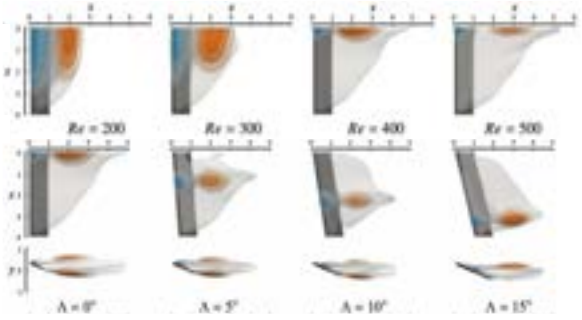

Fig. 2 *Receptivity to momentum forcing (blue) and structural sensitivity (orange) of the leading unstable mode with change of Reynolds number (top) and sweep angle (bottom).*

an effort to arrive at full understanding of the underlying flow dynamics and generate guidelines for their exploitation at practical Reynolds numbers.

Physics-Based Flow Control (high-Re): Two sets of experiments were performed: low-Re in a water tunnel at Re_c = 600 and in a wind tunnel at Re_c = 247, 500 over finite span cantilevered wings. Using the flow physics insights, the focus of the experimental effort was to explore the spanwise location of steady blowing for highest reduction of the reversed flow region over a tapered planform which had a taper ratio λ = 0.27, a 30◦ forward swept trailing edge and an unswept leading edge. This wing was shown to form the inverted ram's horn vortex at post-stall angles of attack that forms near the wing tip and grows in diameter towards the wing root. When active flow control, via steady blowing, was applied slightly inboard of the midspan, it creates a virtual fence where the inverted ram's horn is diverted and the flow is reattached inboard of the jet location.

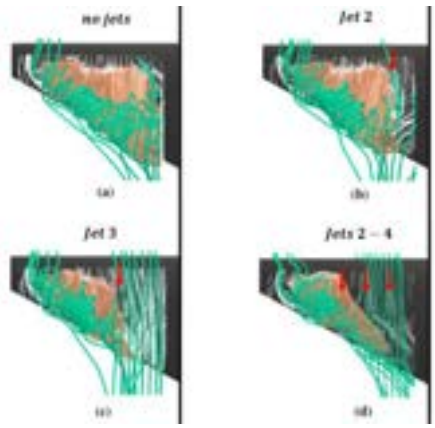

Fig. 3 *Iso-surface of reverse flow region (peach color), with near surface (white) streamlines and 3-D over the surface (green) streamlines, over the (λ, ΛLE, ΛTE) = (0.269, 0◦, -30◦) wing. No jets active (a), jet 2 on (b), jet 3 on (c), and jets 2, 3, 4 on (d) at C_b = 1, α = 18◦ and Re_c = 247, 500.*

The large-scale flow structures measured with SPIV are visualized in Fig. 3. The reverse flow region is identified with U = 0 peach-colored iso-surface, while streamlines are calculated near the surface (white), and above the surface and into the wake (green). The case with no actuation (baseline case, Fig. 3a) exhibits the formation of the inverted ram's horn vortex, as can be clearly seen by the spiraling green streamlines extending from the wing tip to the root. This results in a reversed flow region that grows linearly from tip to root. When jet 2 is individually activated (Fig. 3b), it behaves as a virtual fence limiting the tip-to-root growth of the reversed flow region. Similarly, when jet 3 is individually activated (Fig. 3c), the virtual fencing effect is sustained even at this further outboard blowing location, resulting in a further reduction of the reversed flow region. In addition, the inverted ram's horn is altered, as the virtual fence forces it to reorient in the streamwise direction. When jets 2, 3 and 4 are actuated together (Fig. 3d) the reversed flow region is reduced ever further due to the jets' combined effect.

Resolvent-Analysis-Based Flow Control: We performed active control of the laminar separated wakes around the wings with two primary goals: (i) reducing the size of the separation bubble and (ii) attenuating the wing tip vortex. Instead of preventing separation, we modify the three-dimensional (3-D) dynamics to exploit wake vortices for aerodynamic enhancements. A direct wake modification is considered using optimal harmonic forcing modes from TriGlobal resolvent analysis. For this study, we consider wings at angles of attack of 14 and 22 deg, taper ratios 0.27 and 1, and leading-edge sweep angles of 0 and 30 deg, at a mean-chord-based Reynolds number of 600. For tapered swept wings, the diversity of wake vortices increases substantially, posing a challenge for flow control. To achieve the first control objective for an untapered unswept wing, root-based actuation at the shedding frequency is introduced to reduce the reversed-flow bubble size by taking advantage of the wake vortices to significantly enhance the aerodynamic performance of the wing. For both untapered and tapered swept wings, root-based actuation modifies the stalled flow, reduces the reversed-flow region, and enhances aerodynamic performance by increasing the root contribution to lift. For the goal of controlling the tip vortex, we demonstrate the

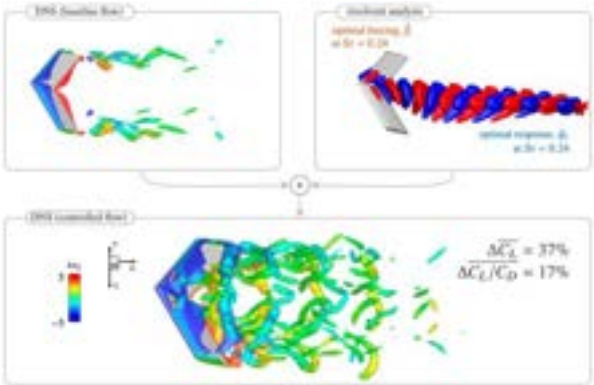

Fig. 4 *Insights from resolvent analysis being used for flow control to achieve enhancement aerodynamic performance of low-aspect-ratio swept and tapered wings.*

effectiveness of actuation with high-frequency perturbations near the tip. This study shows how insights from resolvent analysis for unsteady actuation can enable global modification of 3-D separated wakes and achieve improved aerodynamics of wings.

Reynolds Number Effects on Low-Aspect-Ratio Wing Wakes: Low-aspect ratio wings exhibit a highly impactful tip vortex, which introduces strong spanwise gradients into an already complex flow. We explore the interaction between leading edge flow separation and a strong, persistent tip vortex over a Reynolds number range from 600 to 10,000. In performing this study, we aim to bridge the insight gained from existing low Reynolds number studies of separated flow on finite wings ($Re_c \approx 100$) and turbulent flows at higher Reynolds numbers ($Re_c \approx 10{,}000$). Our study suggests two primary effects of Reynolds number. First, we observe a break from periodicity, along with a dramatic increase in the intensity and concentration of small-scale eddies, as we shift from Re_c = 600 to 2,500. Second, we observe that many of our flow diagnostics, including the time-averaged aerodynamic force, exhibit reduced sensitivity to Reynolds number beyond Re_c = 2,500, an observation attributed to the stabilizing impact of the wing tip vortex. This latter point illustrates how the tip vortex drives flow over low-aspect-ratio wings and provides insight into how our existing understanding of this flowfield may be adjusted for higher Reynolds number applications.

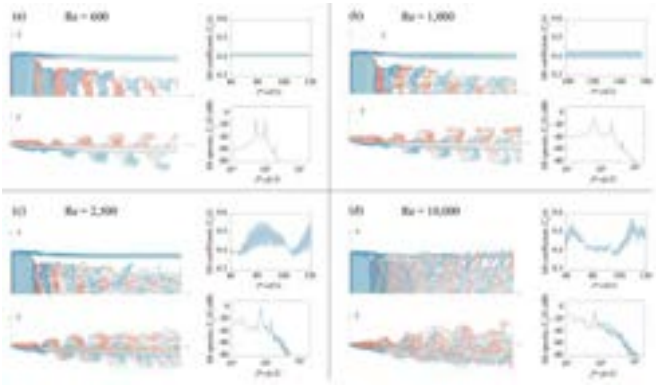

Fig. 5 *Comparison wakes of NACA0012 sAR = 2 wing at 14◦ across a range of Re numbers.*

Journal Publications:

L. Smith and K. Taira, "The Effect of Reynolds Number on the Separated Flow over a Low-Aspect-Ratio Wing," Journal of Fluid Mechanics, in review, 2024.

Carvajal, T., Neal, J., Amitay, M., "Experimental Validation of the Modified Holman Vortex Identification Method", accepted to *AIAA Journal*, July 2024

A. Burtsev, V. Pezlar and V. Theofilis, "Sensitivity of flows over three-dimensional swept wings at low Reynolds number," Journal of Fluid Mechanics, accepted, 2024.

L.V. Rolandi, J.H.M. Ribeiro, C.-A., Yeh, and K. Taira, "An Invitation to Resolvent Analysis," Theoretical and Computational Fluid Dynamics, accepted, 2024.

J.H.M. Ribeiro and K. Taira, "Triglobal Resolvent-Analysis-Based Control of Separated Flows around Low-Aspect-Ratio Wings," Journal of Fluid Mechanics, accepted, 2024.

J.H.M. Ribeiro, J. Neal, A. Burtsev, M. Amitay, V. Theofilis, and K. Taira, "Laminar Post-Stall Wakes of Tapered Swept Wings," Journal of Fluid Mechanics, 976, A6, 2023.

Neal, J. and Amitay, M., "Three-dimensional separation over unswept cantilevered wings at a moderate Reynolds number", *Physical Review Fluids*, 8, 014703 (2023), DOI: 10.1103/PhysRevFluids.8.014703

Conference Papers:

Neal, J. and Amitay, M., "Physics-based control of flow separation on tapered wings", AIAA-2024-0694, SciTech 2024, Orlando, Florida, January 8-12, 2024

A. Burtsev, V. Pezlar and V. Theofilis "Sensitivity of flows over three-dimensional swept wings at low Reynolds numbers", 1st European Fluid Dynamics Conference, 6-10 September 2024, Aachen, Germany

Efficient Stabilization of the Adjoint for Turbulent Separated Flows

Dr. James G. Coder, *Associate Professor*
Ian Maul and Viktoriya Giryanskaya, *Graduate Assistants*

1 Overview

Adjoint methods represent untapped potential for unlocking fundamental physical understanding of turbulent, separated flows through numerical simulations; however, a technical barrier is present in that adjoint solutions exhibit unbounded growth for chaotic dynamical systems. This research directly addresses that technical barrier in order to obtain useful adjoint solutions for turbulent, separated flows and use them to generate new knowledge and understanding about the underlying flow physics.

Adjoint costates provide the gradient sensitivities of system response to instantaneous flow features and external control inputs (such as boundary shape modification or active flow control). From a practical aerodynamic perspective, it is desirable to predict the onset of separation-related flow phenomena before they occur in order to apply the desired control (e.g. vehicle maneuver, shape deformation, or active flow control). Accordingly, this research will be able to identify flow structures that have the strongest influence on turbulent separation.

2 Results Summary

Throughout the past year, an approach was adopted in which wall-resolved, implicit large-eddy simulations were performed for flow over an NACA 0012 airfoil at a Mach number of 0.2 with various angles of attack and Reynolds numbers. The unsteady flow solution served as the basis of constructing ensemble-averaged flow fields and constructing localized eddy-viscosity closures. The basic idea is to determine whether or not an adjoint solution can be found for a physically meaningful steady state. To do so, a necessary condition is that this steady state must be a stable fixed point of the governing equations.

2.1 Body-Force Method

An unfortunately reality of using an ensemble-averaged steady state, $\overline{q} = \langle q \rangle$, is that $\overline{q}$ generally does not satisfy the steady Navier-Stokes equations. To overcome this, a body-force method based on the work of Ranjan[1] was implemented into the PI's WRBLES code. This involves modifying the governing PDE as

$$\frac{\partial q}{\partial t} + R\left(q\right) = R\left(\overline{q}\right)$$

in which R denotes the spatial residual. This method was implemented into WRBLES and tested on two cases:

1. NACA 0012 at 20 degrees Angle of Attack (Re = 2,400): Selected for its lower computational expense with vast amounts of leading and trailing edge vortex shedding, based on the case examined by Fernandez and Wang[2].

2. NACA 0012 at 10 degrees Angle of Attack (Re = 100,000): Exhibiting a highly unsteady leading edge laminar separation bubble and turbulent boundary layer.

The mean flow was computed for both cases by taking a sine weighted average of a time series of 5,000 solution files for both cases. For the Re = 2,400 (dt=0.001) and Re = 100,000 (dt=0.0002) cases, solution files were saved every two and five iterations respectively. This ensured the time-averaged mean flows were sufficiently smooth. Upon reading the mean flow into WRBLES, the body force term was constructed and the simulation ran as normal. However, instabilities in the flow grew in both cases, resulting in the smooth initial flow field becoming fully turbulent. It is important to note that despite being unsuccessful at stabilizing the flow field on its own, the solution did exhibit brief stabilization compared to restarting from the mean flow without utilizing a body force term. Regardless, additional stabilization needed to be applied.

2.2 Turbulence Model Method

To enhance stabilization, an eddy viscosity was introduced to dissipate turbulent fluctuations. The time-averaged Smagorinsky, Wall Adapting Local Eddy viscosity (WALE), k-ϵ, and Prandtl mixing length model eddy viscosity fields were calculated for both cases due to their popularity and ease of implementation into a post-processing `FORTRAN` code. The averaging was done in the exact same manner as the mean flow with the same solution files. The k-ϵ model provided the smoothest field for both cases, particularly in the separation bubble and wake regions. For the $Re = 1 \times 10^5$ case, the WALE eddy viscosity captured the separated shear layer and wake region well, but in contrast to the k-ϵ model, did not exhibit high eddy viscosity within the separation bubble region. The WALE model also did not capture a large portion of the wake region for the $Re = 2400$ case compared to k-ϵ. The Smagorinsky and mixing length models did not provide smooth fields that well accounted for the separation bubble or wake regions of both cases.

With that said, the computed k-ϵ eddy viscosity field was read as an additional input along with the mean flow, and added to the viscosity in WRBLES. The solution for both cases diverged from the initial mean flow, but quickly converged to a new steady flow field. For $Re = 2400$, the new steady state eliminated a large amount of the low momentum wake region exhibited near the trailing edge compared to the initial mean flow as seen in Fig. 1. In the $Re = 1 \times 10^5$ case, the separation bubble was almost entirely eliminated from the flow field. Despite the differences between the initial mean flow and the new steady state, the flow fields successfully achieved a stabilized state.

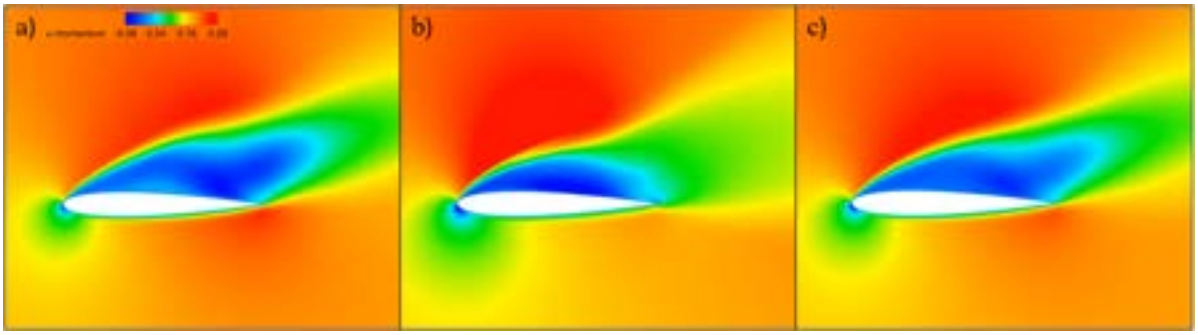

Figure 1: NACA 0012 at 20 degrees ($Re = 2400$): a) Initial mean flow, b) Stabilized flow field with turbulence model alone, c) Stabilized flow field with turbulence model and body force

References

[1] Ranjan, R., Unnikrishnan, S., and Gaitonde, D., "A robust approach for stability analysis of complex flows using high-order Navier-Stokes solvers," *Journal of Computational Physics*, Vol. 403, 2020, p. 109076. https://doi.org/10.1016/J.JCP.2019.109076.

[2] Fernandez, P., and Wang, Q., "Lyapunov spectrum of the separated flow around the NACA 0012 airfoil and its dependence on numerical discretization," *Journal of Computational Physics*, Vol. 350, 2017, pp. 453–469. https://doi.org/10.1016/J.JCP.2017.08.056.

A combined approach using simulations, wind tunnel, and flight experiments for investigating the effects of large wing sweep and unsteady wing motion on transition and separation

Summary of research during the past year
Submitted to
Dr. Gregg Abate, AFOSR
Program Officer, Unsteady Aerodynamics & Turbulence
by
H.F. Fasel (PI) and J. Little (Co-PI) University of Arizona, Tucson, AZ
PI contact: faselh@email.arizona.edu, 520 481 0819

Recent advances in high-strength composite materials have led to the development of wings with high aspect ratios and thus significantly enhanced range and endurance of Air Force aircraft. Current composite wing designs, such as those on the Boeing 787 and the RQ-4 Global Hawk, exhibit considerable structural motion due to unsteady aerodynamic loads, which influences boundary-layer transition and separation. Especially for swept-wing configurations, the interaction between boundary-layer transition and separation is complex and depends on the type of transition physics (e.g., Tollmien-Schlichting instability versus cross-flow instability). Sweep angles in practical applications range from nearly zero degrees (e.g., RQ-4) to about 30° for commercial airliners, and can exceed 40° for unmanned combat aerial vehicles (UCAVs, such as the X-47B).

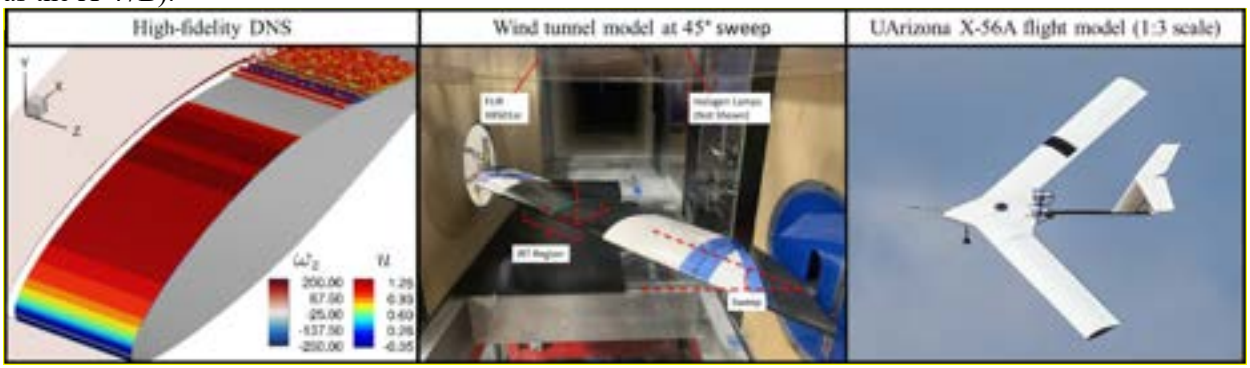

Figure 1: Research approach: High-fidelity DNS. Wind-tunnel experiments, Flight experiments

Research Accomplishments:

A) Development of Research Tools:

DNS/Theory: Improvements of the high-fidelity incompressible Navier-Stokes code to accurately simulate flows at high Reynolds numbers and for three-dimensional (swept) configurations. Expanded the linear PSE solver to handle curvilinear coordinates, enabling analysis of swept wing boundary layer flows.

Flight Tests: Previous X-56A flight model was redesigned for 45° wing sweep. Internal structure and instrumentation were also reworked to provide more stability and intuitive data acquisition.

Wind Tunnel Experiments: New scaled (1:6) wind tunnel models were fabricated to investigate flight stability, wing flutter and deflections. Addition and implementation of a fully automated three-axis traverse to measure time resolved velocity data (CTA) in the wind tunnel. Recording of surface pressure, infrared thermography

Figure 2: Top) Scale model in ALSWT. Bottom) New design with 45° wing sweep

(IRT) and CTA data along with state-of-the-art data analysis tools (e.g., spectral and modal analysis) for direct comparison to stability calculation and DNS (Cotnoir (2023), Frisch et al. (2024)).

B) ***Research Findings:***

Theory/DNS: Direct numerical simulations were carried out for the unwept wing section at Re=600k and zero-degree angle of attack. The results obtained using a random disturbance-input approach (DNS-r) closely matched experimental data and theory (see Fig. 3). Linear PSE based on baseflow obtained with precursor DNS were performed to map out the stability characteristics of the 45-degree swept wing flow at Re=600k, providing insights into the cause of some experimental measurements. Informed by the stability calculations, the optimal spacing and placement of the discrete roughness elements (DREs) was confirmed in the wind tunnel, successfully extending the cases with observable crossflow to cases relevant to flight tests and interactions with LSBs (-2° ≤ AoA ≤ 0°).

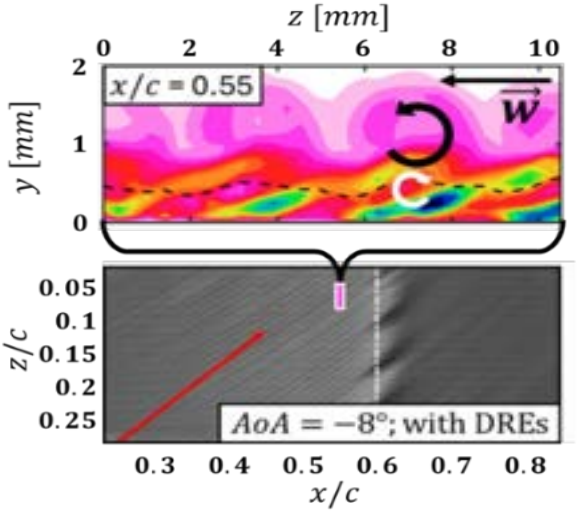

Figure 3: Crossflow downstream of the DREs at AoA= -8, showing the stationary crossflow vortices

Wind Tunnel experiments: Preliminary results from new scaled wind tunnel models (1:6) indicate region of flight envelope where significant flutter may occur and give some indication as to the forces and moments experienced by the model for a range of flight conditions (-5° ≤ AoA ≤ 10°, 10 m/s ≤ U_∞ ≤ 50 m/s). Unsteady measurements for the 45-degree wing sweep model with AoA = -8°, show the growth and development of crossflow instabilities, similar to those predicted by PSE. The interaction of crossflow with the LSB was investigated on the suction side of the wing at moderate angles of attack (AoA = -1°). Frequency content near laminar separation agrees with the dominant frequencies from the crossflow. In the LSB, the dominant frequency band is found to be between that of the crossflow instability and the dominant K-H instability (for the unswept case) and as predicted by PSE, suggesting an interaction of the crossflow with the K-H instability in the LSB.

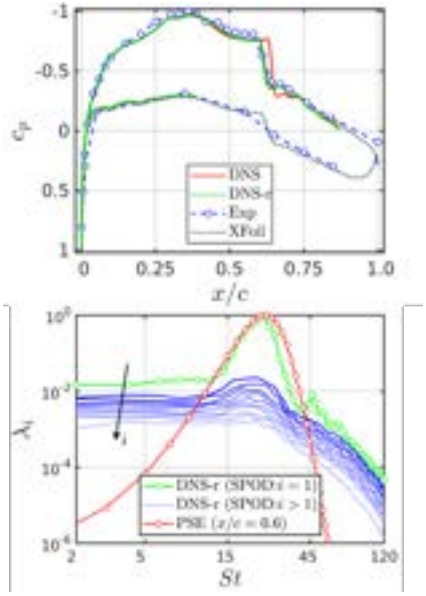

Figure 4: Unswept wing at Re=600k and α=0 (deg). Top) Time- and spanwise-averaged surface pressure coefficients. Bottom) Comparison of spectral POD eigenvalue spectra with linear PSE

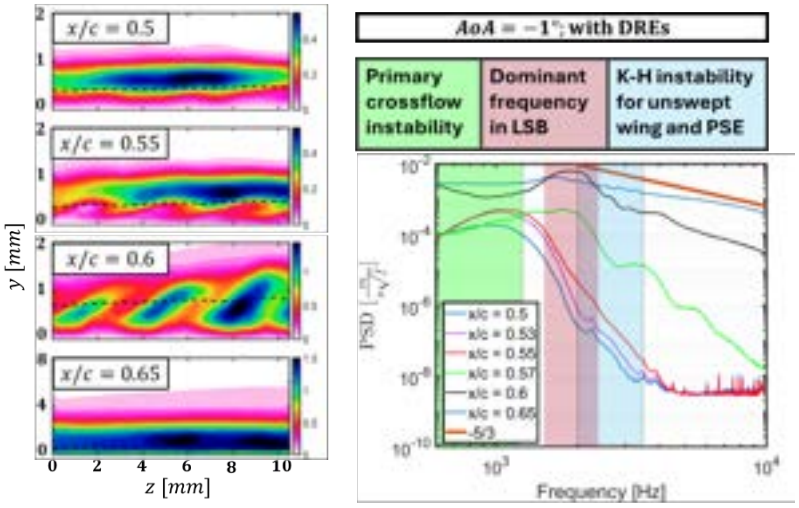

Figure 5: Three dimensionality in the LSB as a result of crossflow, RMS (filtered for primary crossflow range) and spanwise averaged PSD at several streamwise locations in the LSB.

Dynamics and Control of Cargo Aircraft Wakes with Bays and Doors

Prof. Datta V. Gaitonde (PI)
Mechanical and Aerospace Engineering
The Ohio State University, gaitonde.3@osu.edu

Prof. Farrukh S. Alvi (Lead co-PI at FSU)
Mechanical Engineering
Florida State University, alvi@eng.fsu.edu

Background, Motivation and Objectives: The aft-ends of large transport aircraft fuselages differ significantly from those of commercial and fighter vehicles to facilitate cargo and paratroop drops. Two crucial features to accommodate ramp-doors are relatively flat base regions and large upsweep angles, (Fig. 1a). Fundamental research has emphasized a *baseline* setup comprised of low speed (essentially incompressible) flow past a cylinder with freestream-aligned axis and a planar upswept sharp-edged base (Fig. 1b. The flowfield in the base region of this configuration has been characterized in numerous prior studies, and is mainly comprised of an unsteady, meandering counter-rotating longitudinal vortex pair and multiple secondary structures (Fig. 1c). The problem has also been shown to exhibit hysteresis under Reynolds number as well as upsweep angle variation. *These can cause paratrooper accidents and cargo drop error, and increased drag.* The goal of this effort is to *execute an integrated high-fidelity computational-experimental program* to go beyond the baseline approach *to include key distinctive features* of actual cargo aircraft, shown in Fig. 1d, including (i) flight speed to include compressibility (upto Mach 0.6), ii) rounded aft edges that can introduce new low-frequency instabilities into the wake, iii) effects of cargo bays and acoustic interactions and iv) evolution of control strategies based on theory and experimentation.

Achievements during second year:

Compressibility effects: An extensive volumetric and planar PIV campaign was performed to examine the flow at $M = 0.30$ and $M = 0.60$. With increasing Mach number, vortices with increased strength and enlarged core radii were observed. These effects were hypothesized to relate to an increase in vortex meandering amplitude and TKE. This is accompanied by an increase in the recirculation region length and height, and decreases in the growth rate of the vorticity thickness, shear layer growth and fluid entrainment in the recirculation region. Reynolds number identified a decrease in overall pressure fluctuations with increasing Reynolds number for incompressible speeds, but constant fluctuations at compressible speeds. As such, *compressibility yields larger and weakened recirculation regions and lower drag.*

Edge rounding effects: Unsteady pressure sensitive paint and high-speed shadowgraphs of the unsteady wake field reveal downstream convecting pressure waves that are related to vortex mean-

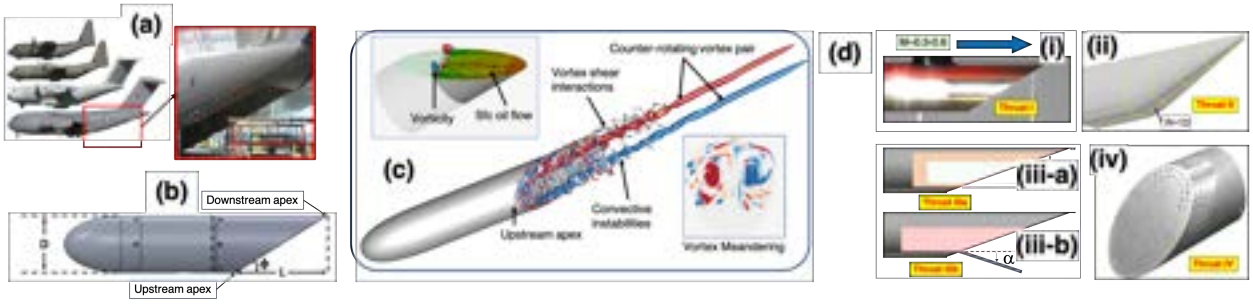

Figure 1: (a) Upswept aft fuselage (b) Baseline configuration (c) Vortical structure (d) Proposed efforts

dering. The effect of edge rounding results in slower, longer, and weaker waves. The slant angle on the rounded-edge model also affects overall pressure fluctuations and wavelengths on the model surface. Analysis of a new centerline attached vortex state display no identifiable peaks in the unsteady surface spectra of pressure probes, pressure-sensitive paints or shadowgraphs. Surface pressure fluctuations of the centerline-attached vortex state may be too weak to be resolved with the utilized methods. Therefore, *edge rounding affects the unsteady content, and the results may be a stronger function of Reynolds number than the sharp-edged configurations.*

Cross-section effects: Since some cargo aircraft cross-sections have relatively rectangular, as opposed to cylindrical sections, the effect of rectangular configurations was explored to better allow the incorporation of cavities and doors. Three dimensional streamlines over this geometry, Fig. 2a, indicate the absence of a horseshoe-shaped vortex that was evident earlier (Fig. 1c). Rather, they are formed separately at the upstream corners, segregated by a centerline separation bubble, and have larger cross-sectional area with lower coherence. Frequencies are generally lower, and associated with interactions between centerline separation and the primary vortex pair, with the existence of asymmetry. The downstream corners also yield corotating streamwise vortices. *The cross-section has a significant influence on the origination of the vortex pair, and long-lasting asymmetric states, together with potential for hysteresis*.

Bay effects: $3D$ streamlines for square and cylindrical cross-section bodies with cavity bays are shown in Figs.2b and c. Vortex generation is delayed, and are more diffuse and dissipate more rapidly than their no-cavity counterparts. In this case, higher frequencies near the upstream separated shear layer may be attributed to structures near separation having a more global influence. An additional mechanism, flow impingement on the cavity wall near the downstream apex, driven by the centerline recirculation bubble, whose effects are being characterized. *Bay effects may thus trigger instabilities due to the interaction of acoustic content inside the cavity with the wake.*

Immediate next steps:

Ongoing research is focused on the following aspects: i) Complete characterization of the unsteady wake, especially Reynolds number effects on different wake states. ii) Further analysis of new potential instabilities in rounded edge case and development of an active flow control campaign on the rounded-edge model. iii) Square body bistable flow analysis and iv) Influence of cavity bays.

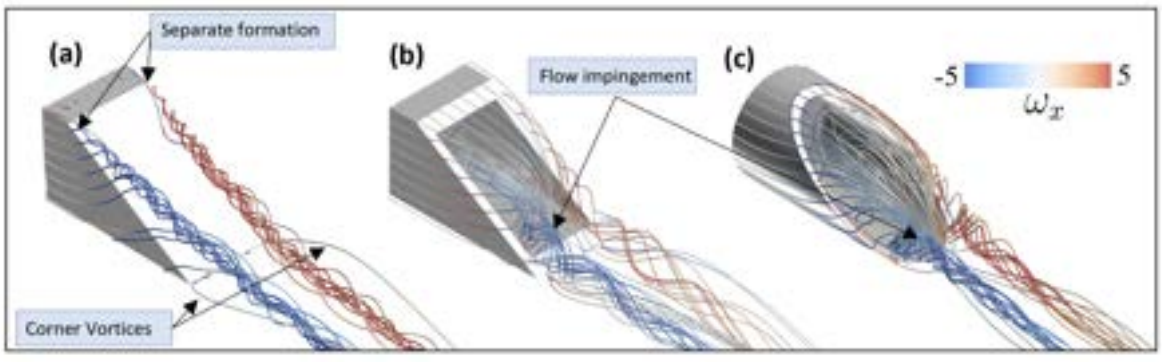

Figure 2: 3D streamlines over the (a) square, (b) square cavity and (c) round cavity geometries

Birth and control of three-dimensional Lagrangian separation: Optimal control

PIs: Gustaaf Jacobs (San Diego State University), Maziar Hemati (University of Minnesota), Geoffrey Spedding (University of Southern California)

AFOSR Award: FA9550-21-1-0434 P00002

Objectives

The main objective of the proposed project is to uncover early Lagrangian material upwellings or "the birth of separation" in three-dimensional separated flows and discover, define and test optimal multi-objective dynamic actuators that control this birth and efficiently reduce the effects of global separation. To this end, we plan to combine the development of Lagrangian separation theory and robust dynamic optimal Lagrangian control theory with computational and experimental testing on the three-dimensional separated, and transitional flow at the junction of a wing and an end-wall. Progress was made in four main themes that are covered by the following Thrusts:

THRUST I: UNCOVER 3D LAGRANGIAN SEPARATION IDENTIFIERS

Building on a frame-invariant theory of material spike formation during flow separation over a no-slip boundary in three-dimensional flows with arbitrary time dependence, we have developed a heuristic measure to identify the location of early upwelling near asymptotic separation manifolds. The heuristic is a special case of the more general, first principle theory that is based on finite time curvature changes and alleviates challenges related to determination of the high-order derivatives dependencies in a experiment or realistic setting. The new measure identifies the backbone within 20% of its exact location.

THRUST II: DEVELOP DYNAMIC CONTROL THEORY

An optimization framework has been formulated to identify sparse and spatially-localized finite-amplitude perturbations that maximize the amplification of energy over finite-time intervals in nonlinear systems. This framework establishes a path toward identifying optimal actuator locations for which the nonlinear response of desired quantities of interest will be most sensitive to control. The proposed optimization problem has been solved with a variational approach, resulting in an iterative direct-adjoint

looping algorithm for computing sparse optimal perturbations. The utility of the proposed analysis technique has been demonstrated on a series of low-order fluids models.

Our optimization framework is ready, but what is needed now is a low-order model that faithfully predicts the complex dynamics of three-dimensional Lagrangian separation. To this end, we have developed a new variant of the sparse identification of nonlinear dynamics (SINDy) that ensures our data-driven reduced-order models satisfy known physical constraints (e.g., energy conservation) and guarantees that model predictions will be long-term bounded (i.e., the models are stable). This is an important step toward our ultimate goal because to date, all of the state-of-the-art approaches for data-driven reduced-order modeling we have investigated have failed to yield predictive models for our flow of interest—both in terms of poor predictive capability over short time-horizons and with regards to model predictions being long-term unbounded (i.e., the models are unstable and aphysical). In addition, we have developed an approach for closure modeling that can be augmented with any existing model—including those we are obtaining from SINDy, but also from reduced-order models obtained by other means—to enhance predictive fidelity without modifying the stability properties of the existing model. Preliminary results based on our recent developments are shown below.

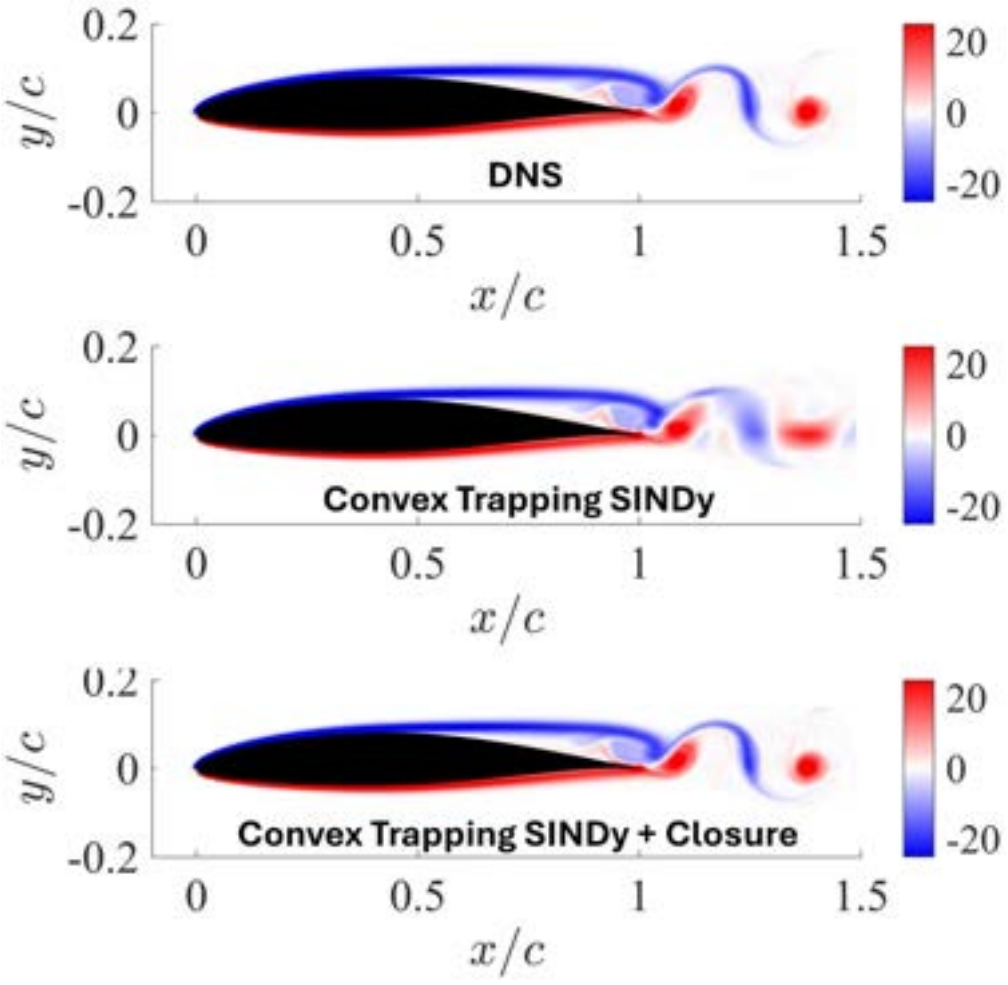

THRUST III: PERFORM DNS OF 3D SEPARATED FLOWS AND CONTROL

An extensive parametric 2D DNS study has been performed on the effect of location and timing of a pulsed control for several angles of attack. The results show that a timing and location that coincides with the dynamics of the backbone has the most effect on changes on separation angles and lift to drag ratio. Results are summarized in databases and are used for the dynamics study conducted in Thrust II.

It is shown how several instabilities coincide and lead to a lock-in behavior of the vortex system in the separation region. Moreover, the wake instabilities are shown to have significant feedback both in 2D and 3D DNS, which together with other tonal instabilities lead to complex flow development that challenges existing reduced models.

3D DNS has been conducted at the critical angle of attack for a blade with an endwall at 7 degrees angle of attack (see Figure 1). A 3D DNS simulation with pulsation near the backbone location shows that the spanwise vortices in the near wake straighten which leads to an increased lift.

Finally, to assess accuracy of RANS for moderate flow conditions and a control study, a 3D RANS simulation of the blade-with end-wall was conducted using the SST transitional model and compared to DNS. RANS results capture the separation location well. Because the pressure distribution is within engineering accuracy, the lift coefficient is predicted within 5% of DNS. The flow field in the separation bubble, wake show significant differences, and the skin friction field deviates considerably. As a result, RANS underpredicts the drag coefficient by 50%

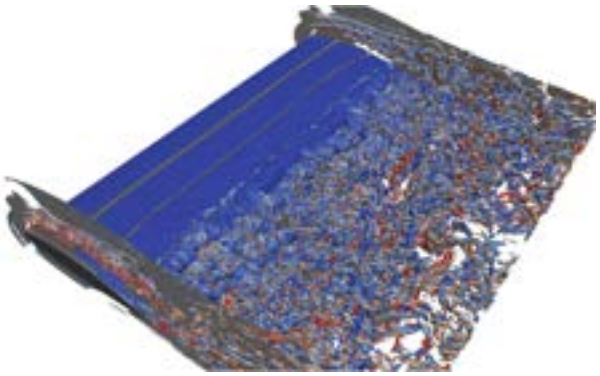

Figure 1. DNS of a blade with end-wall at 7 degrees angle of attack.

THRUST IV: EXPERIMENTS ON 3D SEPARATED FLOWS AT WING-BODY JUNCTIONS

The effect of acoustic forcing on separation and transition has been investigated in the Dryden Wind Tunnel (DWT; DrydenWT.usc.edu). A number of wind tunnel models were made, either 3D printed from PLA or machined from aluminum. The PLA models were constructed from multiple pieces for testing of local acoustic forcing through embedded miniature MEMS array speakers. Speaker arrays were placed at 9 evenly-spaced spanwise locations, and at chordwise positions x/c = 0.1 – 0.6 in increments of 0.1c. The Reynolds number based on chord varied from 20k to 80k, and angles of attack varied from -5^{o} to 15^{o}.

Each set of acoustic experiments begins with an unforced sweep through α, then at each αcrit, a frequency sweep was conducted for 2.7 <= St <= 15 for array actuation at x/c = 0.1. Once the best forcing frequency, St* is established, then the sweep through α is repeated, forcing at St*. This implies a single optimum St* at each Re, which was tested. The procedure is repeated for each Re, and then for each forcing location from 0.1c to 0.6c. The response of the signal amplifier and of the speakers themselves was not linear, particularly at the lower St, and was measured and corrected through a lookup table of forcing function amplitudes. The mean value and variance of Cl, Cd and Cm were measured at each condition. Mid-span planar PIV data were taken for selected α and St, and three separate planes on, and around actuator locations were interrogated. The objective was to locate optimum actuator locations, and to compare these with DNS and reduced model predictions. As a third, independent prediction, the location of a characteristic band of higher than ambient kinetic energy fluctuations (Fig. 2) was also tested.

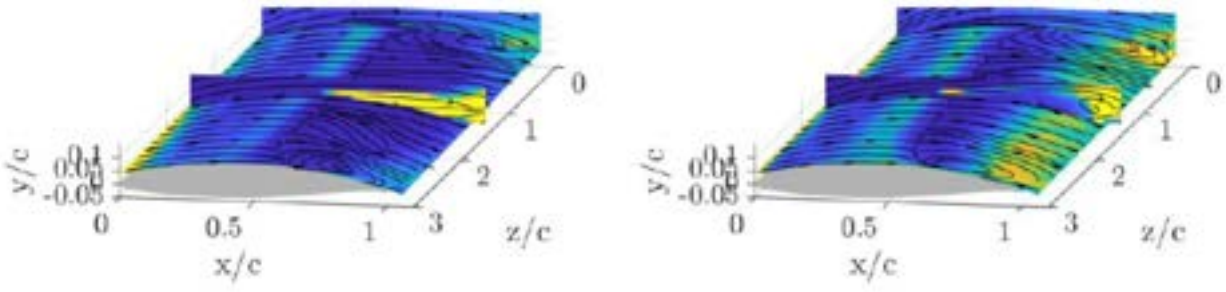

Figure 2. Kinetic energy fluctuations at Re = 40k for a = 4º and 6º. The spanwise yellow bands at about 0.4c show increased variability at a point that always lies upstream of the mean separation line.

There is now a large database of aerodynamic performance data (L, D, M, and normalized derivatives) as functions of forcing location in x, angle of incidence, α, Reynolds number, and forcing frequency. Fig. 3 shows how an optimum St* can be found for acoustic forcing, uniform in amplitude and phase along a spanwise array of embedded speakers. Following each set of lines with the same color in Fig. 3, a clear variation with forcing location can be seen. The optimum location is usually closest to 0.1c. Close to αcrit, the mean separation line is significantly further downstream, at approximately 0.5c (Fig. 4). Fig. 3 shows that forcing is more effective at intermediate Re (40, 60k) which correspond to flow states with more spanwise uniform separation lines.

Currently, Sound Pressure Level (SPL) maps are being measured across the tunnel test section and wing suction surface for internal and external excitation. The database is also being organized for a rules-based, multidimensional lookup table that can be interrogated for suitable forcing conditions, given flight conditions at prescribed α and Re.

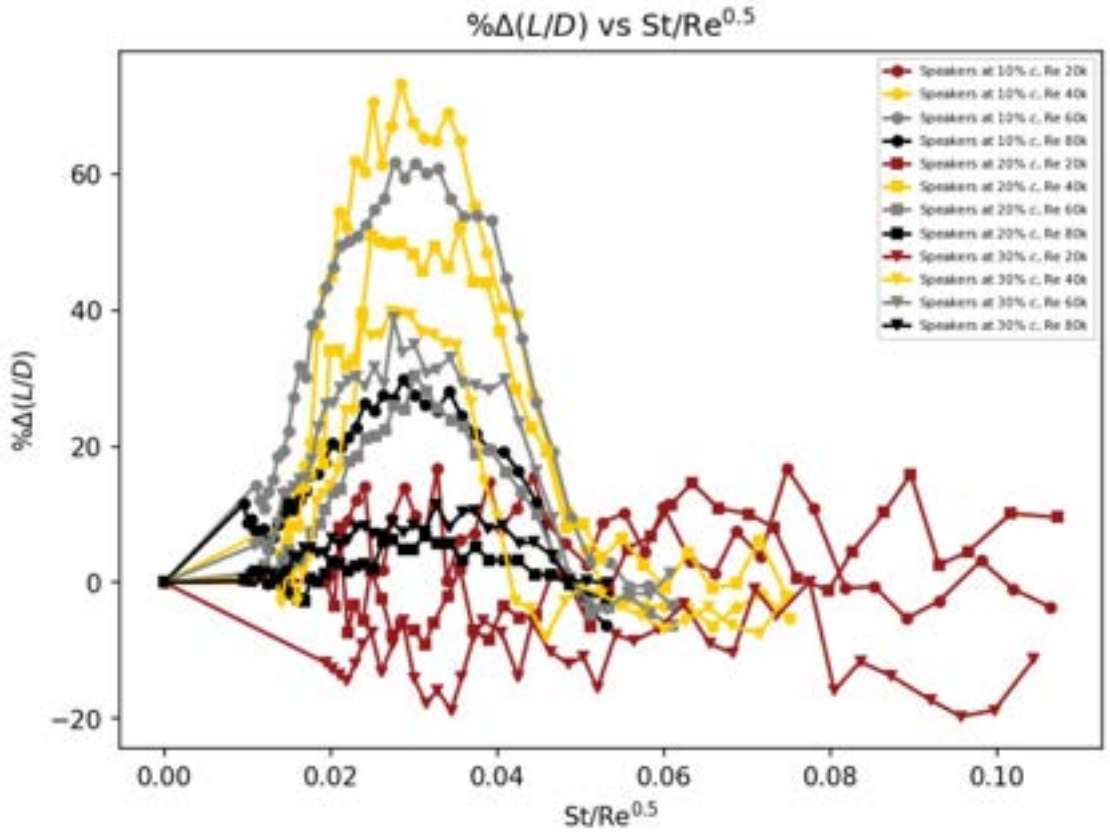

Figure 3. The relative change in lift/drag ratio with speakers actuated at 0.1c (circles), 0.2c (squares) and 0.3c (triangles) for Re = 20k (magenta), 40k (yellow), 60k (grey) and 80k (black). The forcing frequency is scaled on boundary layer parameters.

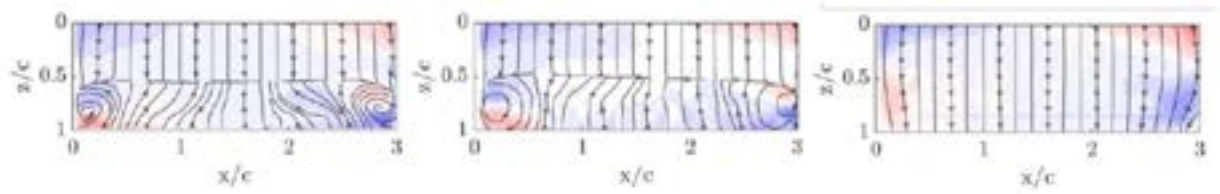

Figure 4. Streamlines and spanwise velocity in color on the suction surface for Re = 40k and a = 4, 6, 8o. The rapid change of flow state between 6 and 8o occurs abruptly at some critical angle.

(YIP) Towards real-time, 3D coherent structure estimation for flow over finite wings

Francis (Frank) Lagor, *University of Virginia*

I. Background & Objectives

Coherent flow structures can dramatically influence the unsteady aerodynamic forces on wings by impacting unsteady lift generation, the phenomenon of dynamic stall, and the mechanisms that govern the onset of stall. Laminar flow separation and the formation of unsteady, coherent flow structures such as the Leading Edge Vortex (LEV) and the Trailing Edge Vortex (TEV) significantly influence the lift force at low Reynolds numbers (approximately 1×10^5 or less) for high angles of attack and unsteady motions, and coherent flow structures continue to play an important role in the aerodynamic forces for increasing Reynolds numbers, although the physical mechanisms differ. Being able to regulate lift for agile flight at low Reynolds numbers will require understanding of the physical mechanisms governing the evolution of these structures and estimation of the state of the flow field, represented through the configurations and strengths of the coherent structures. Recent developments in Dynamic Mode Decomposition (DMD) and Koopman operator theory have made it possible to estimate the flow vector field near a wing using embedded pressure sensors and an estimator that is trained on data that is usually obtained from Particle Image Velocimetry (PIV) measurements or Computational Fluid Dynamics (CFD) simulation [2]. DMD-based estimation is able to correctly represent many pertinent features, such as the general location, magnitude, and shedding phase of a large vortical structure in the flow. To date, the estimates have only been two dimensional (2D). However, experiments and computations on finite wings have revealed the importance of three dimensionality of coherent structures on impacting lift (e.g., see Fig. 1). 3D effects play an important role in its evolution, and rich information about the state of the coherent structure is clearly present in the surface pressure distribution. Since it is impractical to require dense sensor coverage, estimation must be achieved with sparsely arranged sensors, but where should sensors be placed to take the most informative measurements that maximize our understanding of the flow field?

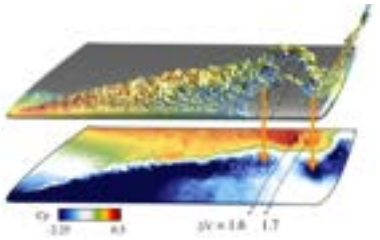

Fig. 1 Stagnation density isosurface of an arch vortex and the associated surface pressure image during dynamic stall [1].

The long-term goal of this research is to achieve accurate, real-time estimation of 3D coherent flow structures over a finite wing. To reach this goal, the objective of this project is to construct a principled framework for optimal pressure sensor placement and subsequent real-time estimation of 3D coherent flow structures that is extensible beyond operating points of the training data. An additional objective is experimental demonstration.

II. Summary of Results

The data-driven estimation approach pursued in this research combines Kernel Dynamic Mode Decomposition and Koopman Observer Form to enable use of the flow model in a standard, discrete-time Kalman Filter to generate flow-field estimates given pressure measurements. The following research findings are based on this framework.

- **Optimal sensor placement framework for flow estimation [4].** We developed a framework to optimally place pressure sensors on the surface of an airfoil (2D) or finite wing (3D) for the purpose of flow-field estimation. The framework maximizes an information measure of the state covariance matrix associated with the sensing array and a Kalman filter operating at steady-state. The information is maximized in the solution of a resource allocation problem that weights each of the candidate sensors. The unique solution of the resource allocation problem can be efficiently achieved with semi-definite program solver. To choose individual sensors, we introduced two methods for sparsification of the resource allocation: orthogonal selection and complementary selection. Numerous numerical simulations demonstrated that the framework produces sensor arrays that are highly effective for pressure-based flow estimation. Some additional noteworthy findings are:
  - **Design for multiple operating points.** We showed that the designing arrays for each desired operating point and selecting the one that maximizes the minimum information for all operating points is a good indicator of which array will have the best filtering performance of each of the conditions considered.
  - **Physical interpretation of sensor locations in 2D.** We showed that the arrays produced by the framework prefer to place sensors at the locations where the impinging saddle points (i.e., stagnation points) associated with large vortical structures appear or disappear on the surface of the airfoil (see Fig. 2a).
- **Flow estimation demonstrated in 3D [3].** We showed in both simulated and experimental data that sensor

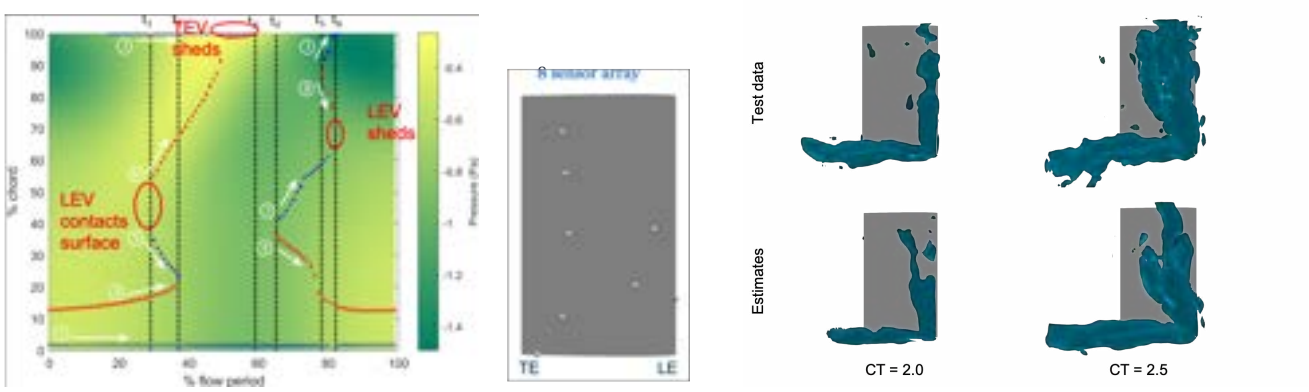

(a) (b) (c)

Fig. 2 a) Plot of saddle point motion during the shedding period for flow past a 2D airfoil, which identifies times of coherent structure contact on the wing. b) Information-based sensor array on a finite wing. c) Γ_2 iso-surfaces identifying vortical structures in 3D flow-field estimates based on towing tank experiments [3].

placement framework and the flow estimation framework extend to 3D without modification, owing to the occurrence of model truncation early in the process, which results in computationally tractable 3D models. Fig. 2b shows a sensor placement layout on a wing for estimation of the 3D coherent flow structures shown in Fig. 2c. Estimation performance captures large features of the LEV and wing-tip vortices, such as time of onset/formation, strength, and orientation. However, some spurious structures are present in the estimates far from the sensor locations, which is a subject of ongoing work.

- **Construction of nonlinear models from data using Least Angle Regression [5].** The grant has also supported research into the construction of mathematical expressions that best represent the dynamics of system under study directly from their data. We contributed an adaptation of Least Angle Regression for selection of terms to capture the dynamics of multiple vortices interacting in a background flow.

III. Current and Future Work

Publication preparation is in-process for the results of 3D flow estimation in experiment. Additional ongoing efforts (GRA: Takahito Isobe) have focused on assessing the performance of neural network based estimation approaches for flow-field reconstruction in order to compare to the DMD-based Kalman filter framework. Additional future work will focus on improving coherent structure estimates in the DMD-Kalman filter framework by incorporating covariance localization techniques to reduce generation of spurious structures. Estimate uncertainty thresholding will be used to remove modal contributions that are too uncertain.

References

[1] Medina, A., Rockwood, M., Garmann, D. J., Visbal, M. R., and Ahmed, A., "On the Characteristics of Three-Dimensional Dynamic Tip Stall on a Swept Wing," 2019. doi:10.2514/6.2019-2324.

[2] Gomez, D. F., Lagor, F. D., Kirk, P. B., Lind, A. H., Jones, A. R., and Paley, D. A., "Data-driven estimation of the unsteady flowfield near an actuated airfoil with embedded pressure sensors," *AIAA J. Guidance, Control, and Dynamics*, 2019.

[3] Graff, J., Isobe, T., Medina, A., and Lagor, F. D., "Experimental pressure-based flow estimation in 3D over a pitching wing," *In preparation*, 2023.

[4] Graff, J., Medina, A., and Lagor, F. D., "Information-Based Sensor Placement for Data-Driven Estimation of Unsteady Flows," *AIAA Journal*, Vol. 61, 2023, p. 4864. doi:10.2514/1.J063015.

[5] Graff, J., and Lagor, F. D., "Construction of Nonlinear Dynamic Equations from Data Using Least Angle Regression with an Orthogonalization Step," AIAA, 2021. doi:10.2514/6.2021-1850.

Dissecting the Flow Physics of Store-Induced Effects on Wing Aerodynamics and Limit-Cycle Oscillations

FA9550-23-1-0010

Rajat Mittal (Professor) & Jung-Hee Seo (Associate Research Professor) & Jacob Turner (Postdoc)

Research Summary for 2023-2024

Background

Aeroelastic wing flutter is problematic in high-performance aircraft, particularly in the transonic regime due to the 'transonic dip' phenomenon. Non-linear damping and shock formations cause limit-cycle oscillations, impacting aircraft fatigue, targeting, and pilot comfort. Wings with external payloads are more susceptible, necessitating deeper investigation into shock-fluid interactions.

Research Objectives

This project aims to understand instability mechanisms causing flutter growth and limit-cycle oscillation (LCO) formation in transonic flow due to aerodynamic instabilities. Using high-fidelity numerical simulations with ViCAS3D, a compressible immersed boundary solver, we examine shock features and vortex dynamics. The first objective involves time-accurate simulations of clean wings to understand fundamental pitching and heaving oscillations. Next, we explore three-dimensional wings to determine the impact of 3D flow and shock features on instability mechanisms. Lastly, we will investigate how external stores like fuel tanks affect aeroelastic performance and flutter mechanisms. Currently, the first two objectives are complete, providing a solid theoretical understanding of flutter mechanisms in 2D and 3D transonic flow, including the source of pitching instability and damping leading to LCOs, achieved through both forced and flow-induced vibration simulations.

Results Summary

In the previous year of the project, we developed the flow solver (ViCAS3D) for a wide range of compressible flow problems including both forced vibration and free vibration flutter. The new solver was used to collect a large dataset of two-dimensional single-degree-of-freedom (SDOF) pitching airfoils at a range of Mach numbers, reduced velocities and pitching amplitudes. An energy map approach, based on sinusoidal prescribed motion, was used to identify the flutter boundary for NACA0012 airfoils including LCOs. Using this dataset we have developed a fundamental understanding of the role of compressibility on flutter instabilities and the origin of the well-known transonic dip.

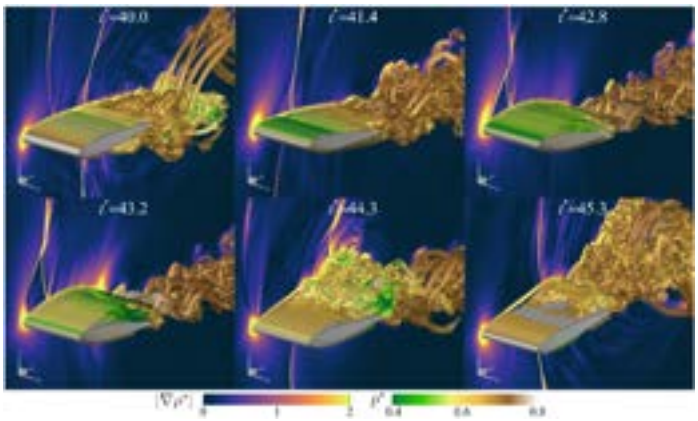

Fig 2: Numerical simulation of a 3D NACA0012 airfoil undergoing sinusoidal pitching motion at M=0.7 and Re=10,000 with a pitching amplitude of 10°. The flow is visualized by iso-surfaces of Q-criterion colored by pressure and contours of density gradient magnitude (numerical Schlieren).

Three-dimensional direct numerical simulations have been carried out to confirm the generality of the identified shock-stall mechanism. Fig. 1. shows the resulting flow field obtained by a NACA0012 airfoil at M=0.7 and Re=10,000, with a pitching amplitude of 10 degrees. The figure highlights the complex nature of the flow including shock boundary layer interactions, separation and transition to turbulence. Fig 3 shows the cycle averaged pitching moment and power extracted from the flow by the wing for 2D and 3D solutions, highlighting the effect of various energy transfer mechanisms identified in our research. Although the primary shock-boundary layer interaction resulting in flutter is broadly similar for 2D and 3D flows, we find that subtle changes in shock formation, trajectory and the timing of shed vorticity inevitably influence the predicted flutter boundary. Additionally, a secondary energy extraction mechanism caused by vortex-induced shocks in two-dimensional flow is found to be damped in the three-dimensional solution due to the spanwise breakup of shed vorticity.

In addition to prescribed motion simulations, we have conducted several fluid-structure interaction (FSI) simulations where the airfoil motion is flow-induced. This includes pitch (SDOF) and pitch & heave problems (Two DOF). Fig 2 shows the outcome of SDOF FSI simulations of a two-dimensional NACA0012 airfoil at M=0.63. Using this approach we have revealed that induced velocity caused by shed counter-rotating vorticity is a likely candidate for flutter damping at high angles of attack, possibly resulting in LCOs. We have also simulated TDOF flutter for several flow conditions in two dimensions. Limit cycles in both pitch and heave dynamics are identified for transonic conditions. The LCO behavior depends strongly on the Mach number and pivot point. At high Mach numbers, classical small amplitude transonic buzz is observed, while at low transonic speeds, high-amplitude shock-stall is possible, similar to SDOF flutter.

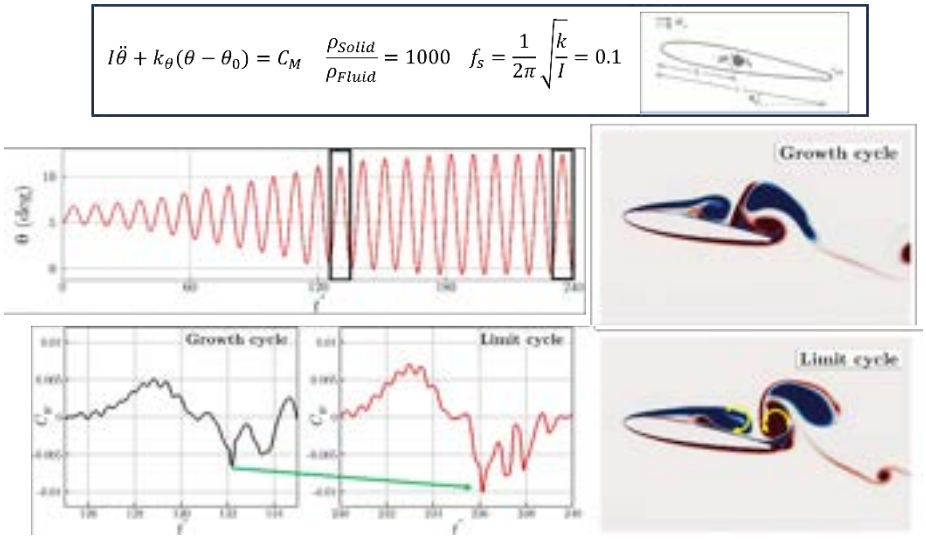

Fig 2: Single degree-of-freedom FSI simulation of a NACA0012 airfoil at M=0.63 and mean angle of attack $\theta_0 = 5^\circ$. Flow induced vibration simulations are used to investigate the non-linear damping mechanism leading to LCO. Time history of pitching angle is shown alongside power coefficient during a growth cycle and limit cycle. Vorticity contours are used to visualize the flow during the damping feature (negative power) labeled on the figure.

Future Work

In year 3 of the project, we will continue our analysis of TDOF flutter to identify the cause for different LCO amplitudes observed at low and high transonic Mach numbers. Additionally, we will investigate the effect of underwing stores on the flutter instability mechanism identified for clean wings. We have conducted preliminary simulations of 3D delta wings with cylindrical stores, thus demonstrating the capabilities of the current methodology for this purpose. Both forced vibration and FSI simulations of wings with stores can be conducted with ViCAS3D. Furthermore, we have developed a compressible variant of the force partitioning method. Using this technique, we can carry out a regional analysis of the flow to identify the key flow and shock features responsible for imparting energy to the structure.

Publications and Presentations

- "Two-dimensional time-resolved subsonic compressible flow characteristics of NACA0012 airfoils", AIAA Journal, 2024, Under Review
- "Time-Accurate Fluid-Structure Interaction (FSI) Simulations of Transonic Flutter", AIAA SCITECH Forum, Jan. 2024, doi: 10.2514/6.2024-1354
- "A High-Order Sharp-Interface Immersed Boundary Solver for High-Speed Flows". Journal of Computational Physics, 2024, 500, 112748
- "Sinusoidally Pitching Foils in Transonic Flow: Insights into Flutter from Time-Accurate Simulations". AIAA Journal, 2024, 62 (3), 1148-1158
- "Limit cycle wing flutter in the transonic regime: Insights from immersed boundary FSI simulations", APS Division of Fluid Dynamics 76th Annual Meeting, Nov 2023.
- "Analysis of the Flow Physics of Transonic Flutter Using Energy Maps", AIAA SCITECH Forum, Jan. 2023, doi: 10.2514/6.2023-0083
- "Investigating the interplay between vortex dynamics and compressibility in transonic airfoil flutter", APS Division of Fluid Dynamics 75th Annual Meeting, Nov 2022.

Populating the wall layer, one eddy at a time: Resolvent analysis for Wall-Modelled LES

Ugo Piomelli
Department of Mechanical and Materials Engineering
Queen's University
Kingston (ON), Canada

Beverley McKeon
Graduate Aerospace Laboratories
California Institute of Technology
Pasadena, CA, U.S.A.
Current affiliation: Stanford University

Abstract

Computational cost precludes direct simulation of non-equilibrium turbulent flows in realistic conditions. Wall-modelled large-eddy simulations (WMLES) and hybrid RANS/LES methods can be used to analyze them at much decreased cost, but require modelling of the near-wall layer. Effective models exist for equilibrium boundary layers, but they are not accurate in more complex configurations. In this research we propose to advance the state-of-the-art of WMLES by using low-order resolvent-based models to populate the wall layer of WMLES with realistic eddies, enabling modelling of local and instantaneous values of velocity and stresses and providing the means to improve the inner/outer-layer coupling that can limit the effectiveness of current WMLES in non-equilibrium flows.

Accomplishments in the Preceding Year

In this year's work, we have finalized and implemented a model based on resolvent modes to augment the Reynolds stress in the near-wall region, considering for now only modes that are confined below the inner-outer interface (located within the first few points of the wall). We have prepared resolvent models of the near wall region using representative modes determined from DNS of turbulent channel flow. The relative weightings of the modes are determined at the model stage, see Figure 1; then we determine a global scaling factor to provide a certain portion of the peak Reynolds stress (Figure 2). The outer layer solution is matched at the interface under the optimal scaling (Figure 3).

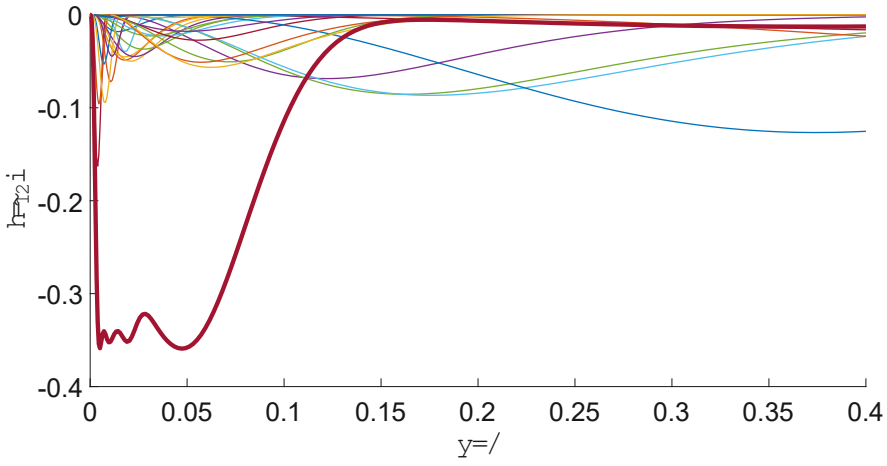

Figure 1: uv Reynolds stress associated with resolvent mode model. Individual resolvent modes (thin lines) and summed contribution (thick line).

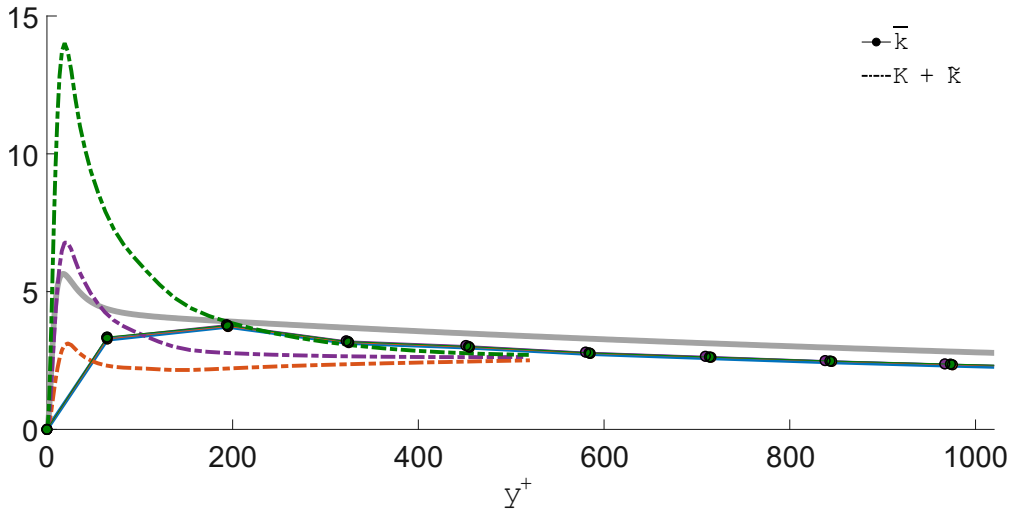

Figure 2: Resolvent contribution to the normal Reynolds stresses in the near-wall region with various scaling factors (dashed lines; red: 15%, purple 35%; green 65%) compared with the outer layer LES solution (symbols) and true (DNS) solution (solid gray line).

The results at friction Reynolds number 5,200 are promising. The next step will be to take into account an expanded range of scales in the log region by increasing the number of resolvent modes in a principled manner, exploiting the self-similar scaling of the mean velocity profile. Further, we will investigate implementing an internal means to determine the resolvent-model scaling by matching inner- and outer-layer quantities (such as the Reynolds shear stress and its derivatives) at the inner-outer layer interface.

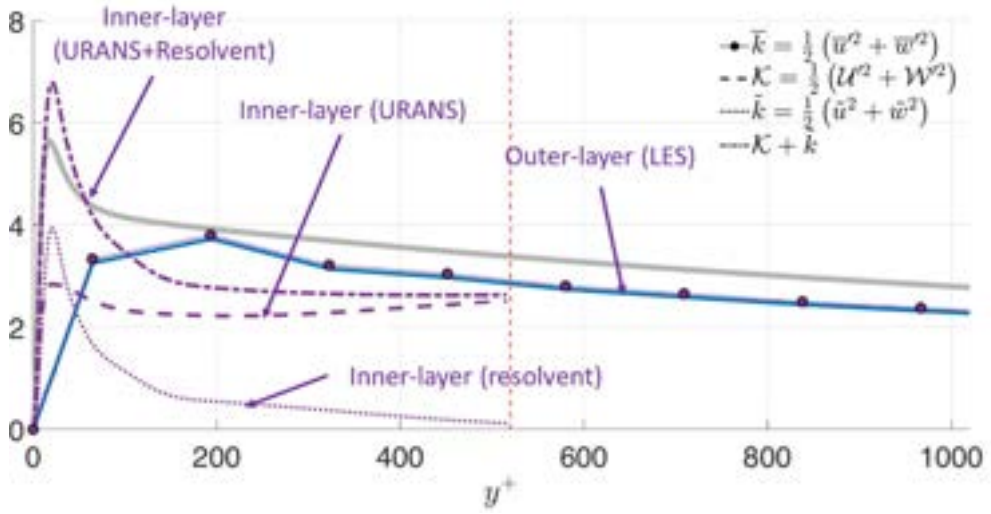

Figure 3: Full solution, showing the contributions to the plane-parallel turbulent kinetic energy of the wall parallel components due to the resolvent model, inner-layer URANS and the match of the sum to the outer layer LES for the optimal scaling factor in the resolvent model.

Discovery of nonlinear flow physics using Bispectral Mode Decomposition

O. T. Schmidt, UC San Diego, Dept of MAE

2024 Update, FA9550-22-1-0541, Gregg Abate

Motivation

Bispectral Mode Decomposition (BMD, [1]) is a powerful modal decomposition technique designed for the physical discovery and reduced-order modeling of large-scale flow data. Similar to Proper Orthogonal Decomposition (POD) and Dynamic Mode Decomposition (DMD), BMD can be applied to both numerical and experimental datasets. While POD and DMD are effective in extracting significant flow features and providing accurate low-dimensional representations of nonlinear flow dynamics, they fall short in offering direct and quantitative insights into the nonlinear interactions that govern these dynamics. BMD addresses this gap by identifying the flow structures associated with dominant frequency triads and pinpointing their interaction regions.

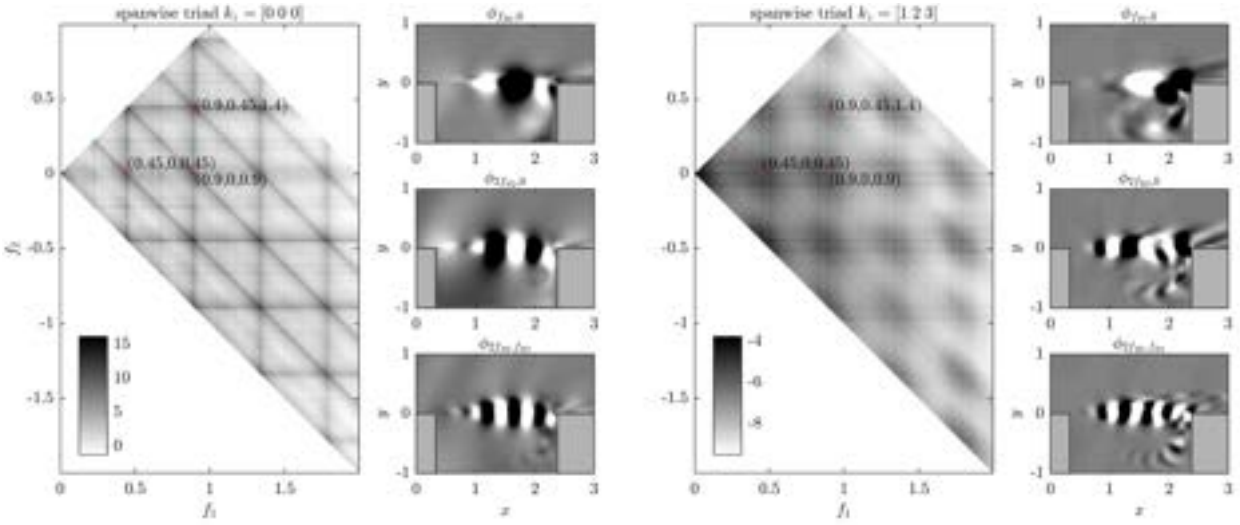

Figure 1: **Bispectral mode analysis of the open cavity flow DNS:** The bispectral modes corresponding to spanwise wavenumber triplets $k_z = [0\ 0\ 0]$ (left) and $k_z = [1\ 2\ 3]$ (right) are visualized. Three distinct bispectral modes identified in the bispectrum are highlighted for each case. The MATLAB implementation of BMD used in this project is freely accessible at https://www.mathworks.com/matlabcentral/fileexchange/83408-bmd.

Open cavity flows are characterized by rich nonlinear dynamics, driven by complex interactions between shear-layer instabilities, acoustic pressure waves, and low-frequency oscillations. A key unsteady phenomenon in these flows is the emergence of Rossiter tones, which arise from the intrinsic Kelvin-Helmholtz-type instability. This instability causes the shear layer to roll up and impinge on the trailing edge, establishing a feedback loop over the cavity's finite length via acoustic feedback. The finite cavity length permits only discrete wavenumbers at integer fractions of the cavity length,

leading to the manifestation of Rossiter tones as distinct frequencies. Both the Rossiter instability and a second low-frequency instability, known as the centrifugal instability within the recirculation region of the cavity, are linear instability modes that can be identified through hydrodynamic stability theory. However, linear theory cannot predict the nonlinear interactions that give rise to the harmonic frequency components observed in real data.

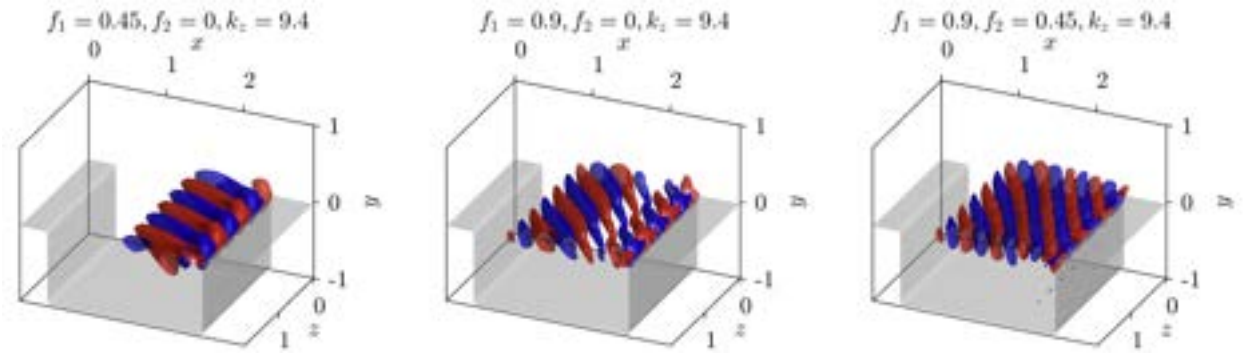

Figure 2: **3D visualization of the bispectral modes.** The same modes as in Figure 1 for $k_z = [1\ 2\ 3]$ are shown. The two isosurfaces correspond to $0.1 \times \max(v)$ (red) and $-0.1 \times \max(v)$ (blue).

Preliminary Results

In this study, we systematically investigate the nonlinear interactions and phase-coupling between various instability modes within the direct numerical simulation database by [2]. Our goal is to develop a comprehensive catalog of the linear and nonlinear dynamics in this flow. On the left side of Figure 1, we present the bispectrum and associated modes for the $k_z = 0$ self-interaction. The bispectrum reveals lines at the frequencies of Rossiter and centrifugal modes, with nodes at their intersections clearly indicating nonlinear interactions between these mechanisms. Two Rossiter modes and a third mode, resulting from their interaction, are highlighted. Given that the flow is periodic in the spanwise direction, it is essential to consider triadic interactions between spanwise wavenumber components that are triadically compatible. As an example, the mode spectrum and representative modes for the spanwise wavenumber triplet $k_z = [1\ 2\ 3]$ are shown on the right. Figure 2 provides 3D visualizations of the corresponding modes. It is observed that higher frequency modes exhibit a longer spatial extent over the cavity and a greater obliqueness angle. Ultimately, these findings will guide the development of nonlinear model-order reduction techniques aimed at creating predictive models that account for the interactions of the most significant modal flow structures.

[1] O. T. Schmidt. Bispectral mode decomposition of nonlinear flows. *Nonlinear Dynamics*, (102(4)):2479–2501, 2020. ISSN 0924-090X. doi: 10.1007/s11071-020-06037-z.

[2] M. Mathias and M. F. Medeiros. Global instability analysis of a boundary layer flow over a small cavity. *AIAA paper 2019-3535*, 2019. doi: 10.2514/6.2019-3535. URL `https://arc.aiaa.org/doi/abs/10.2514/6.2019-3535`.

AFOSR ANNUAL PROJECT REPORT - YEAR 2

Data-Enhanced Hybrid Method for Turbulent Aerodynamics

award # FA9550-23-1-0016

Prepared for the Air Force Office of Scientific Research

July 31, 2024

PERIOD OF PERFORMANCE: Aug 2023 – July 2024

PRINCIPAL INVESTIGATORS: Dr. Paul Durbin and Dr. Anupam Sharma
GRADUATE STUDENTS: Karim Ahmed, Sarasija Sudharsa, Sudeep Menon, and Dylan Sitarski

AFOSR PROGRAM: Unsteady Aerodynamics & Turbulent Flows
PROGRAM OFFICER: Dr. Gregg Abate

REPORT PREPARED BY:
Anupam Sharma and Paul Durbin

Department of Aerospace Engineering
Iowa State University, Ames, IA, USA, 50014

1 Accomplishments

In this period of performance, we have made progress in the following areas: (1) Field inversion for transitional and turbulent flows, (2) machine learning models to predict the correction field identified during field inversion, and (3) use of Field Inversion Machine Learning (FIML) for improving RANS for turbulent and transitional flow predictions. These are summarized in the following sections. One conference paper [Ahmed *et al.*, 2024] directly based on this work and a journal paper [Sudharsan & Sharma, 2024] on a related topic are products of this research.

1.1 Field inversion for transitional flows

We have successfully used field inversion with the shear stress transport (SST) $k-\omega$ model and the laminar kinetic energy (LKE) model of Pacciani *et al.* [2014] for simulating flows with separation-induced transition. Field inversion is used to infer the intermittency field (γ_{eff}) for the SST $k-\omega$ model and a correction field to the transport equation for laminar kinetic energy (k_l) in the LKE model. The details of the implementation are in Ahmed *et al.* [2024]; we summarize key results here. The focus on separation induced transition is driven by the observation from LES results of dynamic stall that stall onset is triggered by the bursting of the laminar separation bubble (LSB).

Two sets of fluid flow problems are considered: (1) flat plate with adverse pressure gradient, and (2) NACA 0012

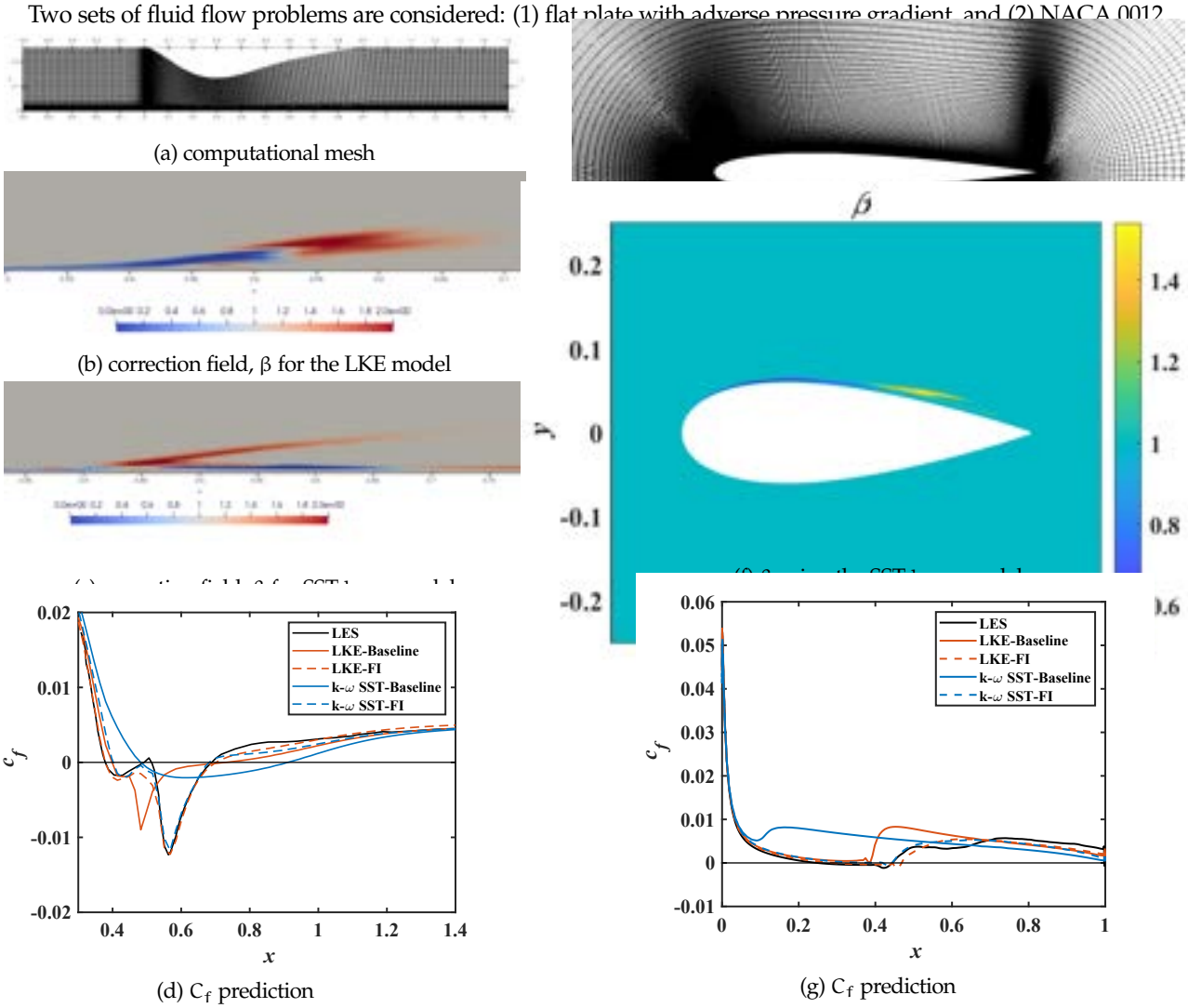

Figure 1: Flow over a flat plate with adverse pressure gradient (left) and over an NACA 0012 airfoil at α=4° (right), simulated using the laminar kinetic energy (LKE) and SST $k-\omega$ models. Correction fields (β) for the two models are in panels b and c for the flat plate case and in panel (f) for the airfoil. Skin friction coefficient (C_f) predicted after field inversion (FI) are compared with baseline predictions in panel d for the flat plate case and in panel g for the airfoil.

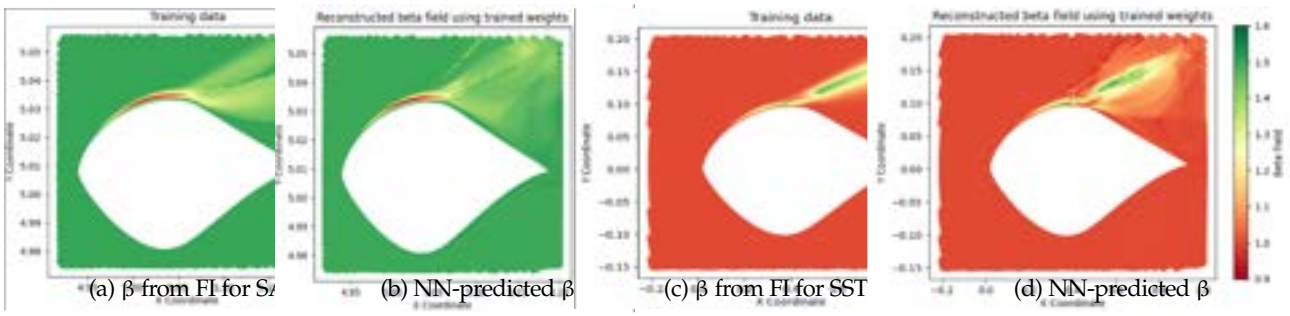

(a) β from FI for SA (b) NN-predicted β (c) β from FI for SST (d) NN-predicted β

Figure 2: Optimized β field compared with that predicted by a trained neural network (NN) model for the Spalart Almaras (SA) model in panels a and b, and for the SST $k-\omega$ model in panels c and d.

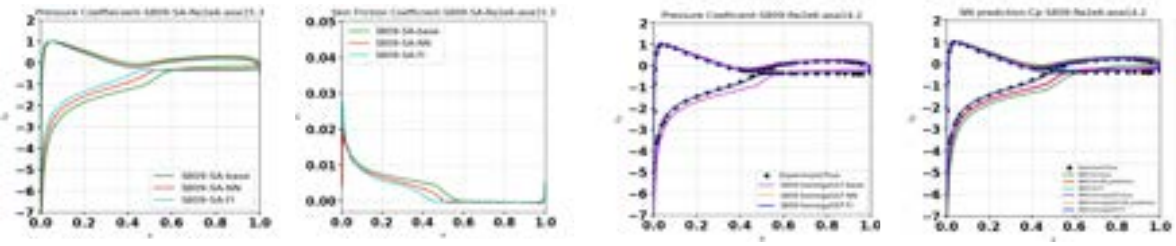

(a) C_p; SA (b) C_f; SA (c) C_p; SST $k-\omega$ (d) C_f; SST $k-\omega$

Figure 3: FIML prediction of the surface pressure coefficient, C_p and the skin friction coefficient, C_f on the S809 airfoil surface using NN-based ML models for estimating the correction field, β using flow features, η.

airfoil at different angles of attack. Figure 1 presents sample results from these simulations. Laminar separation and laminar-to-turbulent transition are accurately captured with field inversion with both models.

1.2 Machine learning

We next train machine learning (ML) models that can predict the correction field, β based on select flow features, η, i.e., develop a data-based model for $\beta = \beta(\eta)$. We have attempted ML models based on Neural Networks (NN) and Random Forest (RF) with moderate success. Figure 2 is a sample result of NN-based ML models to estimate β based on η. For this verification, the η values are obtained from the optimized (field inversion) RANS solutions; hence it only tests the accuracy of the ML model. Note that this testing has so far been limited to turbulent flows; we are working on extending this to transitional flows.

1.3 Field inversion machine learning (FIML)

The ML model is incorporated into the RANS solver in OpenFOAM to evaluate the correction field, β using the flow features, η obtained from the solution at the current iteration. Figure 3 compares FIML-enhanced RANS prediction results for the S809 airfoil.

2 Impacts

The project is at an early stage. It is intended that it will have an impact on models for transitional and turbulent flow prediction.

3 Changes

No changes are anticipated.

References

AHMED, KARIM, SITARSKI, DYLAN, SHARMA, ANUPAM & DURBIN, PAUL 2024 Enhanced rans modeling using field inversion. In *13th International Symposium on Turbulence and Shear Flow Phenomena*.

PACCIANI, ROBERTO, MARCONCINI, MICHELE, ARNONE, ANDREA & BERTINI, FRANCESCO 2014 Predicting High-Lift Low-Pressure Turbine Cascades Flow Using Transition-Sensitive Turbulence Closures. *Journal of Turbomachinery* **136** (5).

SUDHARSAN, SARASIJA & SHARMA, ANUPAM 2024 Criteria for dynamic stall onset and vortex shedding in low reynolds number flows. *Journal of Fluid Mechanics* – (–), accepted.

YIP24: Multi-Modal Interactions in Three-Dimensional Unsteady Flows

Yiyang Sun (Syracuse University)

Background and Motivation

The ability to control fluid flow behaviors can lead to quiet, economical, and efficient systems in fluid mechanics and aerodynamics. Because of high dimensionality, strong nonlinearity, and complexity in fluid physics, the primary challenge to designing effective control strategies comes from the lack of understanding of the fundamental mechanisms of complex three-dimensional (3-D) flow and multi-flow-phenomenon interactions during flow control design. Such challenges can be viewed from three perspectives: (1) a lack of modeling 3-D perturbation assuming all directions inhomogeneous in the current theoretical framework; (2) a lack of understanding of multi-frequency interactions in a multi-flow-phenomenon configuration; (3) a lack of characterizing spatial interactions of a few canonical flow phenomena if they are spatially aligned and connected. For example, as depicted in Figure 1, a small cavity is embedded on the lower side of the airfoil leading edge; when the airfoil is at a high angle of attack, the flow impingement induces a cavity flow oscillation that vortices convect downstream along the airfoil surface to interact with the laminar or turbulent separation area. From a flow control perspective, all these knowledge gaps impose significant challenges in designing an efficient control strategy that can fully leverage the underlying physics of the flow in a practical configuration and trigger favorable interactions, gaining a maximal performance improvement of a highly integrated fluid system. In this YIP project, I aim to fill those knowledge gaps to better incorporate the fundamental physics of canonical fluid flow problems—leveraging cavity flow to eliminate laminar flow separation—into a practical and highly integrated flow system experienced by aircraft, as depicted in Figure 1, contributing to the development of next-generation aircraft systems.

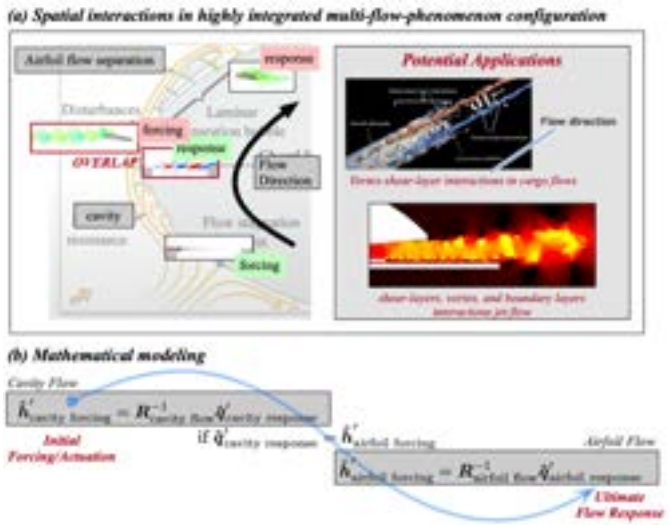

Figure 1(a) Examples of spatial interactions in complex flows. (b) Modeling spatio-temporal interactions in the resolvent analysis for optimal flow response in multi-flow-phenomenon configuration.

Objectives

My *long-term research goal* is to create innovative frameworks and tools to understand complicated aerodynamics and precisely manipulate compressible (high-speed) flow features using flow control techniques. To achieve this goal, *the overarching objective of this YIP project* is to unravel the temporal and spatial interactions of perturbations in the form of modes by developing a 3-D harmonic resolvent analysis for high-speed compressible flow (*for the first time*), and leverage the favorable interactions to suppress boundary-layer separation. There are three key tasks in this project: (1) uncover 3-D perturbation dynamics in 3-D base flow; (2) identify multi-frequency and spatial interactions in unsteady flows using the harmonic resolvent analysis; and (3) characterize temporal and spatial interactions in high-fidelity simulations through a separation control configuration.

Result Summary (new start 2024)

To achieve the goal of eliminating 3-D compressible separated flow using induced cavity vortices by harnessing harmonic resolvent analysis, we are simultaneously developing and validating (i) the 2-D harmonic resolvent analysis incorporating frequency coupling; (ii) the 3-D linearized Navier—Stokes governing equation for compressible flows. As a start, the theoretical tools have been applied to 2-D laminar cavity flows and 2-D laminar separation bubbles, respectively, as discussed below, to uncover the nonlinear coupling and high-frequency perturbation modes that are overlooked using the conventional linear framework.

- *Incompressible flow over NACA0012 airfoil as validation*

Identifying the nonlinear perturbation dynamics developing around a time-varying high-speed base flow requires the compressibility consideration to be incorporated in the harmonic resolvent analysis (HRA) framework. We formulated the theoretical framework of the HRA for the first time using the full compressible linearized Navier—Stokes equation. To validate our code, we performed HRA of the flow past a NACA0012 airfoil at an angle of attack 20°. We performed the analysis at Reynolds number of 200 and Mach number of 0.05 to match the incompressible flow condition used

in the study of Padovan et. al.[1] . The comparison between the forcing and response modes at the same frequency obtained from our code to those of Padovan et al. [1] is shown in Figure 2, which shows an excellent agreement.

- *Instability of cubic lid-driven cavity flow as validation*

Validation of our linearization of the 3-D compressible Navier—Stokes equations can be achieved by comparing 3-D global linear instability results that are mostly available for incompressible flows reported in the literature. We choose a study of 3-D instability of a cubic incompressible lid-drive cavity flow from Ohmichi and Yamada [2] as a validation reference. To match their incompressible condition, we specify the Mach number of 0.025 which is extremely small that a moving air flow at such a speed is assumed to be incompressible. The Reynolds number has been kept the same as 200 used for incompressible flow. Because the Reynolds number remains identical, the 3-D instability modes should be the same but only be scaled by the velocity ratio used in the incompressible and compressible governing equations. As shown in Figure 8, we have successfully validated the linearization of the 3-D compressible Navier—Stokes equations by obtaining the identical leading global instability mode of the cubic lid-driven cavity flow.

- *Harmonic resolvent analysis of 2-D cavity flows*

We analyzed perturbation dynamics in a cavity flow at Mach number of 0.6 and Reynolds number of 1500. We performed the classical and harmonic resolvent analyses to identify the perturbation amplification around time-averaged base flow and time-varying base flow considering the Fourier mode at the resonant frequency. The optimal forcing and response modes at the dominant frequency and its higher- harmonics are shown in Figure 4. The modal structures at the higher-harmonics are generated by cross-frequency interactions, which are resolved by the HRA in contrast to the classical analysis, which does not allow frequency coupling and results in spurious modes at those frequencies.

- *Comparison among SPOD, classical and harmonic resolvent analyses of a laminar separation bubble*

To identify the receptivity of a laminar separation bubble at Mach 0.3 to perturbations, we applied the classical and harmonic resolvent analyses. The SPOD mode obtained from the nonlinear simulation data, the optimal response modes from the classical and harmonic resolvent analyses are compared in Figure 5. The SPOD mode exhibits the dominant presence of structures within the separation bubble and downstream. The mode from HRA predicts the perturbation to get amplified within the bubble, whereas the classical resolvent mode predicts that amplification will occur further downstream.

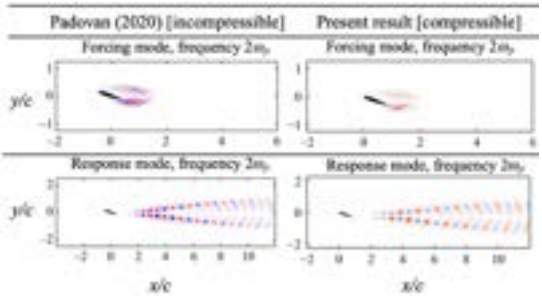

Figure 2 Validation of the HRA framework for compressible flow by comparing forcing and response modes between our result to those reported in Padovan et. al.[1]

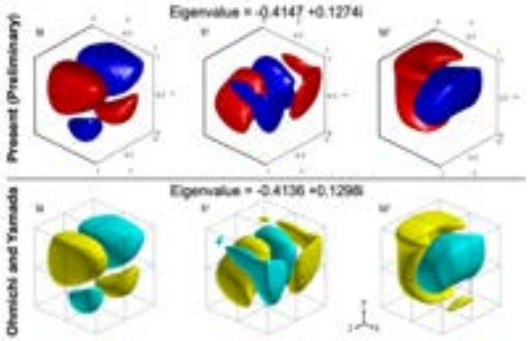

Figure 3 Validation of the linearized 3-D Navier-Stokes equation by comparing 3-D instability in a cubic lid-driven cavity flow reported by Ohmichi and Yamada [2].

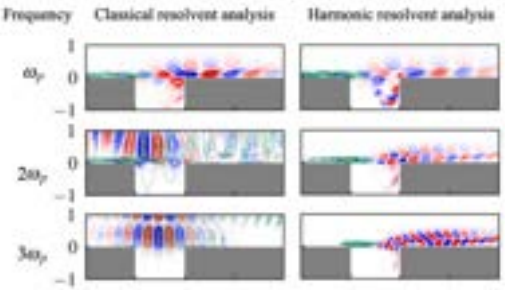

Figure 4 Forcing and response modes obtained from the classical and harmonic resolvent analysis for a cavity flow at Mach number of 0.6.

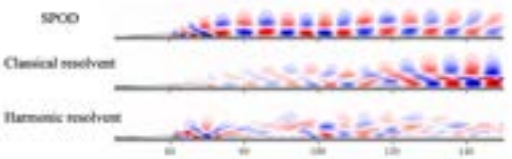

Figure 5 Comparison of modal structures obtained from the SPOD, classical, and harmonic resolvent analysis for a laminar separation bubble on a flat plate.

Future Work

We will extend the analysis from 2-D to 2.5-D configurations to consider spanwise homogeneous flow coherent structures. Meanwhile, instead of investigating the cavity flow and laminar separation separately, these two flow phenomena will be integrated into one model to mimic the scenario of separation control through interactions between cavity-induced vortices and separated shear layers.

Reference

[1] Padovan, A., Otto, S., and Rowley, C. W. Analysis of amplification mechanisms and cross-frequency interactions in nonlinear flows via the harmonic resolvent. *J. Fluid Mech.* 900 (2020), A14.

[2] Ohmichi, Y., and Yamada, K. Matrix-free triglobal adjoint stability analysis of compressible Navier–Stokes equations. *J. of Comput. Phys.* 437 (2021), 110332.

Unsteady Aeromechanic Interactions

SUMMARY OF RESEARCH PROGRESS 2024

Project Title: A wavelet-based resolvent analysis for highly-unsteady transient flows
PI and Co-PI: Jane Bae (Caltech) and Scott Dawson (Illinois Tech)

1 Background and Objectives

Fundamental studies of unsteady aerodynamics and turbulent flow have mostly focused on statistically-steady configurations, where all statistics are invariant under a shift in time. However, in real-world applications of external aerodynamics, truly unsteady transient effects become important. Such events include separation leading to stall, a sudden change in yaw angle or gust encounters, and shockwave formation. The additional complexity of these transient problems makes it harder to perform controlled experiments, both numerical and in the laboratory. Our goal is to develop reduced-order models that can be used to understand, predict, and control highly-unsteady transient turbulent flow in various engineering systems.

Resolvent analysis has been a popular reduced-order model for understanding a wide variety of turbulent flows. However, the use of the Fourier transformation in the temporal direction in the formation of the resolvent operator limits the application of resolvent analysis to statistically-steady and quasi-periodic flows [6].

The research objective of this project is to develop an extension of resolvent analysis that allow us to study study time-transient phenomena by considering wavelet (as opposed to Fourier) transforms in time. This gives a means of predicting spatio-temporally localized trajectories that are most highly amplified by the linearized, but time-dependent, Navier–Stokes operator. We will develop and validate this methodology for a variety of systems, ranging from quasi-parallel wall-bounded turbulent flows to spatio-temporally evolving systems. We believe that this analysis tool will ultimately enable the accurate prediction and control of such flows.

2 Summary of Results

We have now developed a comprehensive theoretical and analytical understanding of using a wavelet basis rather than a Fourier basis for resolvent analysis, and of using sparsity-promotion for identifying time-localized resolvent modes and energy amplification mechanisms. For wavelet based resolvent analysis, we found that using an orthonormal wavelet basis for resolvent analysis is equivalent to the traditional resolvent analysis for statistically stationary flows, with the added benefit of being able to study transient behavior and time-varying mean flows. We were able to develop an efficient code for computing the resolvent modes using the wavelet-based resolvent analysis. We validated this code on a statistically-stationary turbulent channel flow by observing that the modes computed from traditional Fourier-based resolvent analysis match those observed from the wavelet-based resolvent analysis. Finally, we applied the wavelet-based resolvent analysis to two temporally varying systems: turbulent Stokes boundary layer and turbulent channel flow with sudden lateral pressure gradient. These results show that the wavelet-based resolvent analysis can be an useful tool for studying temporally transient flows. Currently, we started study the mechanisms of transition through wavelet-based resolvent analysis of a turbulent oscillating Stokes' boundary layer. Windowing in time will highlight the most dominant forcing mechanisms in each temporal segment of the oscillating boundary layer.

We also studied the transient growth mechanism in a turbulent channel flow highlighted by the wavelet-based resolvent analysis. We inject the most amplified forcing mode into a direct numerical simulation of a channel flow to observe how the statistics of the flow change in time. Ensembles of the experiment are then averaged to construct a statistical view of how the most amplified forcing mode changes the flow. This will allow us to study how important the linear dynamics are in a turbulent flow. Results show that for relatively short times, the linear growth is a good predictor of transient growth, and that extreme events can be identified by detecting resolvent forcing modes that predate the growth.

In addition, we developed the theory and implementation of a spatio-temporally sparse variant of resolvent analysis, which modifies the standard optimization problem in resolvent analysis to allow for time-localized modes for both statistically stationary and time-varying systems. We applied spatio-temporally sparse resolvent analysis to statistically-stationary channel flow, to identify the structure of time-localized wavepackets/wavelets that emerge naturally from the relevant optimization problem. For example, when allowing for localization in the spanwise direction, we identify localized modes that, when compared to spanwise-Fourier modes, are more reminiscent of both instantaneous and conditionally-averaged structures and correlations observed in a turbulent flow field.

We have also now applied this sparsity-promoting analysis to both time-varying systems mentioned above, where we find that in certain cases the sparsity-promoting method identifies mechanisms that are distinct from those predicted from regular wavelet-based resolvent analysis. At the same time, we also continued developments in two directions directions that could reduce the computational cost of these methods: timestepping approaches that do not require the formation of large space-time resolvent operators, and analytic approximations that preclude the need to decompose discrete operators altogether.

These results were published in conference papers in the 2023 AIAA SciTech Forum [2, 4] and a conference journal [1], and submitted two manuscripts to the Journal of Fluid Mechanics (both currently under review) [3, 5].

3 Future Plan

We will expand our analysis of various time-varying flows that highlight interesting physics in several ways. We already started investigating transition mechanisms, but we are planning to tackle separation as well as unsteadiness through change in flow direction in time. We will continue to investigate the application of spatio-temporally sparse resolvent analysis to these configurations, and will focus on determining the extent to which the predictions of this approach align with structures and statistics observed in full nonlinear simulations. We will also develop analytic approximations to account for time-varying mean profiles, to investigate the extent to which analytic considerations can predict the effects of a time-varying mean on the shape and amplification of leading resolvent forcing and response modes.

We will additionally look to apply the methods developed in this work to cases where only experimental (rather than numerical) mean data is available, to demonstrate the broader applicability of these methods. We are currently talking to Prof. Theresa Saxton-Fox to apply our methodology to their experimental dataset of temporally-varying pressure gradient turbulent boundary layers.

References

[1] E. Ballouz, S. T. M. Dawson, and H. J. Bae. Transient growth of wavelet-based resolvent modes in the buffer layer of wall-bounded turbulence. In *J. Phys.: Conf. Ser.*, volume 2753, page 012002. IOP Publishing, 2024.

[2] E. Ballouz, B. Lopez-Doriga, S. T. Dawson, and H. J. Bae. Wavelet-based resolvent analysis for statistically-stationary and temporally-evolving flows. In *AIAA SCITECH 2023 Forum*, page 0676, 2023.

[3] E. Ballouz, B. Lopez-Doriga, S. T. M. Dawson, and H. J. Bae. Wavelet-based resolvent analysis of non-stationary flows. *J. Fluid Mech.*, under review, 2024.

[4] B. Lopez-Doriga, E. Ballouz, H. J. Bae, and S. T. Dawson. A sparsity-promoting resolvent analysis for the identification of spatiotemporally-localized amplification mechanisms. In *AIAA SCITECH 2023 Forum*, page 0677, 2023.

[5] B. Lopez-Doriga, E. Ballouz, H. J. Bae, and S. T. M. Dawson. Sparse space-time resolvent analysis for statistically-stationary and time-varying flows. *J. Fluid Mech.*, under review, 2024.

[6] A. Padovan, S. E. Otto, and C. W. Rowley. Analysis of amplification mechanisms and cross-frequency interactions in nonlinear flows via the harmonic resolvent. *J. Fluid Mech.*, 900:A14, 2020.

An experimental dynamical systems approach to aeroelastic instabilities of swept wings

Annual report for AFOSR Grant FA9550-21-1-0462

Aug 2024

Kenny Breuer, Brown University

Goals of program

The goal of the research is to study aeroelastic instabilities on swept wing flows using a variety of experimental and data-driven analysis techniques.

Results

Over the past year our focus has been on two areas: (i) Detailed analysis of PIV data taken in the previous year to examine the formation of Leading edge and Tip vortices from pitching swept wings. (ii) development of the Force-Moment portioning method (FMPM) to quantitatively study the contributions of different components of the flow to the forces and moments on these swept wings.

In the first area, using experimental data previously acquired under this program, we have been focused on identifying reduced order models for the behavior of unsteady vortex-dominated flows over swept wings. We are computing the center of pressure for pitching wings from the force/moment measurements.

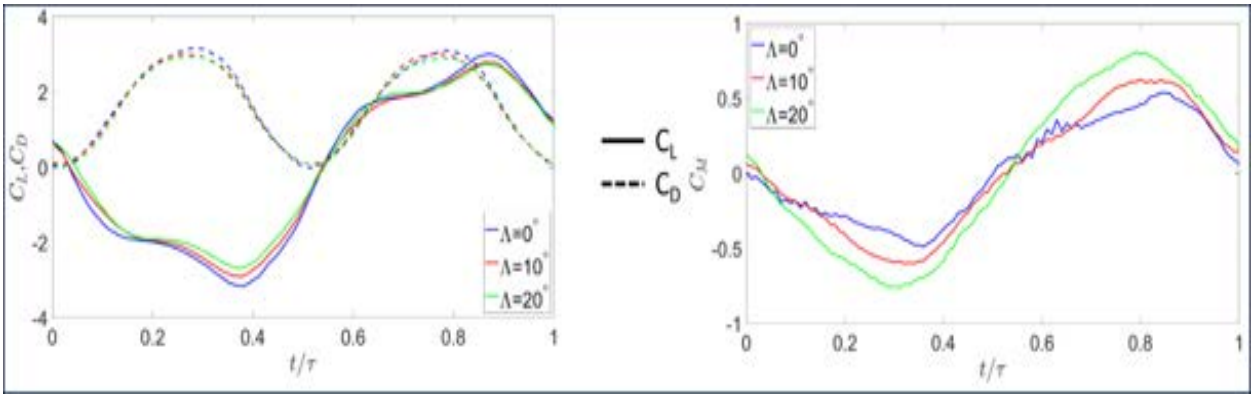

Figure 1 (A) The change in Lift and Drag throughout the pitching cycle (b) Variation of Pitching Moment during the cycle

The phase-averaged lift and drag forces for wings with three sweep angles are shown in Figure 1 with the pitching angle information. The drag is shown by the dashed lines and the solid lines represents lift, and the colors represent different sweep angles. The figure on the right shows

the change in pitching moment throughout the cycle. While the lift and drag curves almost overlap with each other, there is a clear dependency on sweep angle for the pitching moment.

From these measurements we can calculate the center of pressure, which show strong dependencies on the sweep angle due to the changing role of the leading edge, and tip vortices associated with these large amplitude pitching wings.

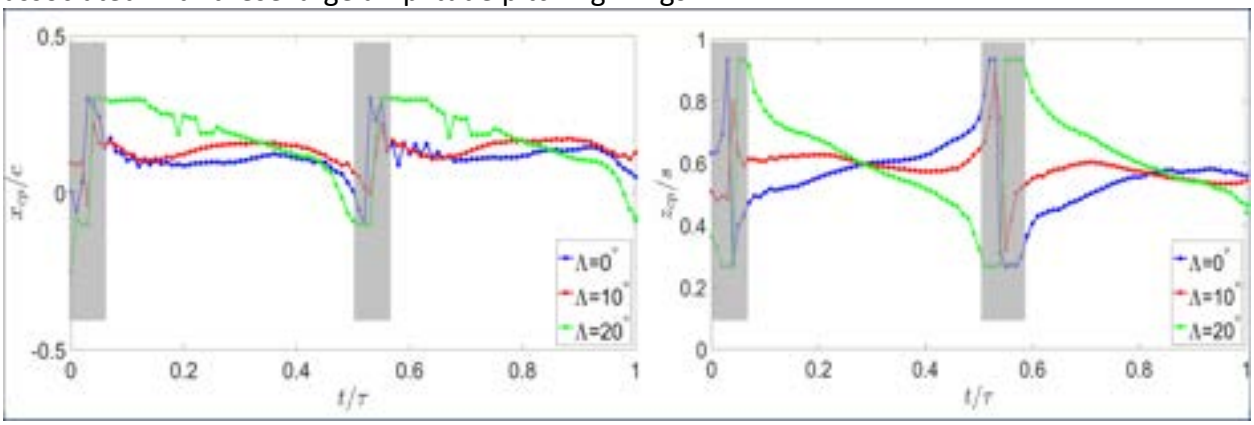

Figure 2 (a) Chord-wise variation of COP (B) Movement of COP in the span-wise direction

We are analyzing this in more detail using Force/Moment Partitioning Method (FMPM), which quantitively assesses the role of flow features to (in this case) the pitching moment. This work is ongoing and will be completed soon (an abstract at the 2024 APS/DFD meeting has been submitted to report on these details.

During the last few months of the project, we plan to take one more set of experimental data to definitively isolate the different roles of tip and leading edge vortices in the varying aeroelastic characteristics of the wing with different sweep angles. This work will be completed in September/October 2024.

Challenges and changes in approach

This past year has experienced two significant sources of delay in making research progress. (1) The previous graduation of the PhD student (Yuanhang Zhu) and difficulties in finding a researcher to pick up the project resulted in a staffing shortage over much of the year. A new PhD student was identified in Jan 2023 and worked on the project from January through September 2023. However, after several months, this student made no progress on the project and left my research group without achieving any significant results. A new Post Doc - Dipan Deb - joined the group (from Taha's group at UCI) in January 2024, and has been working on the project since then, but this too has taken some time to come up to speed. (2) Our key experimental facility was shut down in May due to significant facility problems. It has since been rebuilt and is currently undergoing testing for flow and instrumentation before research can continue (hopefully in September)

The program ends this year, and no renewal proposal has been submitted. However, a no-cost extension has been requested due to the issues described above.

Background/Motivation

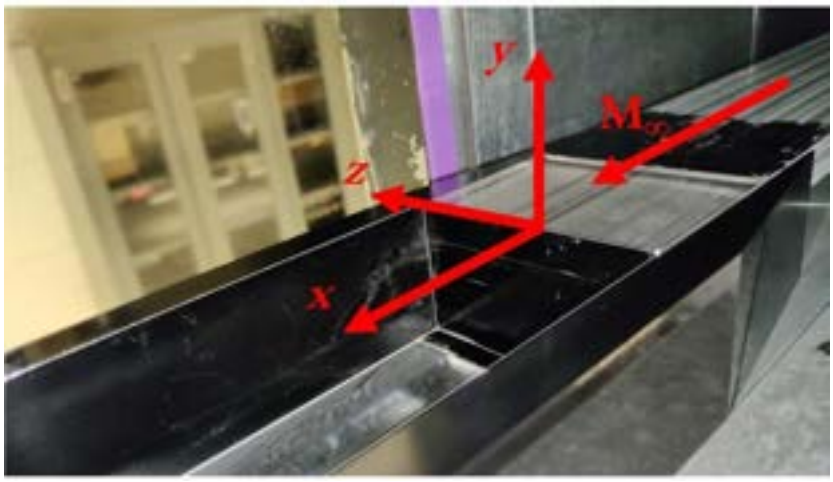

Figure 1: Experimental Setup

A major concern for directed energy applications at high speeds is the establishment of a temporally and a spatially varying shear layer, which can be challenging from an aero-optical standpoint. When a planar wavefront passes through a gas with a varying density distribution, light rays are refracted resulting in wavefront aberration. Such can arise with the passage of a beam through a supersonic shear layer, where strong density fluctuations exist due to the Kelvin-Helmholtz instability. Attenuation of these structures could lead to a reduction in jitter, which would be beneficial for maintaining quasi-steady performance of the directed energy system. Unfortunately, there are not many promising existing techniques available to mitigate these unsteady fluctuations. To address this issue and improve beam performance, we propose a basic, scientific study of the ability of an array of vortex generators to attenuate unwanted large-scale fluctuations within a supersonic shear layer and improve the aero-optical environment at supersonic speeds.

Objectives

The research plan for this proposal is designed to assess the ability of an array of pins to improve the aero-optical environment through a supersonic turbulent shear layer through a combination of different experimental measurements applied to a DOE approach. In general, the objectives move through a series of steps to maximize the pins' potential influence on the aero-optical environment.

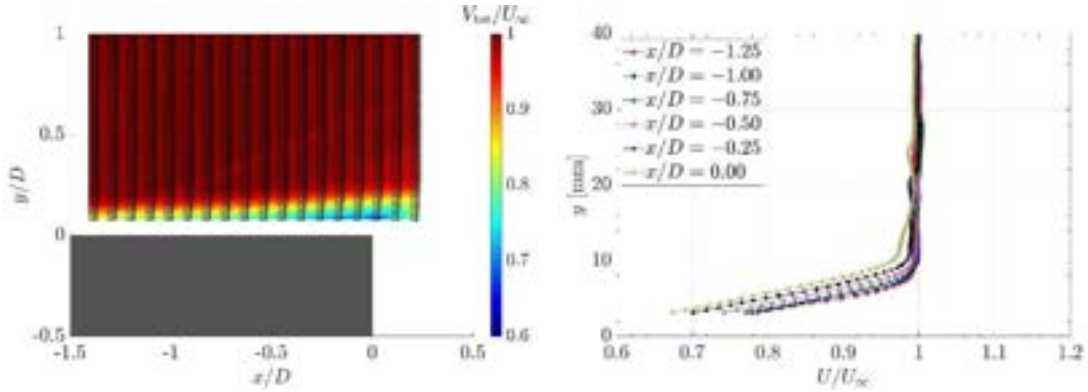

Figure 2: Boundary layer measurements to identify the relevant length scales necessary for sizing the pins.

Objective 1: Explore and quantify the streamwise influence of an array of pins in attenuating the formation of large-scale density variations associated with the Kelvin-Helmholtz instability in a shear layer.
Objective 2: Identify the influence of the pin array on the aero-optics of the shear layer.
Objective 3: Define the influence of three-dimensionalities in resolving the total aero-opticaleffect within a shear layer.

Results Summary

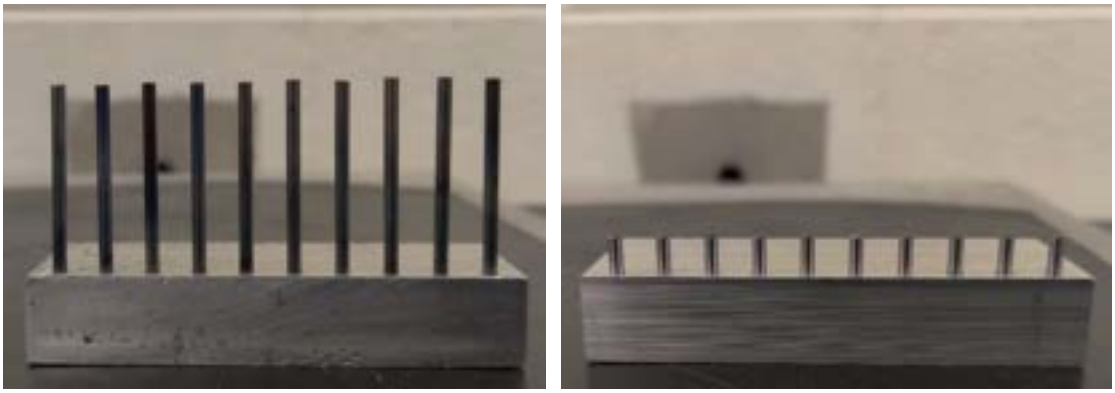

Figure 3: Two pin arrays manufactured for passive flow control testing. The largest and the smallest are completed using press-fitting of steel pins into aluminum.

Since the beginning of the project, we have been able to create our wind tunnel model and begin testing the baseline shear layer. The model is constructed from anodized aluminum to minimize surface reflections (Figure 1). Optical access is achievable through the floor of the cavity, which allows for the PIV laser sheet or imaging. The first phase of the experiments involve measurement of the baseline and the oncoming boundary layer. The boundary layer measurements are necessary to provide a length scale for sizing our pin array, according to historical data. In addition, we are observing the presence of any unwanted three-dimensionalities, along with the quantification of the shear layer in terms of time-averaged statistics.

Experiments are currently underway performing this quantification of the baseline flowfield. The boundary layer has been measured, with additional measurements being performed downstream of the separation point itself; these data can be seen in Figure 2, which shows both the centerline vector field and extracted streamwise velocity profiles. At this time, we have identified a length scale of nearly 9 mm, which can be used to guide the sizing of our pins.

A series of pins have been designed and fabricated to study the influence of passive flow control on the supersonic shear layer. An example is shown in Figure 3. The arrays that have been manufactured are designed using the boundary layer thickness as the characteristic length scale. Experimental data have now been obtained to observe the changes induced to the centerline shear layer as a function of pin array. Along with the SPIV data, Kulite measurements have also been

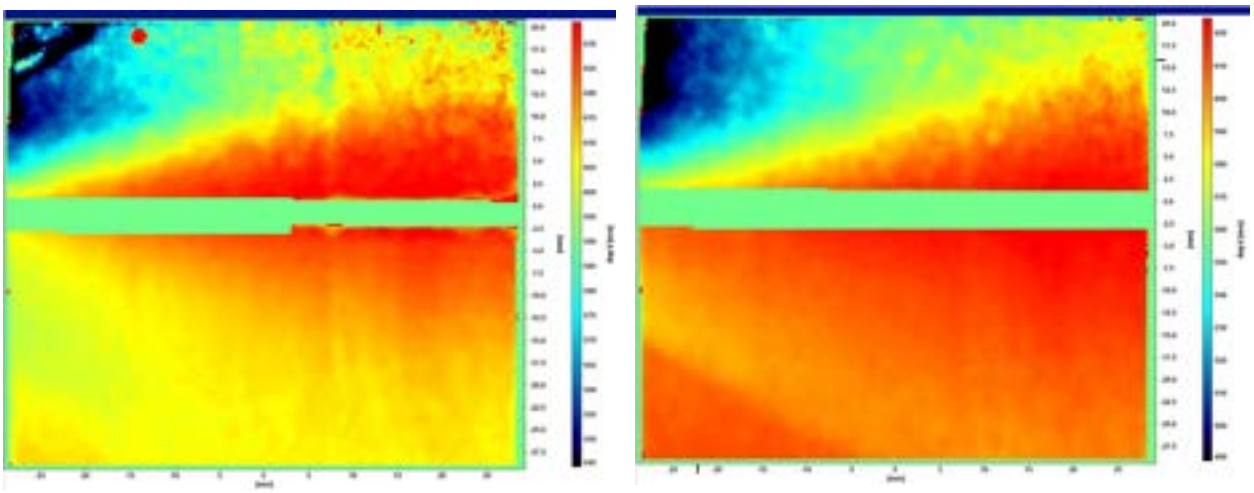

Figure 4: (left) Baseline shear layer; (right) shear layer influenced by pin array of height of 0.5 boundary layer thickness and 0.75 boundary thickness spacing.

made to observe changes in the pressure signal downstream of where the shear layer impinges upon the floor. An example of the SPIV measurements is shown in Figure 4; the floor of the step is towards the top of the images, whereas the edge of the step is towards the lefthand side. These images were obtained about an inch from the leading edge, representing the average of 500 images each. Surface reflections had to be removed along an edge in the middle of each image, yet both the shear layer and an expansion fan are evident in both. The presence of the pins gives rise to a steady shock that is seen in the lower lefthand corner of the right subfigure. These data, which are color contours of total velocity, have been obtained for 10 cases (baseline included) and are currently being processed.

Future Work

We intend to present these results at the 2025 SciTech conference. In addition, Shack-Hartmann measurements are planned for September of this year. To better understand three-dimensionalities induced by the presence of pins, we will be reorienting the laser sheet to run parallel to the streamwise and spanwise directions, to perform two-component PIV to measure downstream of the pin arrays. Finally, Kulite data are currently being analyzed to observe the pressure signals within the flowfield.

Active Flow Control of a Complex 3D Supersonic Multi-Stream Nozzle Flow

Mark Glauser (Syracuse University), Yiyang Sun (SU), Fernando Zigunov(SU)
and Datta Gaitonde (The Ohio State University)

Background and Motivation

The complex unsteady features associated with high Reynolds number three-dimensional (3-D) turbulent flows exert substantial influence on the design and operation of current and anticipated air vehicles. Active flow control offers a method to optimize performance over a wide range of operational parameters. To date however, such techniques have been primarily developed and implemented in relatively simple low Reynolds number flows. In this effort, we propose to extend and demonstrate an active flow control strategy on a realistically complex 3-D high Reynolds number turbulent and supersonic nozzle flow with the *primary goals of; (1) manipulating shock structure, (2) reducing the unsteady loading on the aft deck which mimics aircraft integration and (3) affecting the tonal far field noise.*

Our demonstration platform is distilled from a configuration of intense current interest to the U.S. Air Force, as it seeks new exhaust systems that maximize the efficiency and performance of future aircraft. We consider specifically the rectangular multi-stream Single-sided Expansion Ramp Nozzle (SERN) notionally mounted over a wing (or deck) and containing primary mixed core and fan streams and a third (deck) stream introduced to protect the wing surface. The resulting flowfield contains multiple 3-D interacting free and bounded shear layers undergoing absolute and convective (Kelvin-Helmholtz) instabilities, as well as shock interactions leading to open flow separation and corner flows (Fig. 1a).

A particularly influential phenomenon is the shear layer formed between the core and deck streams. This layer evolves and subsequently interacts with the deck boundary layer resulting in complex preferential vorticity interactions that affect merging and sub-harmonic generation. The net consequence is the genesis of large coherent structures and significant tonal content with a strong influence on the primary flow features in the entire configuration. This flowfield constitutes a much-needed next level of generalization for the study of active flow control, because of the compounded interactions of non-linear phenomena that appear pervasively in numerous applications and usually degrade the effectiveness; in this case, of the deck stream in providing a thermal and acoustic barrier protecting the wing surface.

Objectives

The objectives of this project are to use our advanced set of highly integrated experimental, computational, and analytical methods to develop, implement and demonstrate an active flow control technique (Fig. 1c). For this purpose, we combine high-resolution diagnostics, 3D linear perturbation techniques (input-output theory) and high-fidelity LES. Specifically, we use these approaches synergistically, in conjunction with reduced order models and advanced data analytics, to efficiently explore a broad actuator parameter space which delivers open and closed-loop control strategies using steady and unsteady blowing. In addition to specific configurations, the proposed effort will showcase an experiment-computation-theory paradigm (Figure 1) to overcome the challenges associated with the application of active flow control at high Reynolds number in flowfields of far greater complexity than previously attempted.

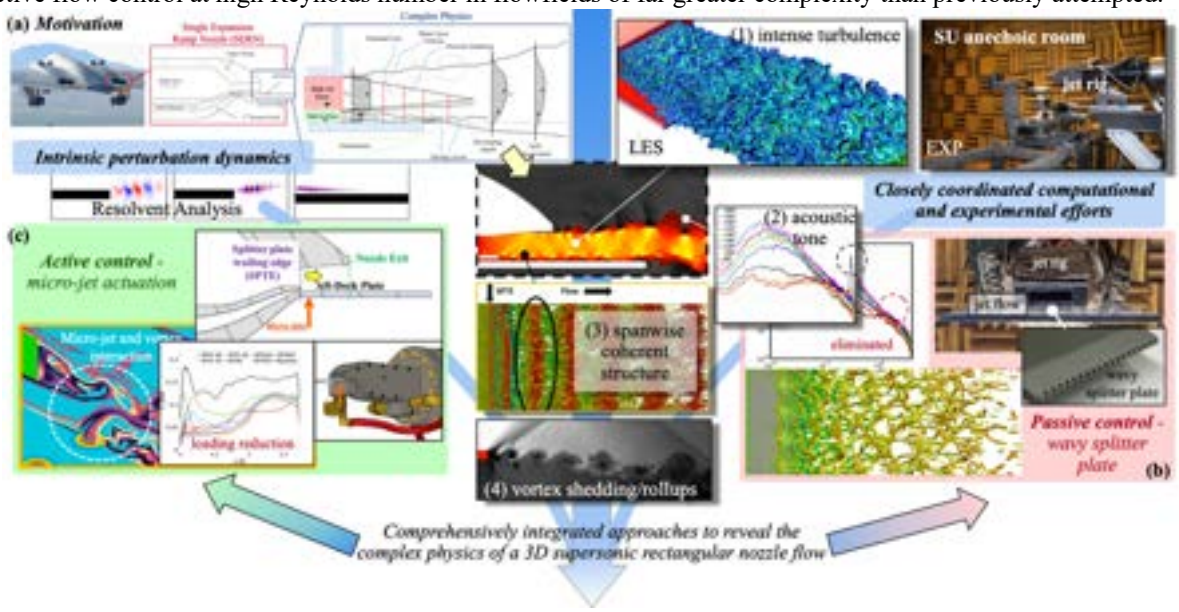

Figure 1 Strategy of integrating theoretical, computational, and experimental efforts to investigate the complex 3-D multi-stream nozzle flow physics and control mechanisms to reduce the adverse effects of large-scale and tonal flow unsteadiness.

Result Summary: ***Active Flow Control*** **(**2023-2024 Progress)

- *Microjet actuation experiments.*

An active flow control experimental campaign was performed with steady blowing through microjets at the splitter plate trailing edge (SPTE). This strategy completely eliminates the shedding tone in the far field as measured by microphones and time-resolved shadowgraph, without affecting the remaining bands of the spectrum (Figure 2). More surprisingly, however, is that active blowing is not even required, as the geometry with jets off also eliminates the shedding tone. After a deep investigation comprising 26 different SPTE geometries tested, it was established that the "passive-fluidic-actuation" strategy leveraged is a boundary-layer bleed that occurred due to a mechanical gap between two parts in our new experimental setup. The direction of the bleed has not yet been established. This newfound strategy requires no energy input and is a completely novel "passive-fluidic-actuation" strategy. Further experiments and analysis are ongoing to further understand the fluidic actuation mechanism using the available state-of-the-art diagnostics in the facility, including shadowgraphs of the interior of the nozzle as seen in Figure 2.

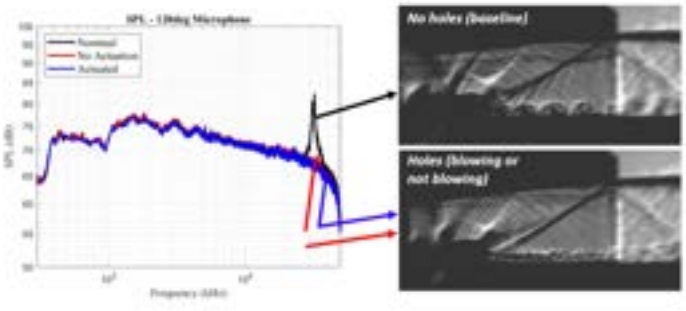

Figure 2 – Spectrum of far-field noise and corresponding shadowgraphs inside the nozzle showing the elimination of coherent structures.

- *Microjet actuation simulations.*

LES were used to analyze different blowing arrangements including those used in experiments, as well as other locations to explore the sensitivity of the flow. These 3D simulations considered a spanwise periodic problem for simplicity, since sidewall effects on the targeted shedding phenomena are minor. In addition to active blowing, various characteristic-condition-backed and wall-backed cases were simulated using round and square cross-section ducts. In general, relatively steady blowing yielded superior results, both from the standpoint of reducing the tone, as well as to reduce the strengths of shocks in the system. Ongoing data-driven analysis techniques are guiding a better understanding of the underlying non-linear dynamics. Meanwhile, extensive two-dimensional (2-D) simulations and resolvent analysis are performed to primarily examine the 2-D flow phenomena in response to 2-D actuation control, as shown in Figure 3. Actuation at the splitter plate trailing edge surface most effectively reduced surface loading due to the generation of smaller shedding vortices, which also consequently weakened the strength of the primary shock. We found that the various shear layer instabilities became more responsive to perturbations when blowing was introduced towards the deck plate, while blowing into the core stream stabilized the shear layers. Additionally, blowing at various angles displayed certain control authority over the development of the shock system.

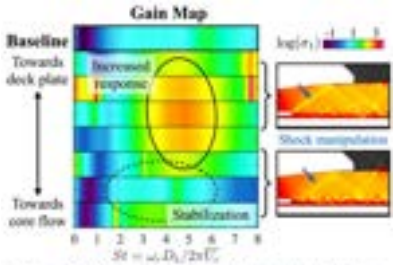

Figure 3 Splitter plate trailing edge actuation and dynamics revealed by resolvent analysis.

- *Input-output dynamics of perturbation.*

To narrow down the parameter space of microjet actuation, we leverage state-space restricted input-output analysis to identify the optimal forcing-response correlation between forcing and response in the flow. All combinations of input and output show higher energy amplification at the resonant frequency. The current results highlight the splitter plate trailing surface as the most receptive region for introducing an actuator that maximizes flow response, as shown in Figure 4. In contrast, forcings from the upper and lower surfaces of the splitter plate primarily generate high-amplitude pressure waves from the input location and are less effective in modulating the shear layer. The theoretical predictions of the input-output analysis are further validated through simulations with applied forcing, which confirm the coherent structures predicted by linear analysis remain active within a nonlinear turbulent shear layer flow.

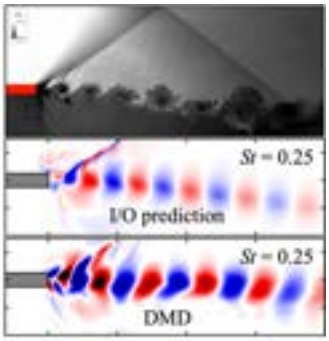

Figure 4 Mode prediction and validation using I/O analysis and DMD.

Future Work

The future experimental campaign will seek to perform targeted diagnostics on the active and "passive-fluidic" flow control cases to understand and establish the dynamics of the interactions observed that culminated in the elimination of the tone with companion simulations. Online data-driven feedback control will be developed as a diagnostic tool to exploit control mechanisms.

Air Force Office of Scientific Research
Unsteady Aerodynamics and Turbulent Flows

AFOSR Grant FA9550-18-1-0225

AERODYNAMICALLY-ADAPTIVE AERO-STRUCTURES USING FLOW-INTERACTIVE CONTROL BY DISTRIBUTED BLEED ACTUATION

Summary of Research Progress Aug 2024

Gabriel Peyredieu Du Charlat and Ari Glezer[1], & Luca De Beni and Massimo Ruzzene[2]
[1]Woodruff School of Mechanical Engineering, Georgia Institute of Technology
[2]Department of Mechanical Engineering, University of Colorado Boulder

Background & Motivation The reciprocal interactions between a wing and the embedding cross flow and therefore the aerodynamic loads are regulated by active distributed air bleed for realizing an adaptive aero-structure having flow-induced tunable aeroelastic characteristics. Bleed actuation is driven through the aerodynamic surfaces by inherent pressure differences in flight (e.g. between and the pressure and suction surfaces) and is controlled by low-power, surface-integrated louvers. The control authority of bleed actuation is derived from modification of the aerodynamic loads by its interactions with the cross flow on the convective time scale over a broad range of angles of attack when the base flow is either fully attached or partially stalled. Control of the apparent aeroelastic characteristics by exploiting the aerodynamic loads can enable reduction of structural vibrations and flutter and ultimately can lead to on-demand wing stiffening and bending-twist coupling for improved maneuverability. The use of distributed aerodynamic bleed for aeroelastic control represents a significant departure from earlier structural control approaches that have relied on direct mechanical deformation or on moving control surfaces with power, weight and response time penalties.

Objectives The present investigations have focused on elucidation of the fundamental mechanisms of coupled spatial and temporal interactions between distributed bleed actuation and the flow over static and dynamic flexible wings with the objective of effecting desired, adaptive aeroelastic characteristics. Detailed wind tunnel investigations using modular 3-D half-span flexible wing models are used to explore the flow structures that lead to regulation of sectional circulation and aerodynamic loads over the wing and their coupling to its near wake. These flow mechanisms are exploited for demonstrating the effectiveness of feedback controlled, bleed-induced aerodynamic loads for suppression of structural vibrations. The effects of the bleed on spanwise distributions of the sectional circulation and aerodynamic loads during vibration control are assessed from time-dependent measurements of the flow evolution in the wing's near-wake using high speed stereo PIV. The link between experimentally-identified bleed-induced aerodynamic loads and aeroelastic properties are analyzed theoretically and numerically using a confluence approach by leveraging reduced order models (ROMs) and developing a properties confluence algorithm (PCA) that incorporate the alteration of the apparent structural properties of the wing (e.g., its stiffness and damping) by the bleed. A central objective of the program is to lay the technical foundation for control of flexible aero-surfaces by regulated bleed actuation.

Results Summary The utility of bleed actuation (shown notionally in Figure 1a) for on-demand time-dependent regulation of the aerodynamic load distributions on the convective time scale of the flow was demonstrated in wind tunnel experiments at Georgia Tech on a 3-D semi-span Clark-Y wing model (s = 60 cm, c = 30 cm). The model is equipped with four spanwise segments of controlled bleed ports (Figures 1b) and the bleed is regulated by low-power, surface-integrated louvers without the need for an auxiliary air supply. The induced variations of the cross-sectional lift are depicted in Figure 1b and show that for a given bleed opening (<6% of planform area) the range of lift variations increases

monotonically with α below stall. Furthermore, for a given angle of attack, the lift can be regulated *bidirectionally* to provide a local increase or decrease within a predetermined operating range. This work also demonstrated that integrated distributed bleed can enable controlled tuning of the *apparent* structural properties of the lifting surfaces and therefore can provide significant aeroelastic control authority as demonstrated for example by the corresponding spanwise increase in distribution of spanwise stiffness. In contrast to other active flow control approaches, bleed actuation is effective even when the base flow is either fully attached or partially/fully-stalled.

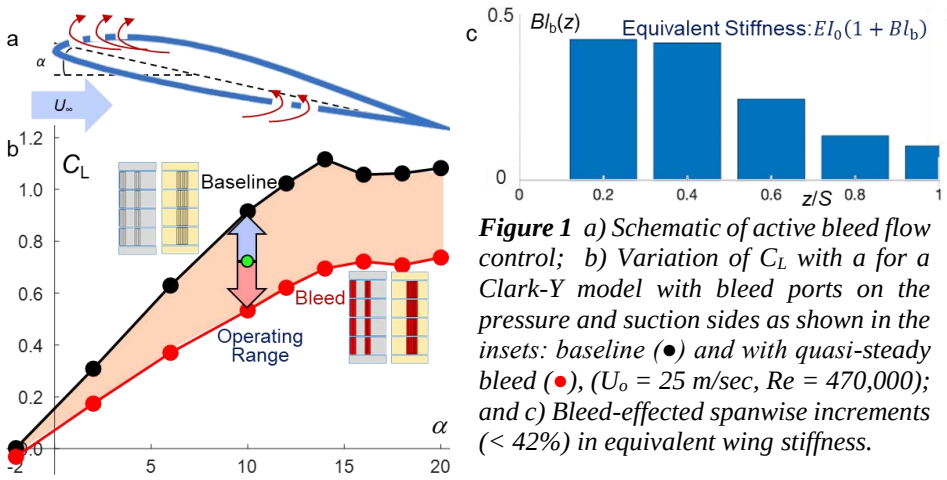

Figure 1 *a) Schematic of active bleed flow control; b) Variation of C_L with a for a Clark-Y model with bleed ports on the pressure and suction sides as shown in the insets: baseline (●) and with quasi-steady bleed (●), (U_o = 25 m/sec, Re = 470,000); and c) Bleed-effected spanwise increments (< 42%) in equivalent wing stiffness.*

The effectiveness of bleed actuation for suppression of induced vibrations of the 3-D semi-span wing model (cf. Figure 1b) was demonstrated in recent wind tunnel experiments. Vibrations of the cantilevered model (amplitude of about 0.2c) were simulated using time periodic variations of the lift by bleed actuation on the outboard segment at 4.5 Hz (τ_n = 0.22 sec) corresponding to the wing's first bending mode in the absence of bleed on the inboard segments. The tip velocity oscillations V_{tip} are monitored using a laser vibrometer (Figure 2a) whose signal is used as the input to an adaptive PD controller that provides the actuation of the bleed louvers in the 3 inboard segments (Figure 3b) and is tuned to provide lift force that would oppose the induced vibrations with an amplitude proportional to the measured tip velocity (the louvers neutral position is set to provide bi-directional control). Control of the vibration is *independent* of the forced oscillations and the controller's objective is to minimize the tip oscillation velocity. The effects of the controller on the tip motion and on the lift at $\alpha = 12^o$ are shown in Figures 3c and d, respectively. The baseline tip oscillations and the corresponding variations in lift are evident for $t/\tau_n < 9$. *When the controller is active ($9 < t/\tau_n < 27$), the RMS fluctuations of the tip velocity and the lift oscillations are reduced by 70% and 32%, respectively. Furthermore, these data show that the reduction or penalty in the time-averaged lift when the controller is active is less than 3% of the uncontrolled lift.*

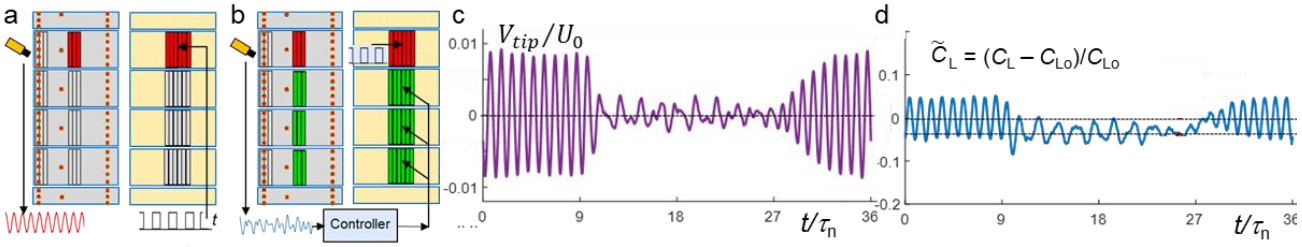

Figure 2 *Vibration control: a) Bleed induced time periodic oscillations near the natural frequency using the wing's outboard segment; b) Adaptive, PD feedback control applied using the tip velocity measured by a vibrometer to activate bleed actuation on the wing's three inboard segments to mitigate the tip-induced vibrations; Normalized time traces (τ_n = 0.22 sec): c) Tip velocity V/U_o (U_o: free stream speed), and c) $\tilde{C}_L$ (C_L and C_{Lo} are lift in the presence and absence of control, respectively).*

The investigations during the past year have focused on the mechanism by which bleed actuation regulates the spanwise distribution of sectional circulation and thereby leads to prescribed variations in lift distributions for structural control of the wing and manoeuvring. To this end, bleed actuation was effected uniformly along the four midchord spanwise segments shown in Figures 2a-b, and the three components of the velocity field were measured using double-plane stereo PIV in the *y-z* (streamwise-normal) plane 0.02*c* downstream of the trailing edge. Color raster plots of distributions of time-averaged spanwise and streamwise vorticity components $\xi_z(y, z)$ and $\xi_x(y, z)$ are shown Figures 3(a, c)

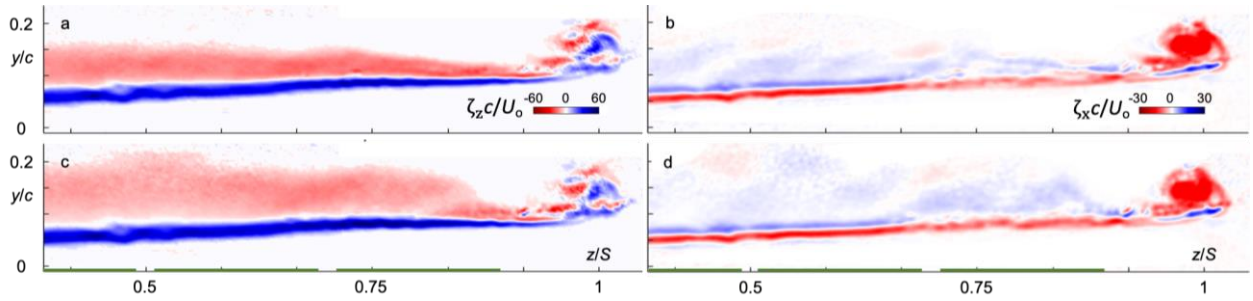

Figure 3 *Color raster plots of time-averaged **CCW** and **CW** vorticity concentrations in the y-z plane 0.02c downstream of the trailing edge: spanwise ξ_z (a, c) and streamwise ξ_x (b, d) in the absence (a, b) and presence (c, d) of midchord bleed actuation (Figure 2). The spanwise extent of the bleed segments of the rigid wing are marked on the x axis.*

and 3(b, d), respectively in the absence (baseline, 3a, b) and presence (3c, d) of bleed actuation. Since the measurements are taken a short distance from the trailing edge the boundary between opposite sense vorticity concentrations is marked by null levels. As shown in Figure 3a, in the absence of bleed, the CCW and CW layers of spanwise vorticity are primarily advected by the streamwise flow while the flow induced by the tip vortex leads to entrainment of spanwise vorticity concentrations of opposite senses from the pressure and suction surfaces that become wrapped about its core and the intensified advection towards the tip leads to thinning of the surface boundary layers. The corresponding concentrations of streamwise vorticity ξ_x in Figure 3b show two distinct layers, namely CCW-ξ_x and CW-ξ_x. The tip vortex that is clearly dominated by CCW-ξ_x and the layers of CCW-ξ_x over the wing surfaces that are associated with opposite-sense spanwise flows (towards the tip and the root over the pressure and suction surfaces) and with streamwise tilting of spanwise vorticity contribute to increase in circulation and lift. However, the tall cross stream layer of CW streamwise vorticity above the suction surface that is apparently engendered by oblique and cross stream shear flows over each surface contributes to a reduction in circulation (note that the spanwise flow induced by the tip vortex over the suction surface effects CW-ξ_x). As shown in Figure 3c, the presence of bleed on the suction surface leads to significant cross stream spreading of the CCW spanwise vorticity layer inboard of the active bleed segment

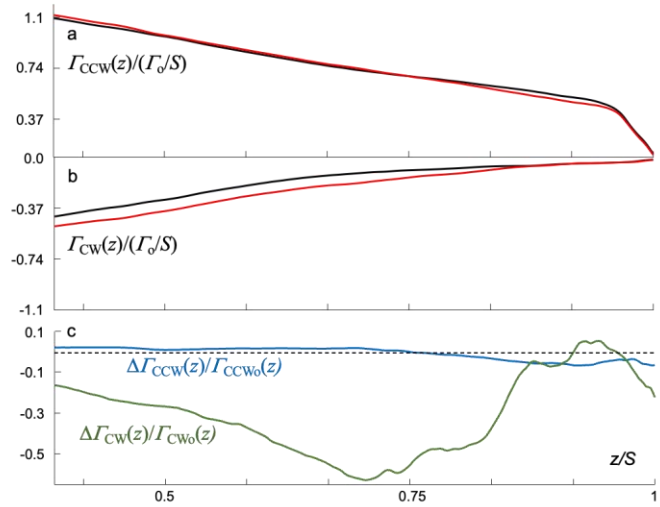

Figure 4 *Spanwise distributions of: (a, b) Sectional circulations of the CCW and CW streamwise vorticity $\Gamma_{CCW}(z)$ (a) and $\Gamma_{CW}(z)$ (b) in the **absence** and **presence** of bleed actuation; and (c) Differences between the circulations in a and b **$\Delta\Gamma_{CCW}(z)$** and **$\Delta\Gamma_{CW}(z)$** each normalized by the corresponding circultion in the absence of bleed $\Gamma_{CCWo}(z)$ and $\Gamma_{CWo}(z)$.*

($z/S < 0.88$) but little or no discernible change in the CW layer or in the tip vortex. This spreading is accompanied by corresponding spreading of the CW streamwise vorticity layer over the suction surface that along with some localized intensifications can lead to increased decrement in sectional circulation and lift distribution. These changes are quantified by spanwise distributions of the sectional circulations of the CCW and CW streamwise vorticity concentrations $\Gamma_{CCW}(z)$ and $\Gamma_{CW}(z)$ in the absence and presence of bleed actuation in Figures 4a and b, respectively where each distribution is normalized by the total wing circulation in the absence of bleed actuation Γ_o. While the magnitudes of $\Gamma_{CCW}(z)$ are nearly unchanged in the absence and presence of actuation, the actuation increases the magnitude of $\Gamma_{CW}(z)$ as a result of the changes in the cross-stream distribution of CW-ξ_x in Figure 3d, and consequently results in a prescribed decrement in lift. Figure 4c shows the spanwise variations of fractional differences between the sectional circulations in Figures 4a and b $\Delta\Gamma_{CCW}(z)$ and $\Delta\Gamma_{CW}(z)$ each normalized by the corresponding sectional circulation in the absence of bleed $\Gamma_{CCWo}(z)$ and $\Delta\Gamma_{CWo}(z)$. These results show that bleed actuation can modify the streamwise vorticity over the wing and thereby regulate the spanwise distributions of sectional circulation (by over 60%) and aerodynamic loads for prescribed apparent structural and aeroelastic characteristics.

It is anticipated that the utility of bleed actuation for harnessing unsteady aerodynamic loads to effect desired structural dynamic characteristics will enable support of control strategies for gust response alleviation and flutter.

Numerical Investigation of Freestream Turbulence Effect on Endwall Flow in Low-Pressure Turbine Passage

Andreas Gross, New Mexico State University, Las Cruces, NM 88003

Air Force Office of Scientific Research; Grant number: FA9550-22-1-0195
Program manager: Dr. Gregg Abate

Large-eddy simulations of the flow through a low-pressure turbine cascade with front-loaded high-lift blades reveal the effect of freestream turbulence on the pressure and suction surface laminar boundary layers and on the endwall flow structures.

Freestream turbulence (FST) in turbomachinery results from upstream wakes and combustion unsteadiness among others. Low-Reynolds number flows, such as the flow through the low-pressure turbine (LPT) of turbofan engines, are known to be sensitive to FST. The trend in LPT design is towards front-loaded high-lift blades. The blade geometry chosen for the present work is the L2F, which was developed by the Air Force Research Laboratory (AFRL) for investigating the aerodynamics of highly-loaded profiles. The objective of this research is to broaden the understanding of the effect of FST on the laminar boundary layer separation and secondary flow losses in a L2F LPT cascade at a chord Reynolds number of $Re = 50,000$. Such improved understanding supports the design and development of more fuel-efficient jet engines that improve the performance of aircraft. Large-eddy simulations were performed using two different grids (coarse and fine). Here, results obtained with the fine grid for freestream turbulence intensities (FSTI) of 0 and 8% are discussed. The FST was introduced with a Fourier mode-based model that permits the specification of the FSTI, integral turbulence length scale, $L = 0.5C_{ax}$, and turbulence spectrum, $E(k)$ (von Kármán spectrum).

Mean flow visualizations for both cases in Fig. 1 exhibit two distinct vortices: The horseshoe vortex (HV) and the passage vortex (PV). The HV, which originates from the interaction of the endwall boundary layer with the blade root, wraps around the leading edge of the blade. The pressure side leg of the HV develops into the PV. The PV extends from the pressure side to the suction side of the adjacent blade and is fed by the secondary flow.

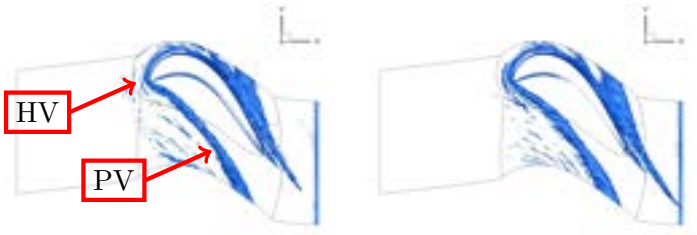

a) b)

Figure 1: Q=20 surfaces a) without and b) with 8% FSTI.

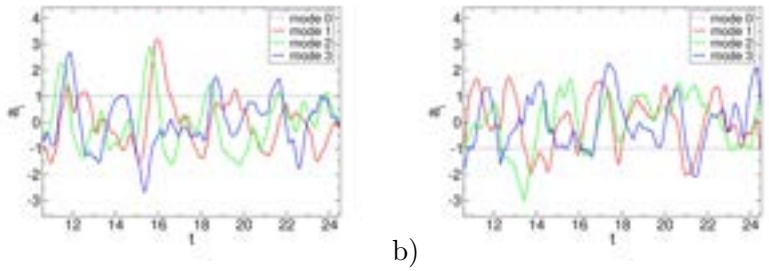

a) b)

Figure 2: Time-coefficients for a) 0% and b) 8% FSTI.

Snapshots of the unsteady flow fields were analyzed with the proper orthogonal decomposition (POD). The POD time-coefficients are plotted in Fig. 2. Modes 1 and 2 for the 0% FSTI case and modes 1-3 for the 8% FSTI case appear related with an approximate phase shift of a quarter period. The modes also share

similar eigenvalue magnitudes which is an indication that the pairs (or triplets) capture traveling waves.

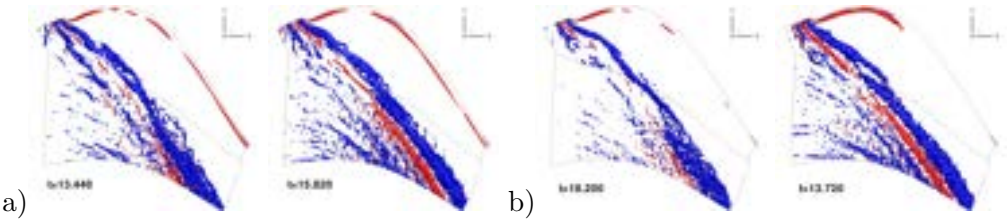

Figure 3: POD reconstructions (Q=100 iso-surfaces colored by ω_x) for a) 0% and b) 8% FSTI.

The flow field was reconstructed from the leading POD modes 0, 1, and 2 (Fig. 3). Intermittently, the PV moves downstream. Whenever that happens, a counter-rotating vortex (marked red in Fig. 3) ahead of the PV gains in strength. The counter-rotating vortex can be traced back to a lift-off or separation of the endwall boundary layer ahead of the PV. The reconstructions in Fig. 3 suggest that these events go hand in hand with a strengthening of the counter-rotating vortex in the junction region. This suggests that the leading edge region unsteadiness affects the PV.

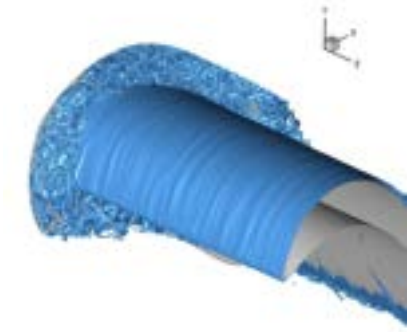

Figure 4: Iso-surfaces of Q=100 for 8% FSTI.

Instantaneous flow visualizations for the case with 8% FSTI display streamwise structures for both the suction and pressure side boundary layer. The suction-side structures (Fig. 4) likely result from FST that is transformed into streamwise aligned vortices at the leading edge. These vortices penetrate into the boundary layer to produce the localized thickening and thinning characteristic of Klebanoff modes.

Contours of the u-velocity (Fig. 5) for the suction (top) and pressure side (bottom) reveal that the suction side structures are entirely missing for the 0% FSTI case. Figure 5 also reveals streamwise structures for the pressure side for the 8% FSTI case. As the pressure side surface is concave, the structures are likely Görtler vortices. The fact that hte Görtler vortices are missing for the 0% case suggests that the disturbance amplification due to centrifugal instability is not strong enough for spanwise disturbances to reach amplitudes high enough for Görtler vortices to be observed.

The results were presented at 3 conferences:

Hoque, M.A., and Gross, A., "Numerical Investigation of Freestream Turbulence Effect on Flow Through Low-Pressure Turbine Cascade," AIAA-2024-4469, https://arc.aiaa.org/doi/10.2514/6.2024-4469

Hoque, M.A., and Gross, A., "Numerical Simulation of Turbulent Boundary Layer with Free Stream Turbulence," AIAA-2023-4336, https://arc.aiaa.org/doi/10.2514/6.2023-4336

Hoque, M.A., and Gross, A., "Large-Eddy Simulation of Turbulent Boundary Layer Flows with Freestream Turbulence," AIAA-2023-72050, https://arc.aiaa.org/doi/10.2514/6.2023-72050

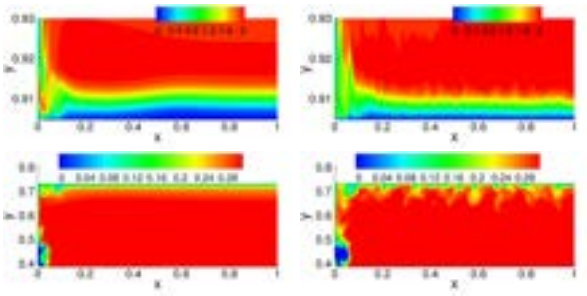

Figure 5: Contours of u-velocity for top (x=0.3839 at wall) and bottom surface (x=0.3686 at wall) for a) 0% and b) 8% FSTI.

Dynamic Response of the Shear Layer to Cavity Door Operation at Supersonic Speeds (FA9550-20-1-0199)

Prof. Rajan Kumar (PI) Prof. Datta V. Gaitonde (PI at OSU)
Mechanical Engineering Mechanical and Aerospace Engineering
Florida State University, rkumar@fsu.edu The Ohio State University, gaitonde.3@osu.edu
In Collaboration with: Ryan Schmit, Rachelle Speth and Scott Sherer, AFRL/RQVI

Motivation: Store separation from internal weapons bays pose significant constraints at high-speeds. When bay doors are neglected, the fundamental phenomena encountered are associated with the shear layer formed between the freestream and the low-speed flow inside the cavity. Major phenomena are associated with various instabilities, including prominently of the Kelvin-Helmholtz type. Depending on the dimensions, specifically ratios of length to width and depth, the flow may remain mostly two-dimensional or may develop substantial three-dimensional structures even in the mean. The overall consequences manifest in highly turbulent flow and an intense aeroacoustic environment in and around the bay. When doors are added, the problem becomes considerably more complex; a sketch of key features is presented in Fig. 1a). However, remarkably few high-fidelity experimental results or trustworthy simulations exist that explore transient dynamics of the shear layer and their connection to, and impact on, the magnitude of pressure fluctuations or resonance characteristics inside the cavity during bay door operation. This motivates the need to study the response of the shear layer (both in time and frequency domain) during the operation of physical doors at a range of freestream supersonic Mach number conditions.

Research Objectives: We obtain a significantly improved understanding of the flow in a more realistic bay operation scenario with moving doors. Specific goals are: i) determine transients associated with bay door operation, shear layer development and the cavity resonance, ii) understand time-dependent onset effects of cavity door operation, iii) acoustic-vortical interactions from pressure waves and influence on the discrete Rossiter model with variable feedback mechanisms.

Summary of Results: A closely integrated experimental-computational effort was conducted (*details in Refs. 1 and 2*) at freestream Mach numbers of 1.6 and 2, with both inner wedge (IW) and outer wedge (OW) doors; the leading-edge shocks are directed into the cavity for the former, and outwards for the latter. Experiments in the FSU polysonic wind tunnel used a pneumatic mechanism capable of opening the doors at relative time-scales much smaller than at full-scale to exaggerate transient effects. In addition to fast-response Kulite pressure transducers at different locations, shadowgraph images and slow-motion videos were recorded at different frame rates.

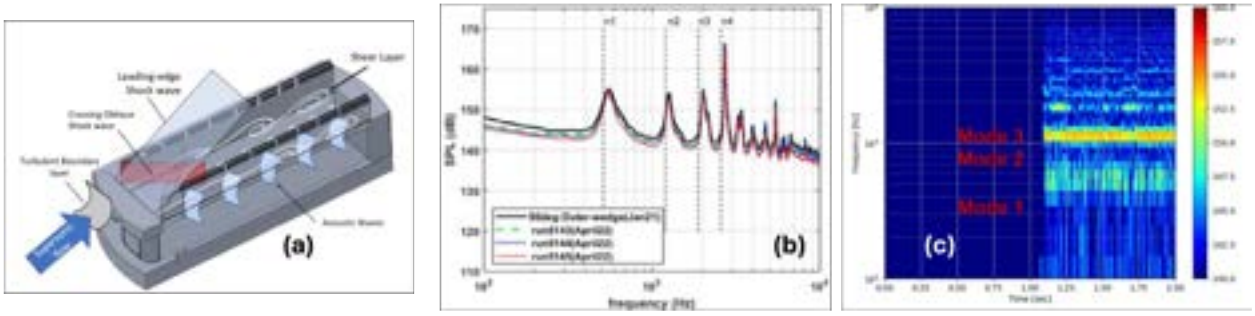

Figure 1: (a) Schematic of flow structures (b) spectral response of outer wedge doors (c) Short-time FFT during door opening

The presence of doors significantly affects the cavity resonance. In all cases, several modes (peaks) are observed; example results are shown in Fig. 1(b) for OW at Mach 2 where the modes are identified by number. When all the results are considered together, the primary effects of doors are observed to be 1) the reduction of broadband levels, 2) mode-shifting to a higher frequency and 3) change in the identity of the most amplified mode. For IW and OW, peaks for modes 1 and 2 are similar, but the amplitudes of other higher frequency modes decrease drastically for IW with a modal shift towards lower frequencies. In terms of dynamic response, the spectra for the rotating doors, regardless of IW or OW, match very well with the static doors case and show repeatability in multiple runs. This suggests that the time-scales associated with door opening are significantly larger than those that establish the flow-acoustic resonance. However, door-opening transients are perceptible. Fig. 1(c) shows modal amplitudes of Short Time Fast Fourier Transform during outward wedge door opening on the cavity rear wall at Mach 1.6. A detailed examination indicates that a pressure pulse is observed during the dynamic door motion before establishment of full cavity resonance. This is accompanied by, and possibly associated, with observed pressure spikes, which may be of practical interest and is thus being explored further.

Simulations were also deployed to explore the primary quasi-static 3D dynamics during the door-opening process. A summary of results from a parametric study indicate that when fully open, the IW doors enforce a degree of spanwise symmetry on the flow inside the cavity; OW doors have relatively smaller effect. In fact, asymmetric behavior in the form of a tornado vortex are obtained under the nominal conditions (first bifurcation). A sample result, shown in Fig. 2(a), indicates the primary (white) recirculation region, and a (red) tornado vortex. Particles from the vortex side travel upstream, bypass and distort the primary recirculation region, and eventually feed the tornado vortex, in which fluid is swirled back up into the shear layer. The back-wall pressure loading is an important indicator of the 3D flow. Beyond a critical angle, another bifurcation arises and three local impingement peaks (as opposed to two) are obtained in symmetric fashion, as shown in Figs. 2(b) for OW doors. This also yields a distorted recirculation region and a twin-tornado vortex system (c) for IW doors.

1. Outten et al. "Effect of Dynamic Door Motion on Cavity Acoustics at Supersonic Speeds," Scitech Forum, AIAA Paper 2024-2731, 2024.

2. Baugher et al. "3D Effects of Quasi-Static Door Opening on Supersonic Cavity Flows," Scitech Forum, AIAA Paper 2024-2729, 2024.

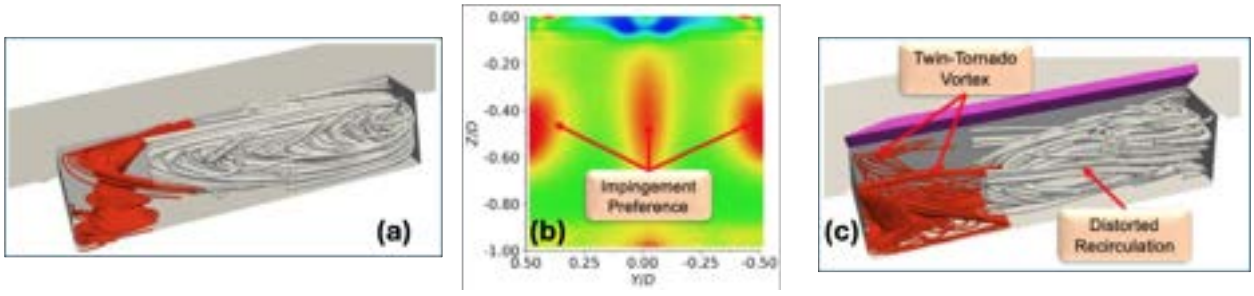

Figure 2: (a) Single tornado vortex (b) Back wall pressure (2nd bifurcation) (c) Twin vortex system

Grant #: FA9550-21-1-0006, University of Notre Dame, PI Dr. Sergey B Leonov (2024 update)

Title: **Rapid (on-Demand) Control of Shock-Dominated Flows by Filamentary Plasma**

Project Objectives. An imperative goal of this work is to mature a plasma-based technique for the effective control of shock-dominated flows. The ***first objective*** of the project is to study the unsteady aerodynamic phenomena realized due to the presence of a near-surface plasma array and its impact on the reflected SW. The ***second objective*** is to study the plasma array's effect on the structure and parameters of shock-dominated, duct-driven airflow, including stabilization of flow unsteadiness.

Current Project state, major results, and upcoming tasks (2024). The 2024 major efforts were related to an active control of unsteady shock train by near-wall electrical discharge. The position of the pseudoshock, a region of increasing pressure that consists of a shock train and a primarily subsonic mixing region, is a function of upstream boundary layer characteristics such as Reynolds number, Re_θ, the confinement ratio, the Mach number, and the downstream pressure. A variety of methods has been used to manipulate these parameters in order to control the pseudoshock position and structure, such as gas injection, BL suction, and vortex generators. Their response times can be orders of magnitude greater than the relevant gas-dynamic time scales. Electrical gas discharges, on the other hand, offer nearly instantaneous response due to their inertia-free action. In this work, three near-wall Q-DC plasma filaments are generated upstream of the shock train leading edge (STLE) in a throttled supersonic diffuser, reducing the pseudoshock pressure gradient and improving overall pressure recovery. The experiments were conducted in the SBR-50 supersonic blowdown wind tunnel facility at the University of Notre Dame. Tests were run at Mach 2 with stagnation quantities of $T_0 = 300 - 600$ K and $P_0 = 1.6 - 3.2$ bar. A diffuser section begins 704 mm downstream of the nozzle exit, which has adjustable wedge faces on the top and bottom walls that can be

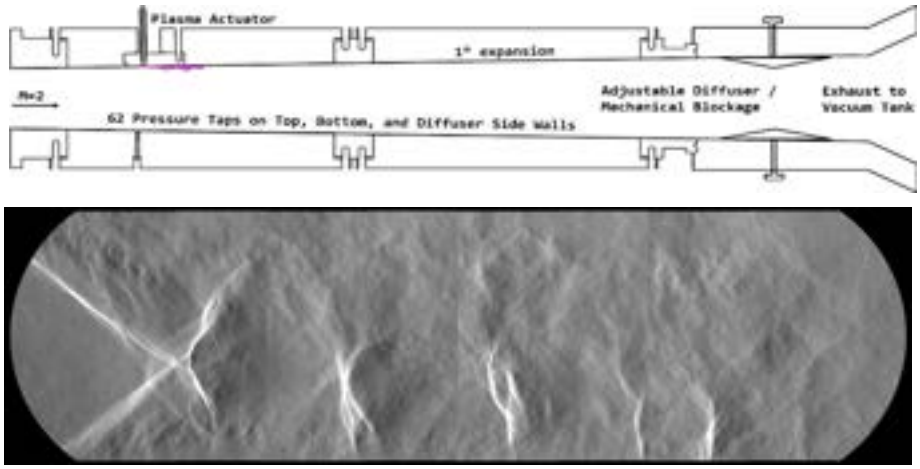

Test duct schematics and Mach 2 shock train captured by SAFS.

set in order to vary the STLE position from run to run. A schematic of the test section is provided in Figure. Instrumentation included a Self-Aligned Focused Schlieren System (SAFS), fast cameras and set of fast pressure transducers.

The presence of plasma modified the flow field, bringing the upper leg of the STLE upstream toward the electrode location. This pattern was observed for the entire 100 ms duration of the plasma actuation. The flow structure is restored after the plasma turned off. Wall pressure distributions for the run with a diffuser angle of $\alpha = 7.75^\circ$ are presented in the graph below.

The graph shows the average pressure distribution prior to plasma actuation and after plasma on over wall in the test section. The uncontrolled shock structure was relatively symmetric as the top and bottom walls. The STLE position for the uncontrolled flowpath was at a nondimensional streamwise distance from the nozzle exit plane of $x/h \approx 3.5$ (h= duct height). Plasma actuation resulted in the upstream repositioning of

the pseudoshock with the top (plasma) wall leg of the STLE being anchored to the electrode location $x/h \approx 1.5$ and the bottom wall leg of the STLE moving a lesser distance upstream to $x/h \approx 2.25$, as also was proved by observation of the schlieren images. The plasma appeared to reduce the shock angle of the top leg of the STLE, which significantly reduced the pressure gradient over the entire pseudoshock region.

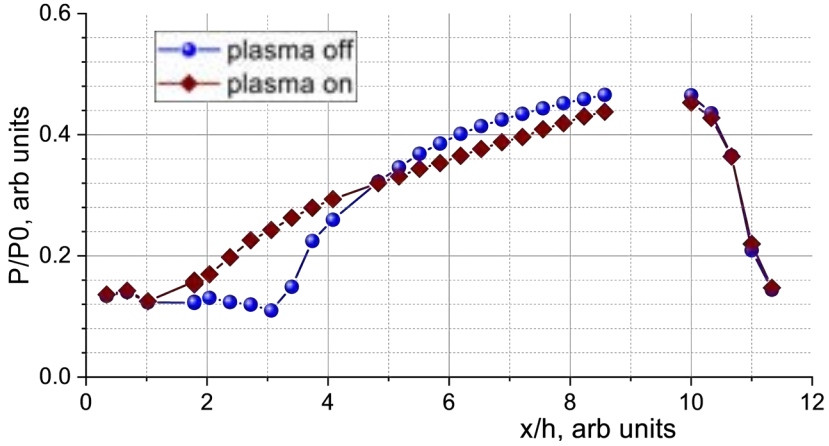

Wall pressure distributions with and without plasma.

For various conditions in M>1 flows, filamentary plasma authority has been well demonstrated. A hot plasma filament produces an extended zone of gas expansion leading to a conical SW production. With multifilamentary plasma arrays, individual SWs interfere with each other, resulting in almost planar plasma-induced SW, which is equivalent to shifting the entire shock train upstream. The physical mechanism of the plasma effect is essentially thermal: with a high local gas temperature, the plasma zone presents an array of longitudinal subsonic jets enclosed in a supersonic flow. Gas pressure is significantly redistributed resulting in pressure bump caused by an impinging SW or compression ramp is mitigated and moves upstream until reaching electrode locations. The negative x-gradient of pressure is reduced significantly due to a presence of flow reversal. It is a paradigm-shifting concept to use plasma as an active trigger action for SW position control. In supersonic or hypersonic flows, narrow subsonic channels generated by plasma filaments are opened to allow pressure to drain into an upstream area, creating a significant pressure redistribution despite a small energy deposition relative to the flow total enthalpy.

Further analysis will focus on the dependence of the pressure gradient reduction on the STLE starting (uncontrolled) position as well as the relationship between the plasma power, plasma morphology, pseudoshock position, and pseudoshock structure. The experimentation is planned at SBR-50 facility in UND and RC-19 test facility at AFRL (Dayton).

Publications and presentations related to the project (2024)

S. Leonov, P. Andrews, T. Ombrello, and E. Braun, “Shock Wave Train Control in Supersonic Duct”, Paper AIAA 2024-1653

S. Leonov, P. Andrews, D. Wagner, and J. Poggie, “SWBLI at Near-Surface Stratified Plasma: Comparison of Test Results to CFD Modeling Data”, Paper AIAA 2024-1655

S. Leonov, “Supersonic Flow Control In Ducts And Over Compression Ramps By Q-DC Discharge”, European Drag Reduction and Flow Control Meeting – EDRFCM 2024, September 10th–13th, 2024, Turin, Italy

- Title of Proposal: Physics-informed reinforcement-learning-based multiple-input multiple-output flow control
- PIs: Qiong Liu, Andreas Gross, Fangjun Shu
- Institution/Organization: New Mexico State University

Executive Summary

We are developing reinforcement learning-based closed-loop active flow control strategies for alleviating laminar separation from the suction surface of a wing section with NLF(1)-0115 airfoil. The impact of key parameters such as actuation location, observed states, and reward function on the effectiveness of the control is investigated for a chord Reynolds number of $Re = 5,000$. The control agent is then tested at higher Reynolds numbers, remaining effective at $Re = 10,000$ and $Re = 20,000$. At $Re = 10,000$, the controller increases lift, while at $Re = 20,000$, it reduces both lift and drag resulting in increased aerodynamic efficiency. A proper orthogonal decomposition (POD) suggests that this change can be attributed to a transition of the primary unsteady mode of the uncontrolled flow from a wake mode to a shear layer mode at $Re = 20,000$. The present study offers insights into estimating the effectiveness of reinforcement learning-based control agents at higher Reynolds numbers based solely on their low-Reynolds number performance. It highlights the crucial role played by flow instabilities in reinforcement learning-based active flow control of laminar separation and it establishes a predictive framework for the scalability of such strategies in aerodynamic applications. Ongoing efforts focus on designing reinforcement learning-based control for a 2.5D airfoil flow and examining the underlying control mechanism both numerically and experimentally.

Introduction

Closed-loop flow control, also known as feedback control, adjusts the control input by detecting changes from sensors. The merits of closed-loop flow control—minimal energy cost and control under off-design conditions—have been demonstrated in both simulations and experiments. However, designing a robust closed-loop control agent that can effectively and efficiently manipulate the flow toward the desired target is challenging. An increasing demand for intelligent airplanes with high performance and adaptability to environmental changes makes closed-loop flow control indispensable choice. The development of closed-loop flow control is aided by ever-increasing computational power and temporal and spatial resolution of sensors and actuators. The majority of existing closed-loop controllers are based on linear theory and limited with regard to performance and computational complexity. Therefore, there is a need for nonlinear controllers for closed-loop active flow control. Neural network techniques have been described as "exceptionally well-suited" for learning nonlinear systems. Reinforcement learning, an important application of neural networks, is widely exploited in various research areas. Here, we attempt to introduce reinforcement learning-based closed-loop flow control to enhance aerodynamic performance over a wide range of on-design and off-design flow conditions. The research is multi-tiered and includes wind tunnel experiments, simulations, and theory.

To ensure the smooth progress of the project, we conducted the following research in the first six months:

1) Integrate a Python-based reinforcement learning algorithm in a CFD environment, specifically the Nek5000 CFD solver.
2) Test the synergistic framework for the closed-loop flow control over 2D airfoil flow at $Re = 5,000$, 10,000, and 20,000, and angles of attack (AoA) of 5° and 10°.
3) Examine the dependence of the reinforcement learning control effectiveness on the open parameters—actuation locations, observed states, and reward function.
4) Vary the Reynolds number to test the robustness of the control and understand the relevant flow physics.
5) Design and build an instrumented wing section for wind tunnel experiments.
6) Instruments, sensors and actuators for the experimental study are currently being tested.

Progress and Achievements

Figure 1 shows the aerodynamic performance for different control setups. The conclusions drawn are that the control actuation locations and observed states have a significant effect on the control effectiveness, while the reward function with a drag penalty has a minor effect. The controller was tested at $Re = 10,000$ and 20,000. Figure 2 shows uncontrolled dominant POD modes and the time history of lift and drag for the tested control cases. The lift coefficient shows a significant increase from 0.31 to 0.574, marking an 85% enhancement with control. Simultaneously, the drag coefficient exhibits a marginal increase from 0.073 to 0.074 or 1.4%. These results demonstrate that the optimal control agent, initially trained at a lower Reynolds number of $Re = 5,000$, effectively enhances performance at $Re = 10,000$. At $Re = 20,000$, the data indicate a moderate decrease in lift and a concurrent strong drag reduction with control. Thus, the aerodynamic efficiency is increased, although the controller fails to increase the lift which was the primary control

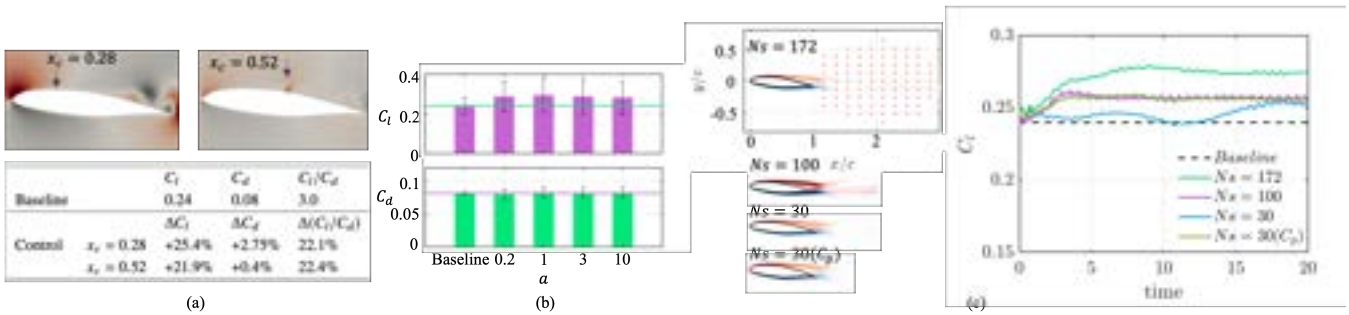

		C_l	C_d	C_l/C_d
Baseline		0.24	0.08	3.0
		ΔC_l	ΔC_d	$\Delta(C_l/C_d)$
Control	$x_c = 0.28$	+25.4%	+2.75%	22.1%
	$x_c = 0.52$	+21.9%	+0.4%	22.4%

Figure 1 The controlled lift coefficient C_l and drag coefficient C_d over (a) different actuation locations, (b) different reward functions $r = C_l - aC_d$ and (c) different observed states.

Figure 3 From left to right: molds for making wing skin; wing skin made from composite material; assembling wing skeleton; wing section before gluing the suction surface; test of DBD actuator and test of microphone pressure sensor.

objective.

This observed trend can be explained as follows: For $Re = 5,000$ and 10,000, the controller reattaches the suction side boundary layer, leading to a significant increase in lift and a reduction in pressure drag. For $Re = 20,000$, the suction side boundary layer is already reattached for the uncontrolled flow, as seen in Figure 2, and the controller mainly reduces the pressure drag. Figure 3 shows the progress for the design and fabrication of the instrumented wing section and tests of the dielectric barrier discharge (DBD) actuator as well as the microphone sensor for detecting pressure fluctuations.

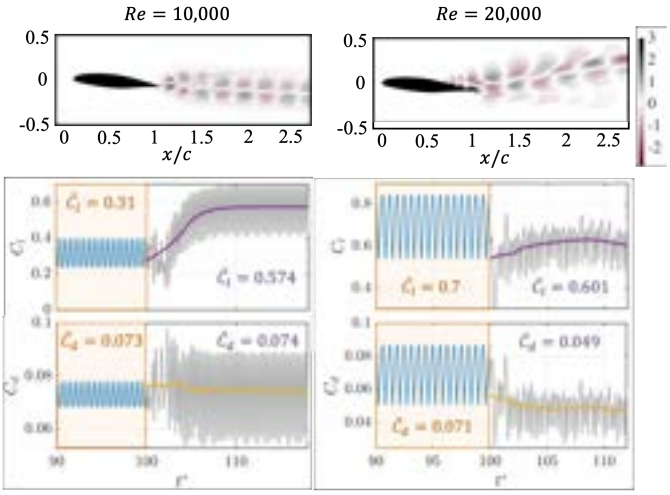

Figure 2 Uncontrolled dominant POD modes shown in u component; time history of the lift and drag for the controlled cases at $Re = 10,000$ and 20,000.

Conclusions and Future Work

We have numerically integrated and tested a reinforcement learning-based closed-loop control for a laminar airfoil flow. The controlled open parameters were optimized and the robustness of the control was tested to an increase of the Reynolds number. As for the experimental work, we designed and built an instrumented wing section; pressure sensors and DBD actuator are currently being tested.

The ongoing work focuses on:

- Extending the approach to 2.5D wing sections which necessitates additional learning parameters such as the spanwise wavenumber for the actuator;
- Comparing the optimal actuator profile from reinforcement learning (RL) with the forcing and response profiles from resolvent analysis;
- Examining the control resilience and the underlying control mechanisms.
- Characterizing and validating the wing section from wind tunnel experiments; implementing control actuators.

Publication

L. J. Trujillo, A. Gross, and Q. Liu. "Active Airfoil Flow Control Based on Reinforcement Learning." AIAA Aviation Paper, July 2024.

DEPSCoR Grant Interim Report Summary

Aditya Nair, Floris van Breugel
University of Nevada Reno

July 21, 2024

1 Project Overview

The DEPSCoR project aims to develop advanced methodologies for predicting and controlling aeroelastic flutter in airplane wings. Traditional approaches often involve complex calculations that are impractical for real-time application, especially in scenarios involving high Reynolds numbers.

2 Accomplishments

2.1 Simulation Platforms

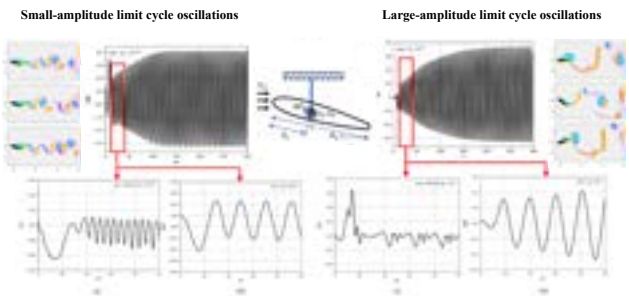

2D Low Reynolds Number Flutter Simulations: Our team conducted simulations at a low Reynolds number (Re = 1000) over a NACA0012 airfoil using the immersed boundary projection solver. The simulations focused on a low equilibrium angle of attack and were validated against the results obtained by Menon and Mittal, showing excellent agreement. The study revealed that the airfoil remains stable at a gust angle of 24.5°, while a critical gust angle above this threshold induces flutter. The difference in limit-cycle oscillation amplitude between stable and flutter conditions was significant, highlighting the sensitivity of flutter onset to changes in flow conditions.

2D Transitional Reynolds Number Flutter Simulations: For flows at a transitional Reynolds number (Re = 88,000), we utilized an overset mesh in the OpenFOAM framework. This approach allowed us to manage large gradients and reduce computational errors at mesh interfaces. The simulations demonstrated large-amplitude pitch oscillations, with the airfoil exhibiting alternate flow separation. The findings were validated against experimental data from Goyaniuk et al., confirming the accuracy of our numerical setup.

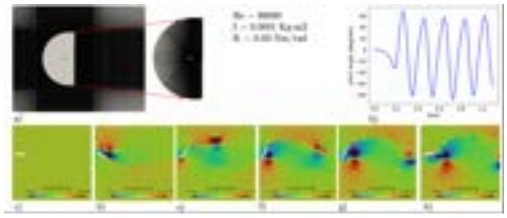

3D Moderate Reynolds Number Flutter Simulations: Initial 3D simulations were performed using CharLES software, leveraging its GPU-based solvers for enhanced computational efficiency. The simulations focused on low-Mach and moving solver frameworks, crucial for studying solid body rotations. The setup process included surface preparation, part meshing, and motion

specification. Future work will involve applying the Force Moment Partitioning Method (FMPM) to analyze the contributions of various forces to flutter instabilities.

2.2 Experimental Platforms

Our experimental setup includes a multi-fan-array wind tunnel designed to simulate natural unsteady flow conditions. The tunnel features a splitter plate that divides the flow into steady and unsteady regions, allowing for the study of complex aerodynamic interactions. We utilized a smoke-generating wick to visualize the plume dynamics under different flow conditions. The experimental data, supported by CFD simulations, provided valuable insights into vortex dynamics and their impact on wing deformation.

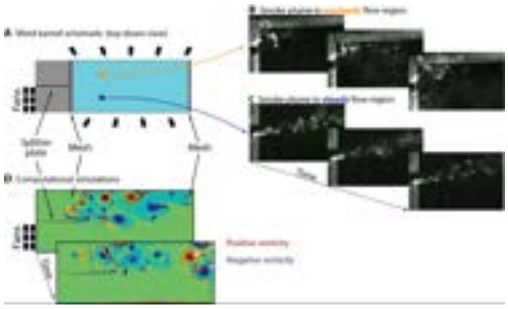

2.3 Methodological Advances

Cluster-Based Autoencoders: To address the limitations of Variational Autoencoders (VAEs), particularly the lack of interpretability in latent space representations, we introduced a physics-informed regularization technique. This method involves clustering the physical state space and aligning latent representations with observable states. By incorporating centroid alignment, we improved the smoothness and physical relevance of latent trajectories, which is crucial for understanding the underlying dynamics of aeroelastic systems.

Cluster Regression Model for Control of Nonlinear Dynamics: Our new approach blends centroid-based unsupervised clustering with sparse regression, enhancing the control of nonlinear dynamical systems. The model effectively captures a wide range of dynamics, including periodic and chaotic behaviors. A notable feature of this method is the "hopping" technique, which manages transitions between different dynamic states, preventing unwanted behaviors such as lobe switching in the Lorenz system. This technique also accelerates vortex shedding in fluid-structure interaction systems while maintaining stable aerodynamic characteristics.

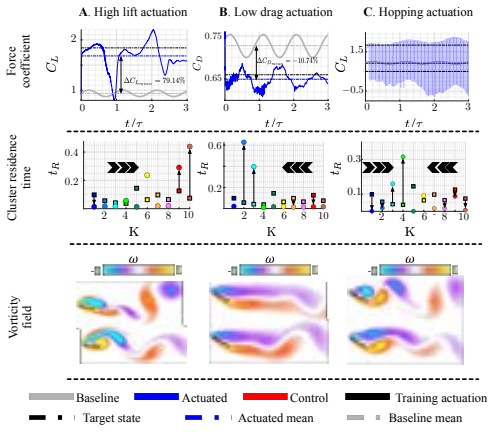

Ongoing Work and Future Directions: We are currently extending our cluster-based autoencoder and cluster regression methodology to include empirical state observability, phase-based and cluster-based controllers. These advancements aim to provide real-time control solutions for flutter suppression. Additionally, we plan to refine our experimental setup to better replicate real-world aerodynamic conditions. This will involve more complex wind tunnel configurations and the integration of advanced data-driven models. Our future work will focus on developing a comprehensive understanding of flutter phenomena, enabling the design of more effective control strategies for aircraft safety.

High-Angle-of-Attack Translating and Pitching Wings Interacting with Finite Obstacles

Grant FA9550-23-1-0170, Program Officer: Dr. Gregg Abate

PI: Dr. Matthew Ringuette, Dept. of Mechanical & Aerospace Engineering, University at Buffalo

Motivation and Background

This research aims to understand the unsteady forces and flow interactions of high-angle-of-attack wings moving past finite-sized obstacles. It applies to agile uninhabited air vehicles (UAVs) maneuvering in complex environments, e.g., urban, indoor spaces, and caves, to enhance the Air Force's ability to obtain local, real-time information. Three obstacle types are studied: channels mimicking air ducts, ceilings, and grounds (Fig. 1). Maneuvers may make the angle of attack, α, or effective angle, α_{eff}, high, separating the flow with leading- and trailing-edge vortices (LEVs, TEVs) and unsteady forces; an α range and pitching will be tested.

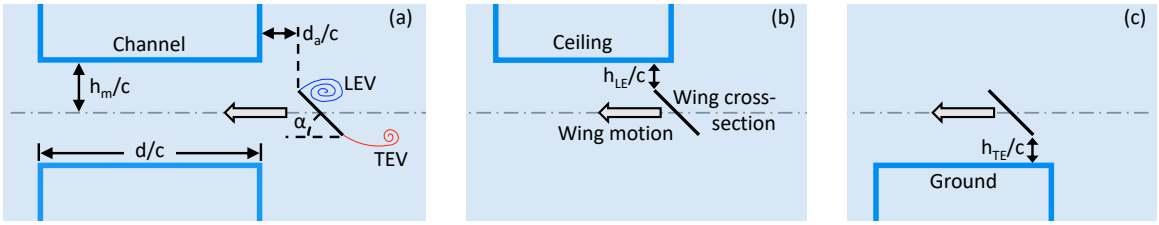

Fig. 1 Schematic of wing/obstacle interaction configurations and parameters.

Prior high-α wing research focused on large/infinite boundaries. In ground effect (GE), blockage below the wing redirects flow over the LE for larger separation, but the pressure rise (ram effect) below dominates. Near ceilings, lift increases for flapping wings, and fixed-wing channel tests found enhanced lift and vortex shedding from flow blockage. A few flapping-wing, finite-obstacle studies showed complex results from the kinematics, and fixed-wing GE work covered wavey grounds but low α. The uniqueness here is simplified motions to understand the flow and forces of a wing encountering a finite obstacle, informing modeling and control.

Objectives

The objectives are: 1) identify how obstacles affect the wing forces for key parameters; 2) understand the unsteady aerodynamics (LEV/TEV behavior, α_{eff}) causing force changes; 3) determine how the forces and flow *scale* (strength and time) with the parameters; 4) characterize wing-pitching effects.

Highlights from Results

The approach is scaled experiments, towing a flat-plate wing in a water tank at Reynolds number 6,000. To simplify the flow to 2D-like large-scale vortices, the aspect-ratio 4 wing's lower end has a $\leq 2\%c$ gap to the bottom (c is chord) to help suppress the tip vortex (Fig. 2). Lift is measured with a transducer, and 2D particle image velocimetry (PIV) captures a flow cross section. Repeated runs with 8 overlapping camera positions cover the full interaction (Fig. 3).

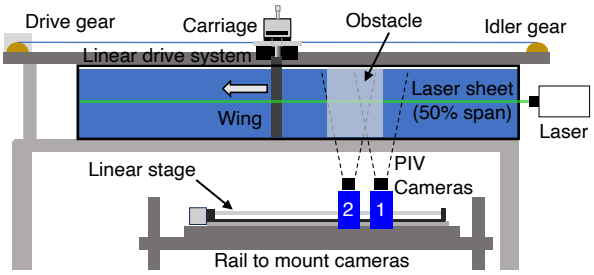

Fig. 2 Towing tank and PIV setup schematic.

Figure 4(a) shows the C_L (lift coeff.) for $\alpha = 45°$ and the narrowest $2c$-gap channels, versus NO (no obstacle), for channel lengths d/c = 4, 6, and 10 starting at s/c = 1 chord traveled. **The C_L rises ahead of the channel from blockage, giving an early warning. Inside it, the C_L peaks from LEV formation are higher and earlier than for NO**: the wing's blockage increases the speed around it, raising its front stagnation pressure and enhancing the LEV and TEV. **The exiting C_L depends on LEV timing.** For $d/c = 4$ the wing exits with a large, intense, attached 2nd LEV (Fig. 5b) and C_L peak (Fig. 5a). This LEV 2 flow forms an opposite ceiling-corner vortex and

Fig. 3 Full PIV vorticity field.

induces an enhanced TEV 3 (Fig. 4c)—both break up LEV 2 and C_L drops. The persistent TEV 3 and exit blockage relief weaken LEV 3 (Fig. 4d), giving the lowest 3rd C_L peak. Instead for $d/c = 6$ (Fig. 3), the wing exits later as LEV 2 sheds, reducing the interactions, trapping TEV 3, for a stronger LEV 3 and 3rd C_L peak.

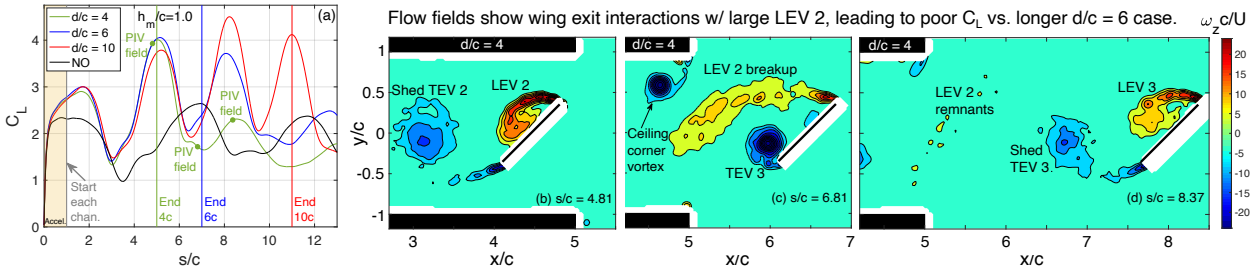

Fig. 4 Channels: (a) C_L; (b)–(d) PIV vorticity fields for $d/c = 4$ (s/c indicated and marked on C_L plot).

Figure 5(a) gives ceiling C_L cases for a small $h_{LE}/c = 0.25$ LE-to-ceiling gap. The LEV 1 is enhanced approaching the ceiling, giving a warning and high 1st C_L peak. Next C_L drops, then has a lower, earlier 2nd peak versus NO. Vorticity for $d/c = 4$ shows that the no-slip ceiling "drags" LEV 1 aft of the wing (Fig. 5b,c), shedding it early, and the flow restriction in the LE gap diverts flow down to enhance TEV 2, causing the the C_L drop. The faster shedding, gap restriction, and stronger TEV 2 lead to an earlier, weaker LEV 2 than NO, and lower 2nd C_L peak. Lastly, opposite ceiling-corner vorticity induced by LEV 2 also weakens it, reducing the C_L faster than for other ceilings (Fig. 5d). **A larger LE gap is helpful, but this proximity yields poorer C_L.**

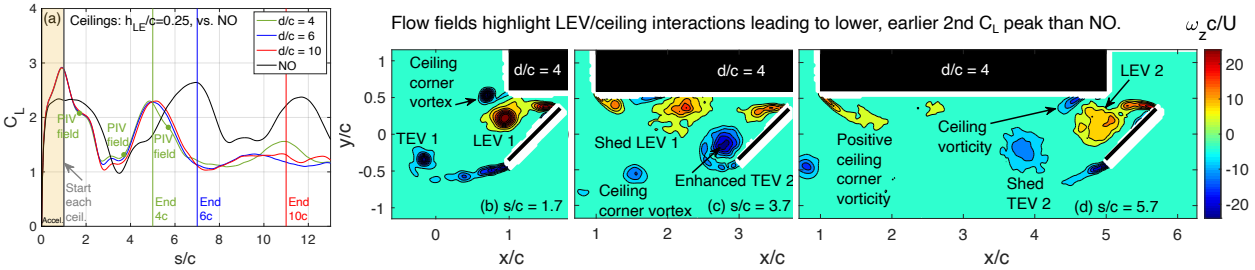

Fig. 5 Ceilings: (a) C_L; (b)–(d) PIV vorticity fields for $d/c = 4$ (s/c indicated and marked on C_L plot).

Ground-effect C_L for a TE ground height $h_{TE}/c = 0.25$ is in Fig. 6(a). **The GE causes a high 1st C_L peak, once the entire wing (including TE) is over the ground.** The LEV 1 strength is similar to the NO, so the C_L rise must be the ram effect: flow restriction below the wing increases the pressure ahead of it. **Later, all 2nd GE peaks are below the NO value.** From the ground restriction, the TEV 2 is larger and closer to the wing than for NO (Fig. 6a,b), ultimately making the GE LEV 2 weaker, which along with the ground ending (Fig. 6d, $d/c = 6$) causes a smaller 2nd GE C_L peak. Before this, the ram effect maintains a higher C_L. **The $d/c = 4$ and 6 GE cases have a C_L loss ahead of the ground ending, giving a warning, likely from relief of the ram effect.**

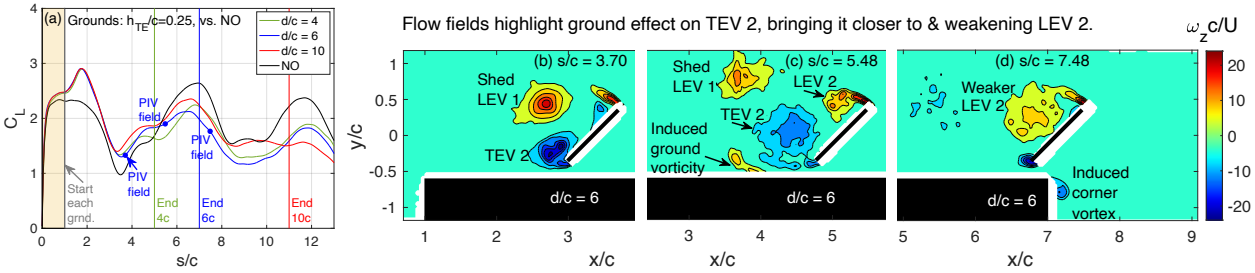

Fig. 6 Grounds: (a) C_L; (b)–(d) PIV vorticity fields for $d/c = 6$ (s/c indicated and marked on C_L plot).

Future Work

Next, vortex circulation (strength) and position will be examined to better understand the C_L trends, also scaling the C_L. A larger facility is in development (right) for longer approaches, to test interactions after the startup flow (SciTech 2025 abstract submitted). Earlier results were published in *AIAA J.*[1] and some of the above (channels) in SciTech 2024[2], with further preparation underway.

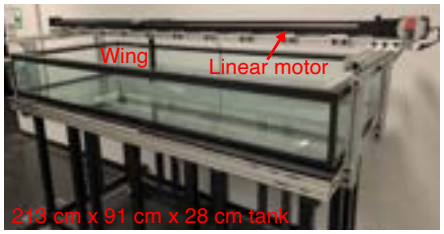

Characterization of Unsteady Flow Physics in the Trailing Edge Region of a Transonic Turbine Cascade

FY 24 Progress Summary

Program:	AFOSR/AFIT MOA Small Grant Program
Technical Period of Performance:	FY 24 – FY 26
Funding:	FY 24: $57,750 FY 25: $53,350 FY 26: $56,430
Principal Investigator:	Dr. James L. Rutledge Department of Aeronautics and Astronautics (ENY) Air Force Institute of Technology 2950 Hobson Way Wright-Patterson AFB OH 45433 (937) 656-6090 James.Rutledge@afit.edu

Distribution Statement B. Distribution authorized to U.S. Government agencies only (P&I, 14 June 2024). Other requests for this document must be referred to AFIT/ENY.

Introduction

Traditional analyses of flows in turbomachinery treat the flow as though it is steady. While this is a reasonable low order approximation, higher fidelity predictions that account for flow unsteadiness are necessary for improved predictions of turbine behavior. This includes the behavior of coolant emanating from a turbine airfoil and periodically impacting on downstream turbine airfoils. This so-called phantom cooling is expected to be increasingly important for advanced airbreathing propulsion concepts. In this project, we are examining flow unsteadiness in a transonic turbine cascade with emphasis on how wakes interact both aerodynamically and thermally with downstream turbine components. There are two thrusts to this study being performed simultaneously. In one, we are using a low speed wind tunnel to examine the way the coolant expelled from an upstream airfoil interacts with a downstream airfoil. This phantom cooling effect is being studied with an emphasis on developing analytical predictive techniques. In the other thrust, we are preparing to perform high speed schlieren visualization of the wake emanating from the trailing edge of turbine blades in a transonic cascade to understand the realistic flow behavior that among other things, governs the behavior of phantom cooling migration.

Dr. Rutledge with his colleagues Dr. Andy Lethander and Ms. Natalia Posada are directing this project. One AFIT graduate student (2d Lt Nathaniel Stout) and four undergraduate level summer research assistants (one Air Force ROTC cadet from Purdue University, two cadets from the US Air Force Academy, and one civilian student from the University of Cincinnati) have been contributing to the project. Additionally, Dr. Molly Donovan and 1st Lt Bailey Hopkins of AFRL are supporting the work. We are further anticipating the matriculation of two additional AFIT graduate students this fall (one Ph.D. student and one M.S. student- both US Air Force officers) that intend to pursue aspects of the project. We are excited about the progress we have made in advancing this research while performing an important educational mission that is giving Air Force officers and future officers experience with laboratory and analytical techniques relevant to unsteady fluid dynamics and aerothermodynamics.

Unsteady Superposition of Phantom Cooling on Downstream Airfoils

Little research has been conducted to characterize phantom cooling, especially in terms of its inherently unsteady nature nor the temperature reduction that it can cause on a downstream airfoil. Instead, most research has focused only on the reduction in adiabatic wall temperature from steady phantom cooling. In addition to addressing both of those shortcomings, we are addressing the issue of predicting the combined effects of phantom cooling with the cooling inherent to the airfoil upon which the phantom cooling acts. In an article recently accepted to the *Journal of Turbomachinery* we developed the first superposition technique for overall cooling effectiveness shown in Eq. (1) for the special case of matched coolant temperatures.

$$\phi_{Super} = \frac{\phi_1 + \phi_2 - 2\phi_1\phi_2}{1 - \phi_1\phi_2} \qquad (1)$$

Further we demonstrated the first successful superposition of overall cooling effectiveness from two different cooling sources and the technique has already been applied by another research group at the University of Texas at Austin. While our overall effectiveness superposition work was performed on a film cooled flat plate, we have recently extended this to a leading edge geometry and presented this work at ASME Turbo Expo. The favorable results suggest we will be able to superpose phantom cooling with leading edge cooling, yielding a powerful new predictive tool for designing cooling schemes. As we proceed with developing the capability to test the technique in this way, we have completed fabrication of a new phantom cooling rig in our low speed wind tunnel. The gray symmetric airfoil seen in Fig. 1 is plumbed to provide trailing edge coolant ejection that will impinge upon the black leading edge film cooling model just downstream

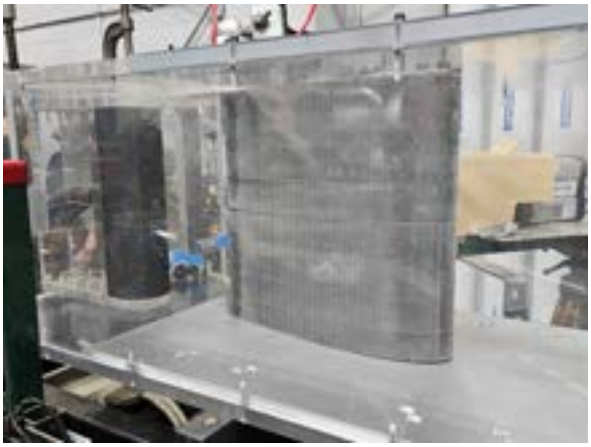

Fig. 1 Phantom cooling airfoil installed upstream of leading edge model with showerhead film cooling

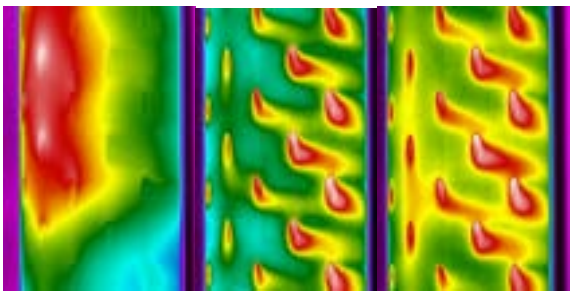

Fig. 2 Unprocessed infrared imagery of leading edge undergoing phantom cooling alone (left), showerhead cooling alone (center), and combined phantom/showerhead cooling (right)

Distribution Statement B. Distribution authorized to U.S. Government agencies only (P&I, 14 June 2024). Other requests for this document must be referred to AFIT/ENY.

(to the left) of it. Just prior to releasing this progress report, on 11 July 2024 we performed the first checkout run of the new facility. Fig. 2 shows raw infrared imagery of a conducting matched Biot number leading edge model exposed to phantom cooling alone, showerhead cooling alone, and a simultaneous combination of phantom cooling and showerhead cooling. The combined effect clearly discernable in the rightmost image, and the ability to predict this combined effect will be helpful in advancing turbine technology. Once this testing regimen is complete, upgrades to the experimental rig will allow for unsteadiness to be introduced into the wake to support further enhancements to the analytical predictive tools to account for wake unsteadiness.

Transonic Turbine Cascade Aerodynamics

Preliminary background oriented schlieren (BOS) imagery has been acquired using the setup shown in Fig. 3. A suitable background pattern with appropriate dot density was produced and a sample of the processed data is shown in Fig. 4. The cross correlation reveals where density gradients exist in the flow, thereby revealing the locations of trailing edge shocks. Nevertheless, it is clear that traditional Z-type schlieren will be more useful, especially in its ability to resolve unsteady flow features with greater detail.

We are proceeding with the planned upgrades to the facility, incorporating windows on both sides of the blade set to allow for light to pass through the entire rig for Z-type schlieren. Design and fabrication are in progress with much of the hardware having been procured. Fig. 5 shows new end wall plates that were recently completed. The rectangular cutouts will accommodate the Schott N-BK7 windows that are now in hand and ready for installation. A redesign is currently under way for a new turbine cascade that will fit within the dimensions of the new facility.

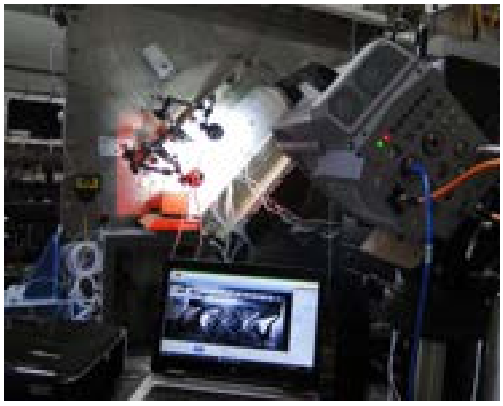

Fig. 3 Transonic Turbine Cascade with BOS capability installed

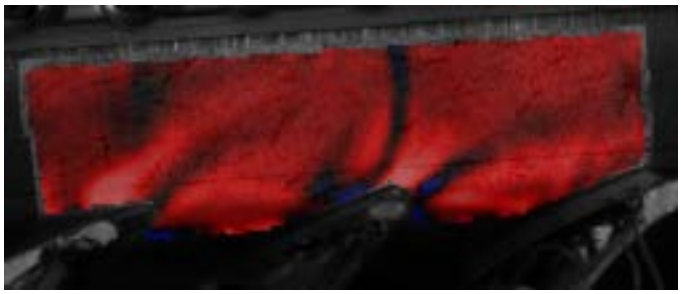

Fig. 4 BOS flow visualization downstream of transonic cascade

Fig. 5 New side plates for transonic cascade with cutouts for schlieren access

Papers Published by the PI During the Reporting Period

1. Hopkins, B.W. and Rutledge, J.L., 2024, "Superposition of Overall Cooling Effectiveness on a Turbine Blade Leading Edge," *ASME Turbo Expo 2024*, Paper No. GT2024-121339.
2. Hopkins, B.W., Hughes, J.A., Bryant, C.E., Rutledge, J.L., 2024, "Biot Number Error in Low Temperature Inconel Overall Effectiveness Experiments," *ASME Turbo Expo 2024*, Paper No. GT2024-124338.
3. Fuqua, M.N. and Rutledge, J.L., 2024, "An Experimental and Computational Investigation of Vortex Tube Heat Transfer Characteristics," *Journal of Thermal Science and Engineering Applications*, Vol. 16, No. 2, February 2024.
4. Wiese, C.J. and Rutledge, J.L., 2023, "Mass-Heat Coupling in Film Cooling Experiments- The Influence of Temperature and Turbulence on the Dufour Effect," *Journal of Turbomachinery*, Vol. 145, No. 12, December 2023.
5. Bryant, C.E. and Rutledge, J.L., 2023, "Scaling Overall Effectiveness in Low Temperature Experiments," *Journal of Turbomachinery*, Vol. 145, No. 12, December 2023.
6. DeMarco, K.J., Polanka, M.D., Bohan, B.T., Rutledge, J.L., 2023, "Design Impacts on Ram Air Vane Cooling in an Ultra Compact Combustor," *Journal of Thermal Science and Engineering Applications*, Vol. 15, No. 10, October 2023.

Distribution Statement B. Distribution authorized to U.S. Government agencies only (P&I, 14 June 2024). Other requests for this document must be referred to AFIT/ENY.

AFOSR – FA9550-23-1-0005

Project Update – August 2024

Since our last meeting at UCF on January 11, 2024, we have (1) built two gust generator systems, (2) built a dual underwater laser setup, (3) characterized uniform and nonuniform gust profiles after improving the flow conditioning, (4) validated our system with published data and Kussner's model, and (5) begun force measurements with different wing morphologies, and (6) conducted force and flow field measurements with a dynamically twisted wing.

To fully understand the flow physics during wing-gust interactions, particularly to measure the circulation around the wing, it is important to measure the flow field around the entire wing with PIV. This cannot be achieved with a single laser plane as a shadow is cast on the opposite side of the wing, especially at an angle of attack or when morphing. Additionally, our blowing and suction bends inside the tank create obstructions to any lasers entering through the side of the tank. Therefore, we built two coincident laser planes, as shown in Figure 1, one coming from each end of the tank to illuminate all sides of the wing.

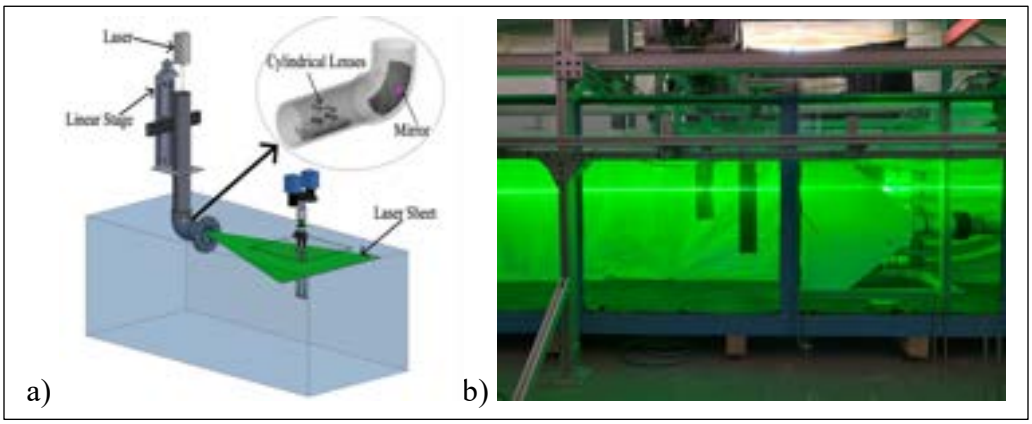

Figure 1: Horizontal laser plane setup for underwater PIV. (a) schematic of laser setup with optics; (b) picture of dual laser planes, one coming from each end of the tank

After moving our gust generator system from our temporary test tank into our permanent 6-m long towing tank, our gust profiles unexpectedly changed, and it was concluded our flow conditioner was at fault. Therefore, we replaced our flow conditioner with an improved version (Figure 2(d)) to achieve the gust profiles shown in Figure 2. This includes the characterization of our uniform and nonuniform gust velocity profiles, at two gust ratios, in both horizontal and vertical planes. Our gust profiles have a width of 2.4c and a shear layer thickness of 0.4c, where c is the wing chord. *GR1* and *GR2* corresponds to gust ratios of 0.84 and 0.48, respectively. The nonuniform spanwise gust profiles, in Figure 2(c), don't exhibit enough of a satisfactory velocity gradient, so further control valve tuning is required.

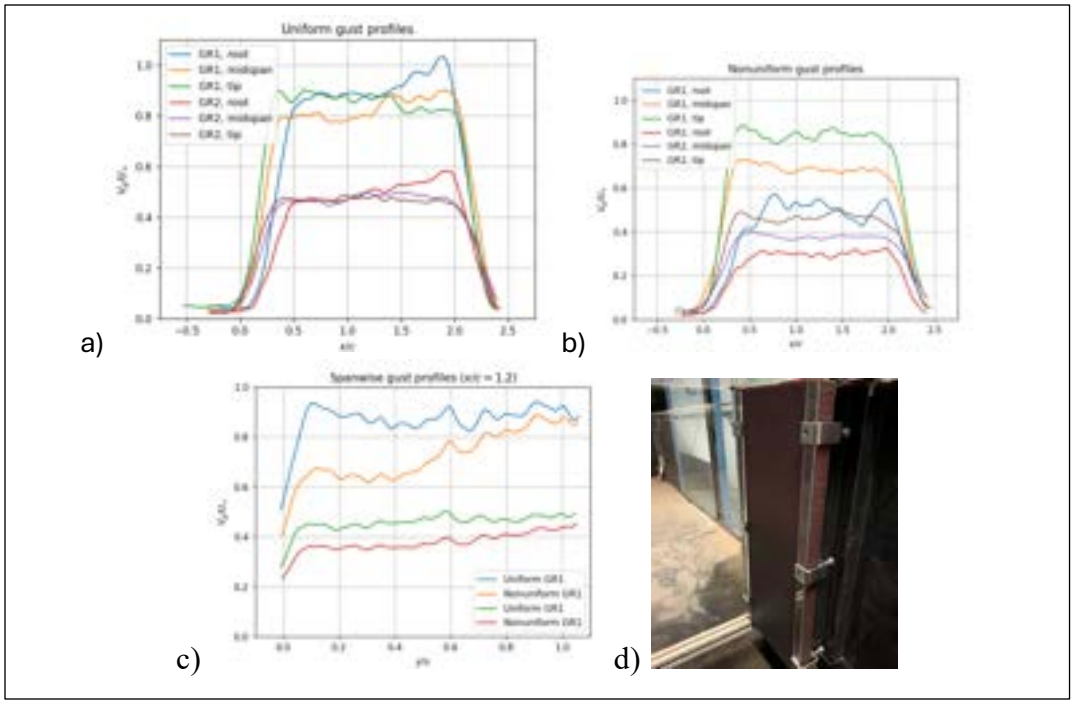

Figure 2: Gust characterization: (a) horizontal profiles of uniform gusts; (b) horizontal profiles of nonuniform gusts; (c) vertical profiles of all gusts; (d) new flow conditioning

We have taken lift force validation data for two uniform Gust Ratios to compare with published data and Kussner's model (Figure 3). These validation cases consisted of a flat plate at $\alpha = 0$ with no morphing at Re = 10,000. We compare our experimental data to published data at the same Re and adjusted for the difference in gust width (Sedky, Gementzopoulos, Andreu-Angulo, Lagor, & Jones, 2022). Our data matches well with the published data, with a 5% difference in lift coefficient peak. We also compare our experimental data to that predicted by Küssner's model, with a 10% difference in lift coefficient peak. Our Küssner model uses a trapezoidal fit, shown in Figure 3(b).

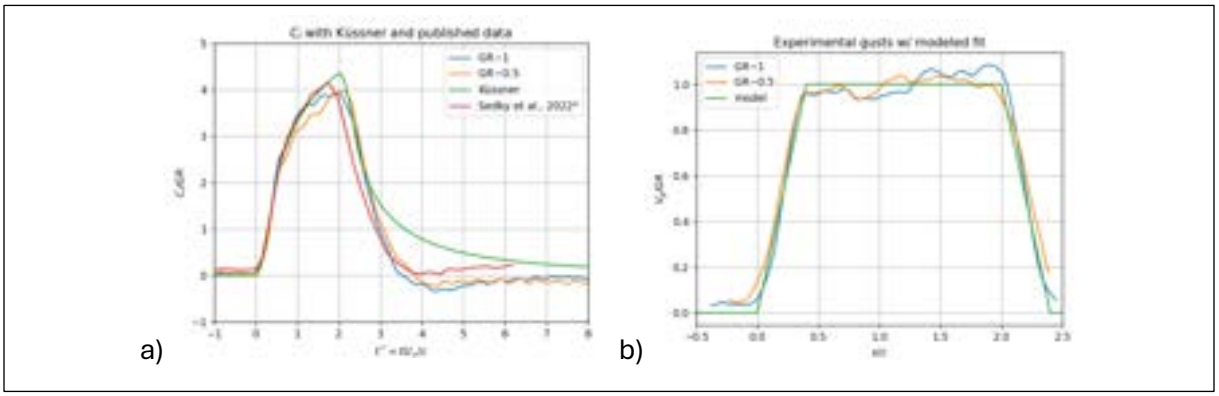

Figure 3: Force validation data with Küssner's model and published data (flat plate, no morphing, α=0)

We have also begun wingtip bending tests using force measurements, with various bending amplitudes or flexion angles, using natural observations from (Lucas, et al., 2024) as bending parameter guidelines.

References:

Lucas, K. N., Johnson, N., Beaulieu, W. T., Cathcart, E., Tirrell, G., Colin, S. P., . . . Costello, J. H. (2024). Bending rules for animal propulsion. *Nat Commun*, 5, 3293.

Sedky, G., Gementzopoulos, A., Andreu-Angulo, I., Lagor, F. D., & Jones, A. R. (2022). Physics of gust response mitigation in open-loop pitching manoeuvres. *Journal of Fluids Mechanics*, A38.

Flow Physics and Optimized Suppression of High-Speed Cavity Flow

L. Cattafesta, K. Taira and L. Ukeiley PI's

AFOSR Award Number FA9550-22-1-0013

Summer 2024 Update

The objective of this effort is to develop a fundamental understanding of three-dimensional cavity flows and leverage this knowledge to develop effective physics-based suppression schemes for high-speed cavity oscillations both in terms of surface pressure and shear layer oscillations. This objective is being accomplished through complementary experimental and numerical efforts that will drive each other to develop optimized control schemes. This coupled approach has demonstrated a link between modal based analysis techniques applied to the numerically generated data sets and control applications in higher Reynolds number physical experiments under both supersonic and subsonic free stream conditions. Over the past year we have made advances;

- with use of windowed resolvent analysis to determine favorable locations of where to introduce control [2]
- in the use of phase reduction analysis for modeling and control of cavity flows
- in the use of modal analysis methods to use experimental data to sync velocity and density fields to understand compressibility effects in the high Reynolds number cavity flow [5]
- in the construction of new facility at IIT and time dependent actuation strategies.

Windowed Resolvent Analysis

Considering supersonic turbulent flow over an open rectangular cavity with a length-to-depth ratio of 6 at Mach 1.4 and a Reynolds number of 10,000. Our previous studies performed resolvent analysis on cavity flows and identified the leading edge as the optimal actuation location and established an unsteady three-dimensional actuation strategy that demonstrated a significant 53% reduction of pressure fluctuations [3]. Motivated by the effective suppression, we performed windowed resolvent analysis to identify additional actuation positions on the cavity walls on the suppression of pressure fluctuations [4]. The overview of windowed-resolvent analysis is shown in Fig. 1. Similar to the leading-edge actuation which results in a shear-layer response, we also identified a secondary actuation location on the bottom cavity wall that results in a similar response. We then investigated the possibility of simultaneous actuation at the leading edge and the bottom wall on the control performance. While we observed that the single leading-edge actuation is highly effective in suppression, we also identified a secondary actuation location and actuation strategy on the bottom wall of the cavity which resulted in a suppression of about 36%. We performed dynamical mode decomposition of the actuated flow fields and identified that sustaining the three-dimensional high spanwise wavenumber in the shear layer is crucial for the suppression of pressure fluctuations. Furthermore, we also identified a saturation of control performance with an increase in momentum coefficient where single leading-edge actuation is effective in the suppression of pressure fluctuations with even a small momentum coefficient of 0.005.

Density-Velocity SAMM

To study compressibility effects relating velocity/pressure coupling of high subsonic cavity flows, time-resolved Particle Image Velocimetry (PIV) and density measurements are utilized. In addition to the SAMM method on the PIV and surface-pressure data [5], we utilize the same method to obtain the correlation between the density field obtained from quantitative Schlieren and time-resolved surface pressure measurements of the same cavity flow at Mach 0.6 [6]. The

reduced order modeling of velocity and density fields are consequentially linked using the surface pressure. The compressibility effect is indicated by the density fluctuations, while positive values are compression and negative values are expansion. Expansion occurs when a positive vorticity is followed by a negative vorticity in the shear layer. In addition, expansion of the flow is associated with positive pressure fluctuations on the cavity surface and vice versa. These observations are consistent at different Rossiter frequencies and can be observed in Figure 2.

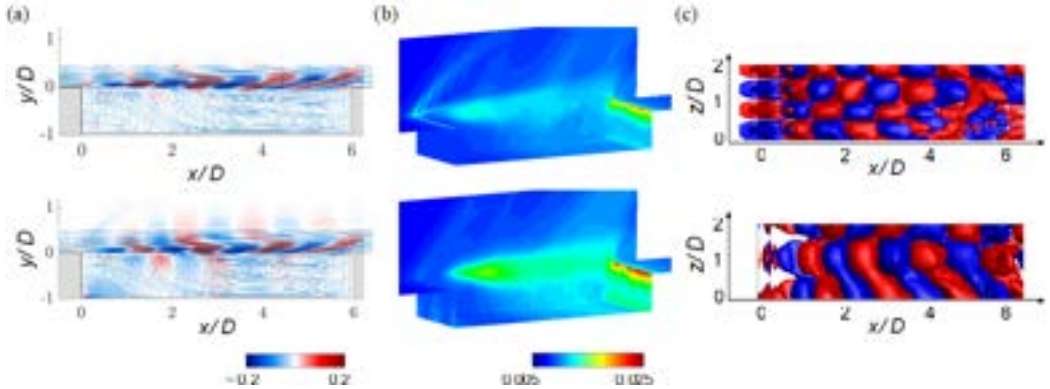

Figure 1. Overview of windowed resolvent analysis-based control for cavity flows at a Strouhal number, $St = 2.49$ using single leading-edge-only actuation (top row) with spanwise actuation wavenumber of 2π and secondary actuation location on the bottom wall at $x = 0.3$ (bottom row) with spanwise actuation wavenumber of π. The streamwise velocity components of the dominant response modes overlayed with the time-averaged streamlines of the baseflow (a), distribution of r.m.s. value of pressure fluctuations on the cavity walls, (c) three-dimensional DMD modes at the actuation frequencies visualized spanwise velocity isosurface of ± 0.05.

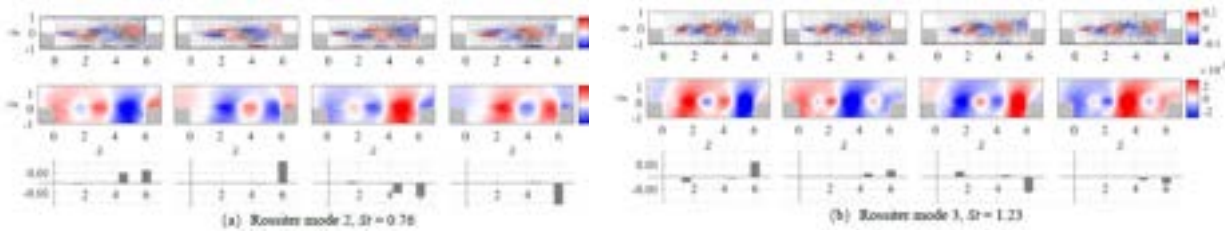

Figure 2. Temporal evolution of flow fluctuation at different phases within a cycle for different Rossiter frequencies. The phases are 0, π/2, π, and 3π/2 from left to right. From top to bottom in each sub-figure are spanwise vorticity, density, and pressure. Vectors are superimposed on the contour of nondimensional spanwise vorticity w_zD/U_∞. Pressure is nondimensionalized by q_∞.

References

1. Godavarthi, V., Kawamura, Y., & Taira, K. (2023). Optimal waveform for fast synchronization of airfoil wakes. *Journal of Fluid Mechanics*, 976.
2. Godavarthi, V., Cattafesta, L.N., Ukeiley, L., & Taira, K. (2024). Windowed resolvent analysis-based control of supersonic turbulent cavity flow, AIAA Aviation, Las Vegas, USA, July 29 – Aug 2.
3. Liu, Q., Sun, Y., Yeh, C. A., Ukeiley, L. S., Cattafesta, L. N., & Taira, K. (2021). Unsteady control of supersonic turbulent cavity flow based on resolvent analysis. *Journal of Fluid Mechanics*, 925.
4. Rosenblum, J., (2024) "Design of a High Frequency Oscillating Fence to Control Cavity Flow," Undergraduate Honors Thesis, University of Florida.
5. Zhang, Y., Cattafesta, L.N., and Ukeiley, L., (2020) "Spectral Analysis Modal Methods (SAMMs) using non–time–resolved PIV." Exp Fluids, 61:226, October 2020, https://doi.org/10.1007/s00348–020–03057–8.
6. Zhang, Y., Cattafesta, L., Ukeiley, L., and Taira, K., (2024) "Modal Decomposition of High-Speed Cavity Flows using Non-Time-Resolved PIV And Quantitative Schlieren," 13th International Symposium on Turbulence and Shear Flow Phenomena (TSFP13), Montreal, Canada, June 25–28, 2024.

Compressibility effects on laminar separation bubbles over airfoils

Laminar separation bubbles (LSBs) have profound impact on loading characteristics of lifting surfaces. However, due to the challenges posed by the small size and highly unsteady nature of these spatio-temporally localized flow phenomena, we have limited understanding of their topology and parametric sensitivities. This result in uncertainties in predicting flow behavior during high-lift configurations, discontinuities in airfoil loading characteristics, and low-frequency unsteadiness detrimental to structural integrity. To address the above issue, we perform a joint computational-experimental campaign that systematically characterizes LSB dynamics and its sensitivities to compressibility effects, over a canonical airfoil. The objective is to identify causal mechanisms that drive these sensitivities through stability and modal analyses, and leverage the insights to develop better-informed flow control strategies.

Key takeaways for the past year's efforts are as follows:

- Matured a high-fidelity computational framework to simulate and analyze the relevant flowfields. Initiated sensitivity studies of LSB over a NACA0012 to varying angles of attack (AoA) with moderate compressibility effects, at M_∞=0.5.
- Developed the experimental setup for the NACA0012 airfoil and performed PIV measurements of LSB related unsteadiness at near-stall conditions.

The dynamic behavior of the LSB at near-stall conditions was consistently reproduced in both computations and experiments. Results are now detailed below.

Computational campaign

Dynamics of LSBs over a NACA 0012 airfoil subjected to a freestream Mach number 0.5 and a chord Reynolds number of 500,000 were evaluated using a high-order implicit large-eddy simulation (ILES) approach. Three angles of attack, α = 4°, 8°, and 12° were investigated.

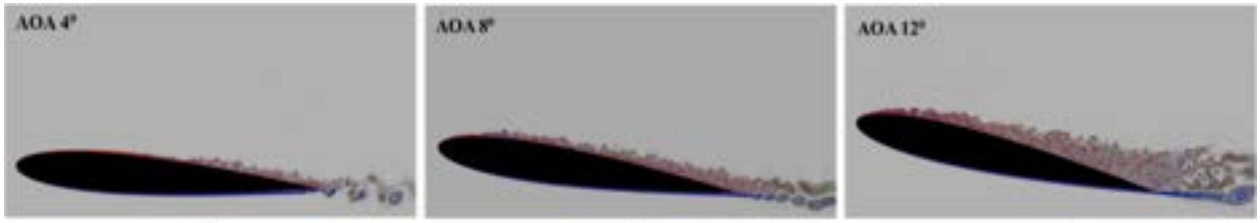

Figure 1: LSB at various conditions shown using vorticity magnitude for (a) AOA 4^0 - No separation bubble, (b) AOA 8^0 - Small separation bubble, (c) AOA 12^0 – State-switching separation bubble

It is observed that at 4° (Figure 1a), the flow remains attached, devoid of a separation bubble. At 8° (Figure 1b), a small separation bubble is formed, indicating leading edge flow separation. However, at 12° (Figure 1c) an intriguing flow behavior is observed, where the separation bubble exhibits intermittent state switching between short and long bubble configurations.

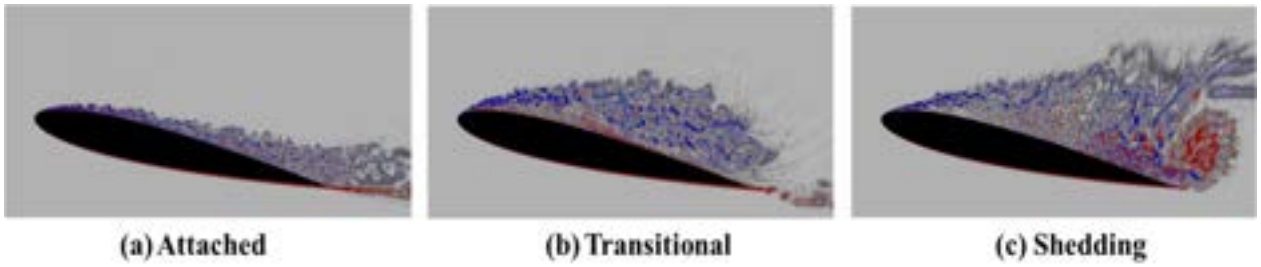

Figure 2: Complex Flow dynamics near the stall condition of AOA 12^0 (a) Attached state, (b) Transitional state, (c) Shedding states

This cyclic behavior, characterized by attached, transitional, and shedding states, resulted in significant loading dynamics near the stall condition (Figure 2). During the attached state, the lift and drag coefficients stabilized at 0.89 and 0.085, respectively. As the bubble elongated in the transitional state, these coefficients surged to 1.38 (lift) and 0.36 (drag) due to vortex-induced effects. When the bubble collapsed, the coefficients dropped to 0.48 for lift and 0.146 for drag (Figure 3). Figure 4 shows representative results using skin friction coefficient, to highlight surface loading fluctuations in time, driven by the size of the bubble (Figure 4).

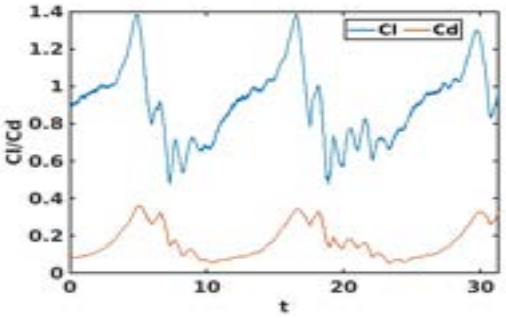

Figure 3: Time history of the lift and drag coefficients at an angle of attack of 12.0^0

A multi-modal behavior of the flowfield was observed at the above near-stall condition, which is also currently being quantified using modal analyses (figure 5). This included low-frequency oscillations near a Strouhal number of 0.08 corresponding to bubble evolution, high-frequency shear layer oscillations at a Strouhal number of 6, and trailing edge vortex shedding at 0.84. This study reveals the complex interplay between flow parameters and LSB behavior, emphasizing the importance of understanding these dynamics for reliable load predictions. Ongoing analyses aim to derive a reduced-order description of this flow behavior using feature identification techniques, and further identify flow control strategies to mitigate the loading fluctuations associated with LSB dynamics. Comparative studies will also be performed at lower Mach regimes.

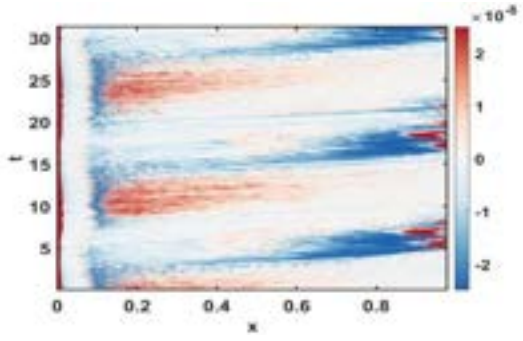

Figure 4: Spatiotemporal contours of C_f at AOA 12^0

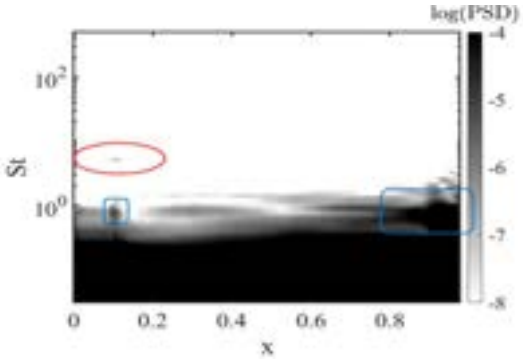

Figure 5: Normalized PSD contours of pressure signals

Experimental campaign

The primary objective of this study is to investigate the switching behavior of a laminar separation bubble between an attached flow near the leading edge and a significantly separated region extending over the NACA-0012 airfoil at a near-stall angle of attack ($\alpha = 12\circ$) with a chord-based Reynolds number of 180,000 ($U\infty = 11.25$ m · s−1). Employing a sophisticated experimental setup and Particle Image Velocimetry (PIV), this research meticulously analyzes the bubble's switching location, size, and temporal evolution. Elucidating these parameters is critical for understanding the global instabilities within the bubble dynamics, which manifest as large-scale oscillatory phenomena influencing the bubble's growth, contraction, and movement. These instabilities can substantially affect aerodynamic performance by altering lift, drag, and flow separation characteristics. The results demonstrate a quasi-periodic switching behavior between an attached and a large separated flow at low frequencies, highlighting the complex interactions that govern bubble stability.

Figure 6(a) illustrates instantaneous streamwise velocity profiles near the airfoil surface, whereas figure 6 (b) depicts the streamwise velocity fluctuations at a single measurement point, crucial for understanding the dynamics of the LSB. This figure provides a detailed assessment of temporal variations in streamwise velocity across the airfoil. The contours, delineated in white and black, signify attached and separated flow regions, respectively. Analysis reveals periods where the entire airfoil surface is characterized by black contours, indicating a fully separated flow state. Conversely, white contours intermittently prevail over the aft region of the airfoil ($x/c > 0.6$), indicating the transient presence of a short laminar separation bubble. In figure 6(b), the pink shaded region represents periods of attached flow, while the purple shaded region indicates periods of separated flow.

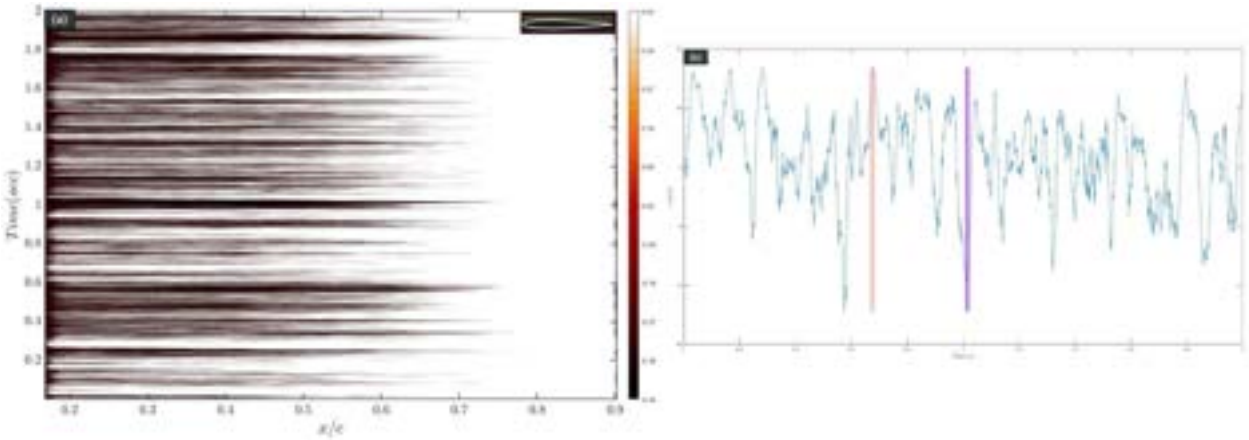

Figure 6: Time resolved streamwise velocity (u/U) profile in time near the airfoil surface. The data is plotted along the yellow line given in the schematic.

Utilizing the data from figure 6(b), the instantaneous streamwise velocity (u/U) has been plotted for both attached and separated flow regions. Figure 7(a) depicts a fully attached flow regime characterized by a smooth velocity distribution without evidence of flow separation. In contrast, figure 7(b) clearly illustrates flow separation on the airfoil surface, as indicated by an adverse pressure gradient and a corresponding flow deceleration near the surface.

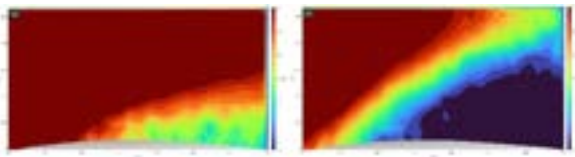

Figure 7: Instantaneous streamwise velocity (u/U) profile near the airfoil surface for attached (a) and separated (b) flow.

Turbulence Studies & Boundary Layer Interactions

Summer 2024 Update

Passive Control of Non-Canonical Flows with Anisotropic Porous Materials

Award Number: FA9550-23-1-0269

Louis Cattafesta (IIT), Rajat Mittal & Charles Meneveau (JHU)

The objective of the proposed research is to examine the characteristics of flows over high-porosity anisotropic porous material (APM) lattices using experiments and computational modeling. Recent advancements in manufacturing have enabled the fabrication of structurally robust porous materials with tunable anisotropic porosities, but the application of such materials for passive control of flows remains underexplored. This work focuses on: the permeability characterization of APMs, APG, and APG TBLs over APM lattices, passive control of a turbulent separation bubble (TSB) via APMs, and the effect of APM substrates on flow over a surface-mounted obstacle (SMO). Over the past year, we have analyzed:

- Characterization of APMs using a zonal-weighting approach for uniform and fully developed flow conditions [1],
- Analysis of inertial flow deflection effects using DNS and experiments to derive an extended Darcy-Forchheimer law [2],
- Analysis of the effects of APM substrates on pressure gradient-induced TSB using Stereoscopic Particle Image Velocimetry (SPIV) and drag measurements [3],
- Computational analysis of bluff body wake control by APM substrates.

Characterization of APMs using a zonal-weighting approach: A zonal-weighting approach where flow region variation through porous lattices dictates the characteristic velocity and hydraulic diameter was considered. However, the zonal division in this method yielded higher errors in convergence across different porosities compared to the projected flow blockage initially used. Dimensionless data analysis for anisotropic cases yielded a good convergence for high porosities. Convergence weakened with decreasing porosity. Comparison between similar-porosity isotropic and anisotropic cases yielded higher pressure losses for isotropic cases. It was concluded that the current scaling law is good for high porosities but not suitable across a range of porosities. For compared anisotropic cases, experimental data are in good agreement with DNS data, while a deviation is seen for isotropic cases [1].

Extended Darcy-Forchheimer law including inertial flow deflection: Inertial flow deflection for the 2D isotropic porous specimen with lattice elements is analyzed using tuft flow visualization and laser-illuminated fog visualization. We see two axes of the flow aligned with the two major axes of the cylinder. Inertial flow deflection estimated from both techniques was comparable within experimental uncertainty and in good agreement with direct numerical simulations. Further investigations are performed by carrying out DNS of various porous media including staggered and random elements. Using the DNS results, an extended Darcy-Forchheimer law which captures the flow deflection effects has been developed and tested. The paper has been published [2].

Effects of APM substrates on APG induced TSB: Stereo PIV analysis of TSB flow with four different APM substrates of high (ϵ =0.8), medium (ϵ =0.5) and low (ϵ =0.15) porosities were conducted on a flat-plate model at $Re_\theta = 760$. A suction setup with a mean suction velocity $\overline{u_s} = 0.44u_\infty$ ($u_\infty -$ free stream velocity at the reference) is utilized to create an APG over the flat-plate model, which induces separation. In general, the average separation bubble vanishes when APM substrates are attached

(example in Figure 1). From inspection of the wall-normal velocity component, we can see that the flow enters and leaves porous cells

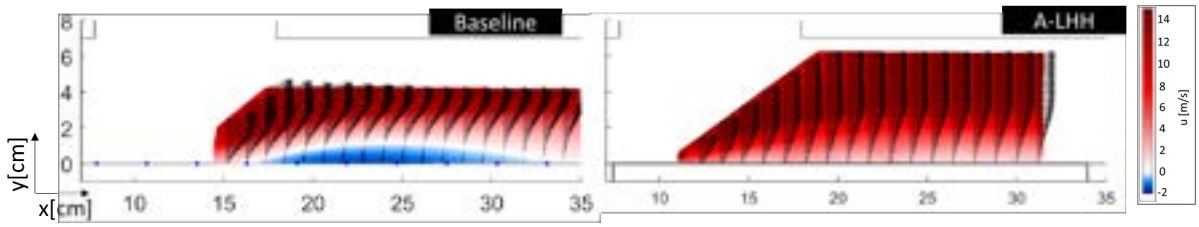

Figure 1: Comparison of u-velocity component for baseline TSB and A-HHL substrate design[3]

periodically, which is validated via sine fits on the velocity profile extracted near the APM-flow interface. Drag measurements were taken for the flat-plate model with and without the substrates by attaching a load cell to the strut supporting the load cell. As illustrated by Figure 2, there is a drag reduction of 20-25% with the substrates, with the highest drag reduction observed for the A-MHH configuration. Validation of the drag measurements is curretly been carried out.

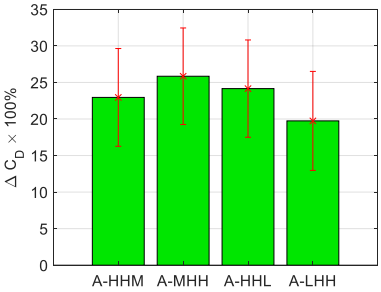

Figure 2: Left – Drag reduction with the APM substrates attached compared to the baseline TSB [3].

Bluff-body wake control by APM substrates: Unsteady separation and vortex shedding in the wake of bluff bodies result in many adverse effects such as drag increase, vibration, and noise. As a possible passive flow control application of APM substrates, the flows over a wall-mounted dome are computationally investigated. We observe that a localliized thin porous substrate under the dome effectivley supprreses flow unsteadiness (Figure 3). Optimal shape and parameters of the APM substrate, including anisotropic substrates with different orientations, will be further studied.

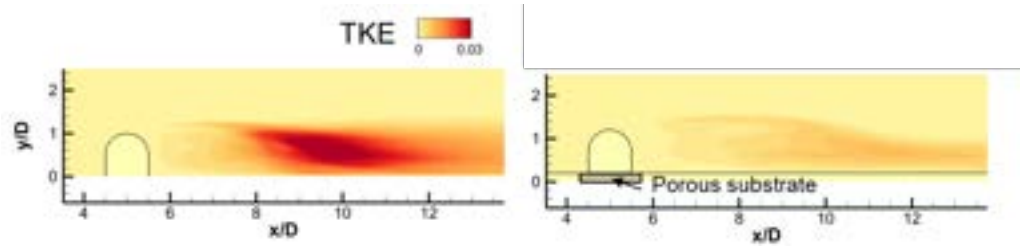

Figure 3: Turbulent kinetic energy (TKE) distribution in the wake of wall-mounted dome. Left – Solid wall, Right – Porous substrate under the dome. Substrate diameter: 1.4D, thickness: 0.2D, where D is the diameter of the dome.

References

[1] "Characterization of Periodic Lattice Anisotropic Porous Materials for Passive Flow Control", AIAA AVIATION Forum, Jun. 2023, doi: 10.2514/6.2023-3448

[2] "Generalized Darcy-Forchheimer law including directional effects", Journal of Fluid Mechanics, 31 January 2024, doi: 10.1017/jfm.2023.1083

[3] "The Effects of Anisotropic Porous Lattice Substrates on Turbulent Separation Bubbles", AIAA AVIATION Forum, Jul. 2024, (Accepted, pending publication)

GRANT FA9550-23-1-0715: 2-PAGE SUMMARY

TAILORED FLOW CONTROL: EXPLOITING TRIANGULAR POROUS TEXTURING ELEMENTS AND ARCHITECTED MATERIALS FOR ENHANCED AIR VEHICLE PERFORMANCE

SUBMITTED TO

DR. GREGG ABATE

Program Officer, Unsteady Aerodynamics & Turbulent Flows

Air Force Office of Scientific Research

PRINCIPAL INVESTIGATOR

DR. ISAAC CHOUTAPALLI

Professor, Department of Mechanical Engineering

The University of Texas Rio Grande Valley

CO-PRINCIPAL INVESTIGATORS

DR. RAJAN KUMAR, DR.S. UNNIKRISHNAN

Department of Mechanical Engineering

Florida State University

DR. KUNIHIKO TAIRA

Professor, Mechanical and Aerospace Engineering

The University of California Los Angeles

Table of Contents

I. Introduction

The primary objectives of our collaborative research is to explore the Triangular Porous Texturing (TPT) elements' influence on near-wall turbulence, with focus on reducing skin-friction and overall drag. In this past year, we have used force measurements, Particle Image Velocimetry (PIV) and computational simulations to analyze the interplay between solid TPT elements (no internal channels) and the flow field both within and outside the boundary layer. The initial experiments at UTRGV were carried out on a NACA 0018 airfoil and a flat plate. The preliminary computational effort and data-driven analysis on the flat plate were carried out by FSU and UCLA respectively.

II. UTRGV's Effort

Completed Tasks: This past year, UTRGV fabricated test articles that included flat plates and NACA 0018 airfoil with and with TPT elements. The initial study consisted of understanding the impact of solid TPT elements (without internal architected channels) on the boundary layer. In our experiments with the NACA 0018 airfoil, the freestream chord-based

Figure 1: *Fabricated test articles with and without the solid TPT elements.*

Reynolds numbers ranged from 68,000 to 206,000. The angle of attack was varied from 0 deg to 20 deg. The TPT elements are 1 mm equilateral triangular prisms, the spacing between the elements in any given row is 5mm (center to center of base) and the spacing between the rows is 4 mm. Force measurements were carried out using a sting balance mounted in the wind tunnel. Additionally, planar particle image velocimetry (PIV) data was collected at three-quarter span from each airfoil at pre-stall, stall, and post-stall angles of attack at several freestream conditions. The experimental and flow field data demonstrate that the addition of TPT elements to the NACA 0018 airfoil, especially at the leading edge significantly improves its aerodynamic performance, particularly at higher angles of attack. The modified airfoil exhibits a lower lift

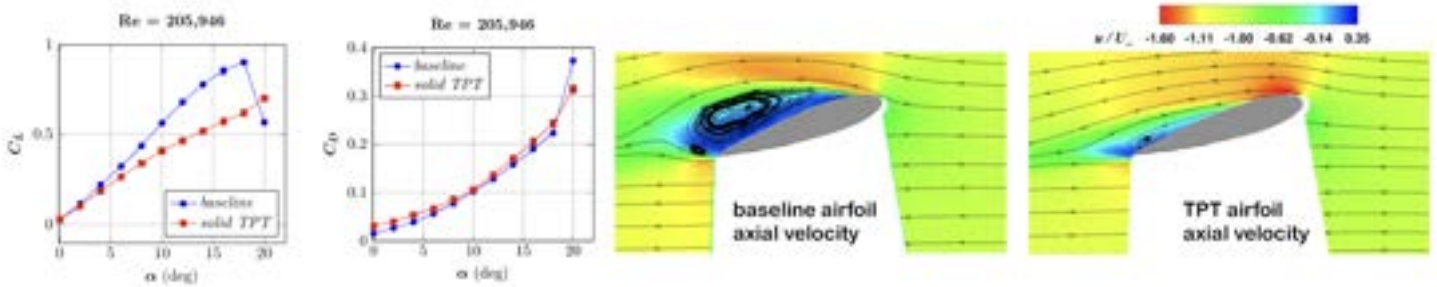

Figure 2: *Airfoil force measurements (a, b) and PIV axial velocity contours of baseline and TPT airfoils (c, d).*

slope and $C_{L,max}$, yet benefits from a delayed stall, occurring at a greater angle of attack compared to the baseline airfoil (figure-2a, b). PIV data at 18° AoA, which is the stall angle for the baseline airfoil, reveal that the TPT elements help maintain more attached flow, resulting in a smaller separation zone and lower turbulence levels behind the airfoil. This is corroborated by reduced drag coefficients observed in the modified airfoil, particularly beyond 18° AoA, indicating improved efficiency in post-stall conditions. Overall, the modifications enhance the airfoil's ability to operate at higher angles of attack with lower drag and improved flow control, making it more efficient and better suited for applications requiring high lift and reduced drag in these conditions.

Ongoing / Upcoming Tasks: Experiments are currently underway to study and characterize the effect of solid TPT elements on a flat plate. In addition, fabrication is also underway to begin experiments on a flat plate and on a NACA 0018 airfoil to understand the combined role of TPT elements and architected materials both within and outside the boundary layer in terms of skin-friction reduction and flow separation control.

III. FSU's Effort

The primary goal of FSU computational effort is to develop necessary solvers and perform high-fidelity simulations of baseline and textured surface boundary layers, complementary to the experimental work performed at UTRGV. In addition

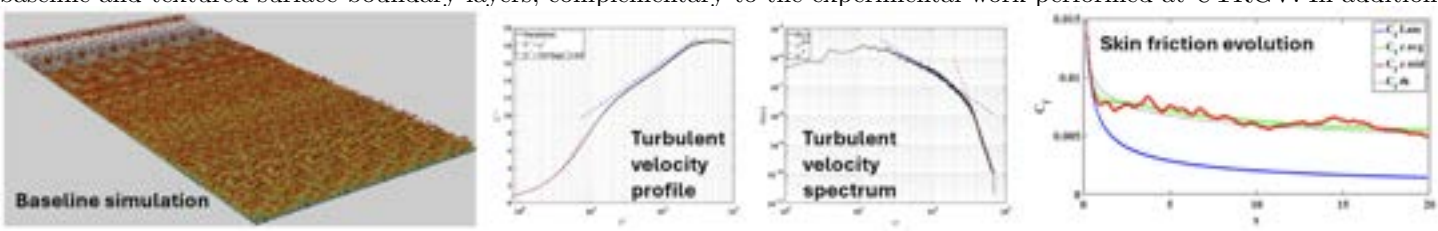

Figure 3: *Simulation and validation of the baseline smooth plate using the newly developed high-order in-house solver.*

to providing first-principles based insights into the role of surface texturing in manipulating near-wall turbulence and wall loading, this effort will generate scale-resolved spatio-temporal data for the data-driven analyses performed at UCLA. Towards

this end, over the past year, we have developed and validated an in-house high-resolution fluid solver, and are currently modeling the textured surface. Details are as follows:

Tasks Completed: To simulate the incompressible speed regime corresponding to experimetns at UTRGV, we have developed a high-order Navier-Stokes solver based on the bulk viscosity artificial compressibility method (BVACM). The solver is formulated in the generalized curvilinear coordinates to handle arbitrary geometries and utilize 10th order central schemes and explicit filters to ensure sufficient resolution of near-wall inhomogeneity induced by the texturing. Figure 3 shows an instantaneous visualization of the baseline simulation on a smooth flat plate, corresponding to the 24 inch plate model tested at UTRGV, at a unit Reynolds number, 80,833/m. Also shown in figure 3 are the validation plots of turbulent velocity profile, velocity spectrum, and skin friction coefficient, with theoretical estimates.

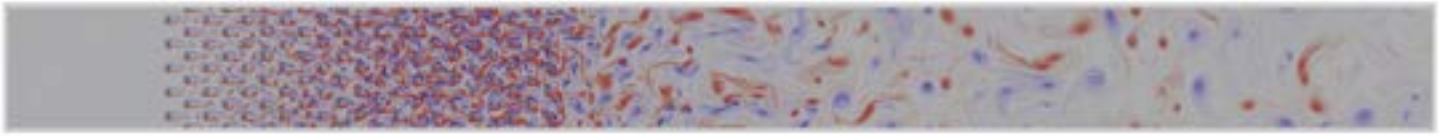

Figure 4: *2D simulation of the 12-inch plate model with square roughness elements.*

Ongoing Tasks: Currently we are in the process of modeling the textured surface by incorporating surface roughness over the smooth plate model. To perform a rigorous near-wall grid-resolution analysis, initial efforts will model square roughness elements. Preliminary result from a 2D simulation on this model is included in figure 4, which corresponds to the 12-inch plate with triangular roughness elements tested at UTRGV. The square elements modeled here have edge length identical to the triangular elements utilized in the corresponding experiments.

FSU's Experimental Effort: The boundary layer will be quantified by employing high-resolution particle image velocimetry (PIV) at a resolution of $75\mu m$. This high resolution of boundary layer measurement allows the characterization of near-wall flow physics. To further investigate the physics between the flow and TPT elements, the resolution of the flow measurements will be further enhanced.

IV. UCLA's Effort

In the present study, we consider data-driven methods of enabling the comparison of turbulent flow datasets from numerical simulations and experiments of varied resolution and spatial availability for the goal of design optimization of TPT elements for drag reduction. Traditional methods of design optimization typically require comprehensive parameter studies over many design configurations, which is costly in terms of both finance and time. We seek to leverage data-driven techniques, such as dimensionality reduction, to direct analysis toward cases that we expect to perform well, to accelerate the development cycle. In many forms of data-driven analysis, we are often tasked with quantifying the similarity of different flow field measurements. While a simple distance metric (e.g., the Euclidean norm) is often used, such measurements require the data to be of the same resolution and spatial structure, which makes it a poor metric for comparing data obtained from different conditions—for example, DNS and PIV—without introducing errors that are difficult to quantify. For this study, we consider representing multi-fidelity datasets using a shared state representation where a similarity analysis can be performed. In the current analysis, we represent our data as a probability distribution over some state, for instance, sensor measurements. This method allows us to consider comparisons between sensor configurations that vary in their spatial resolution and placements. We compare the obtained distributions via the Wasserstein distance, which essentially measures the cost associated with moving between different distributions. We consider a Monte-Carlo method to approximate this distance in a manner that is computationally tractable for use in further data-driven analysis.

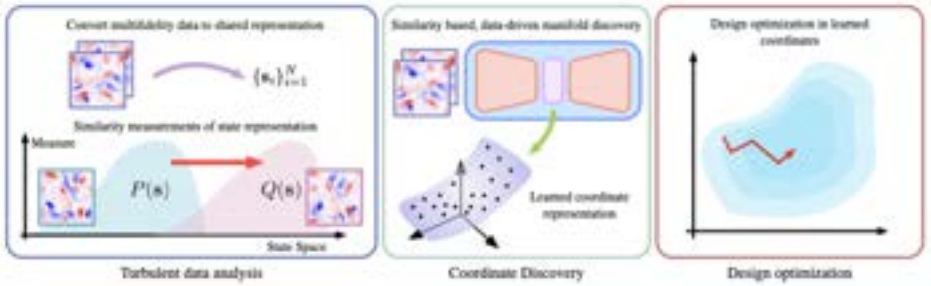

Figure 5: *Overview of data-driven analysis of turbulent flow field data for design optimization.*

V. Capacity Building at UTRGV

The NSP grant has already significantly altered the aerospace research landscape at UTRGV. Highlights are given below.
Student Engagement and Pipeline Development: With AFOSR funding and help from UTRGV's College of Engineering, we were able to hire 9 graduate students and 10 undergraduate students to work on various aspects of the project. There are many more and numerous graduate and UG students who have expressed interest in the field of aerodynamics to the PI over the past several weeks and months. This new grant has spurred aerodynamics interest in many students on campus.
Resource Expansion through Collaboration: Students from UTRGV, FSU, and UCLA hold bi-weekly Zoom meetings to share their research findings and brainstorm ideas. Additionally, all PIs and students convene monthly on Zoom for updates and presentations on each other's work. Collaborating with faculty from FSU and UCLA has significantly boosted UTRGV's research capabilities. To further this exchange, two UTRGV students will spend the Spring 2026 semester at FSU, gaining hands-on experience with advanced CFD and experimental techniques, and utilizing FSU's cutting-edge research facilities.
UTRGV's Financial Investment: After receiving the AFOSR NSP grant, UTRGV has undertaken major building renovation and electrical work to rehouse our existing wind tunnel in a separate building and dedicated it to aerodynamics research. To date, the university has invested nearly $500,000 (and counting) for renovations, electrical work and other building upgrades. The work is still ongoing. Because of this grant and our collaborative work with FSU and UCLA, the department is planning to hire new faculty in aerospace engineering pending approval from UT System Board of Regents.

The Response of Wall Turbulence to Large-Scale, Space-Time Perturbations
Students: Miriam Theobald-Deschine (Ph.D.), Luke Sylliaasen (undergraduate),
Shreyas Madhvaraju (Past - undergraduate), PI: Ebenezer P. Gnanamanickam
Embry-Riddle Aeronautical University (ERAU), Aerospace Engineering, FL

Despite recent advances, the response of turbulent boundary layers subject to systematic space-time perturbations at the wall remains an outstanding basic science task. This work seeks to bridge this gap by studying the response of turbulent boundary layers that are systematically perturbed at the wall both in space and in time. The perturbations are applied via surface deformations that result in traveling wave-like perturbations at the wall (see Fig. 1). The unique aspect of this work is the use of an actuating strategy that utilizes wall deformations to generate space-time (or traveling wave-like) perturbations at the wall. Th
and oblique waves to be gener

Actuating Strategy - The present approach is to use solenoid actuators to generate surface traveling wave-like perturbations at the wall. Each of these actuators, when deformed, generates a "Gaussian bump" at the wall. Hence, these actuators generate a discretized version of traveling waves which are essentially a "wobbly wall" (see Fig. 1). Each actuator has a spring-loaded shaft that is actuated by a solenoid. The actuators push against a flexible surface, generating the surface bump. An array of these actuators are then used and operated in conjunction to generate the surface deformations. In the first year of this work, most of the focus was on conceptualizing and developing the actuation strategy. This included the following tasks, considering carefully various flexible surfaces, developing a mechanism to control actualtion height η (seee Fig. 1) by retrofiting solenoid actuators, developing an Arduino based controller etc. Using this strategy, successful actuator arrays were manufactured. Several four-by-four actuators were built and tested. These tests were primarily used to characterize the actuator controller, measure the response of the surface while undergoing displacement, test the quality of the surface finish, investigate if there was any hysteresis, etc. A video of one such array in action was previously communicated to the program manager. For the purpose of an upcoming conference (APS DFD 2024), a single line of five actuators was built. A single actuator was actuated to characterize the perturbation generated by an isolated actuation. Some preliminary results are presented here.

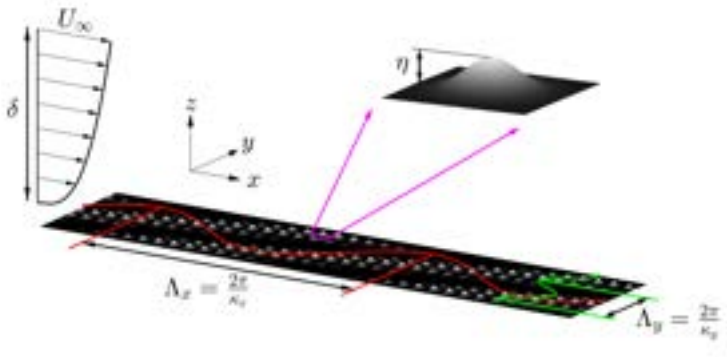

Figure 1: Schematic showing travelling-wave-type, space-time perturbations generated by discrete wall deformations.

Preliminary Results - A single actuator that formed part of an array was actuated while placed on the wall of a zero-pressure gradient boundary layer. The actuator was mounted at a location where the nominal smooth wall friction Reynolds number of the turbulent boundary layer was $Re_\tau \approx 2475$. The actuator was adjusted to provide a maximum surface perturbation of $\eta^+ \approx 23$ (0.64 mm). The frequency of actuation was $f_a = 0.85$ Hz. Hot-wire anemometry was used to carry out measurements of the velocity field at several downstream locations. These measurements were carried out while the surface was being

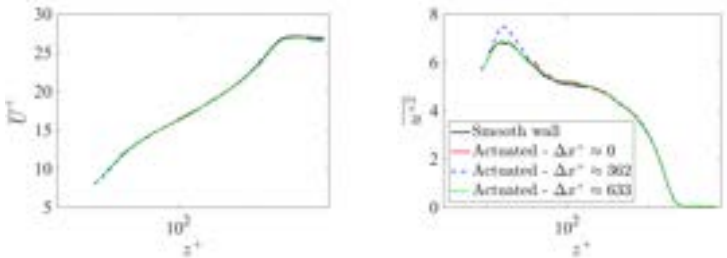

Figure 2: (right) Mean velocity and (left) turbulence intensity profiles at various downstream locations (Δx) while the surface was being actuated. The smooth wall profiles are shown for reference.

actuated. This included a location directly over the actuated surface ($\Delta x = 0$ in the figures). However, directly over the deformed surface, due to the deformation of the surface, measurements close to the surface were not carried out to avoid damage to the how-wire sensor. Smooth wall (no actuation) measurements were also carried out for reference. The inner-scaled mean velocity profiles $\overline{U}^+$ at several downstream locations are shown in Fig. 2. It is clear that there was no significant change in the mean velocity profile while the surface was being actuated. The corresponding inner-scaled turbulence intensity profiles are shown in Fig. 2. In this case, at the most upstream location ($\Delta x^+ \approx 362$), there is a clear increase in turbulence intensity at the location of the inner peak. At further downstream locations, there is no discernible difference in the turbulence intensity profiles when compared with the smooth wall.

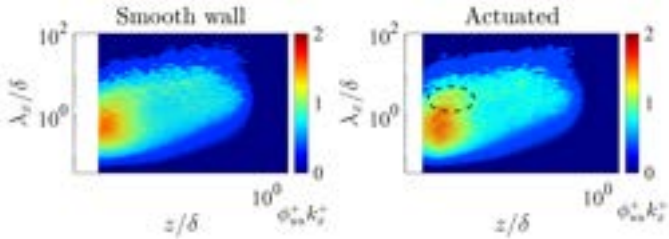

Figure 3: Pre-multiplied one-dimensional energy spectra in the case of the flow over smooth wall (left) and that about $\Delta x^+ \approx 362$ behind the actuated surface (right).

The pre-multiplied one-dimensional energy spectra $\phi^+_{uu}k^+_x$ for the flow over the smooth wall is shown in Fig. 3 (left). Here, k_x is the streamwise wavenumber. The corresponding spectra for flow behind the actuated wall are shown in Fig. 3 (right). This spectra was measured about $\Delta x^+ \approx 362$ downstream of the actuated surface. It is clear that there are no significant changes in the overall spectral content. However, an area of increased energy was observed (highlighted by the black ellipse). This was at a wall-normal location of $z^+ \approx 18$. This is close to the location of the inner peak, which explains the increase in turbulence intensity in Fig. 2. However, these scales had a larger wavelength ($\lambda_x = 2 - 4\delta$) than th

To obtain an estimate of the average perturbation caused by a single actuation, a phase average of the velocity field $\hat{U}^+$ was calculated. Here, the average was calculated from the onset of actuation, capturing a complete up-and-down motion of the surface. The phase averaged mean velocity fields at several downstream locations are shown in Fig. 4. Note that the vertical ordinate is in logarithmic scale. It is clear that the primary perturbation caused by the actuation is a low-speed region in the near-wall region. This is seen as a blue "blob" in Fig. 4. Fig. 4 also shows the clear downstream convection of this perturbation. This low-speed region was confined to wall-normal locations that lie below $z^+ < 100$. In a temporal sense, the perturbation lasts about $\Delta t^+ \approx 1120$. The strength of the perturbation is also seen to rapidly dissipate with increasing downstream distance. The footprint of this perturbation is barely visible at a downstream location of $\Delta x^+ \approx 1265$ (Fig. 4(bottom)). The strength of the perturbation was about twice the friction velocity at its maximum. Note that Fig. 4(top) is saturated to maintain a constant colormap level across all three contour maps. Hence, to summarize, a single actuation resulted in an average perturbation that persisted for about 1200 viscous length and time scales while being confined to the near-wall region.

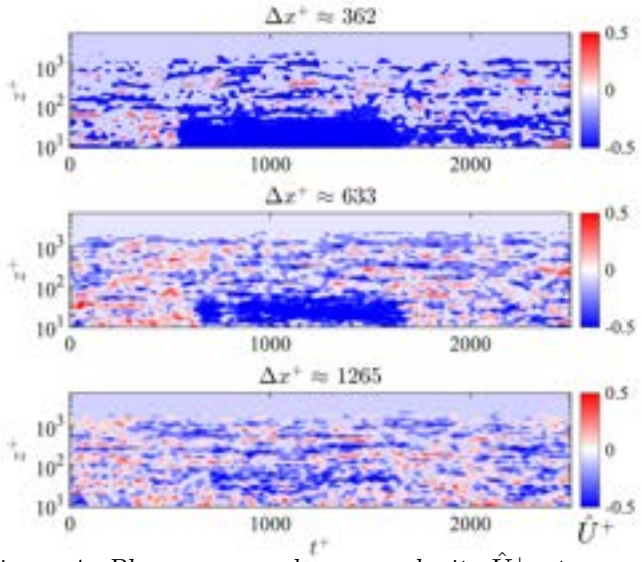

Figure 4: Phase averaged mean velocity $\hat{U}^+$ at several locations downstream (increasing from top to bottom) of the actuation location.

1 Motivation

The goal of the project is to harness phononic materials for unsteady aerodynamic flow control, by combining high-fidelity computation, design, and experiments. Comprehensive control of aerodynamic phenomena is crucial for the design of maneuverable and disturbance-robust unmanned aerials vehicles (UAVs). Yet, such a control paradigm remains elusive because the associated dynamics are high-dimensional, nonlinear, and exhibit a challenging range of space and time scales. *Phononic materials* are periodic media that support tailored frequency-dependent dynamics and offer a compelling paradigm for *passively adapting to and thereby controlling unsteady aerodynamic flows*, which are driven by shear layer and vortex shedding processes with characteristic frequency content. Figure 1 conceptualizes our vision for *phononic flow control* in a next-generation aircraft. We note that beyond this aim, phononic flow control has broad-reaching implications in Air Force-relevant problems driven by characteristic frequency signatures, including flutter instabilities, resonant cavity scenarios and hypersonic flight. We also highlight that this program is part of an ongoing collaboration with AFRL RXAS/RQ, in which experiments, simulations, and phononic material modeling to understand phononic flow control in a transitional boundary layer flow over a flat plate. Our focus on an airfoil configuration and consideration of different phononic material behaviors provide synergistic insights into this burgeoning interdisciplinary topic. Moreover, we hold periodic meetings to exchange computational methodologies, fabricated materials, and key scientific results.

Figure 1: Concept of *phononic flow control* for next-generation UAVs.

2 Objectives

Our objectives are to (i) use accurate computations to determine how phononic materials interact with nonlinear, unsteady aerodynamic flows and synthesize dimensionless parameters that capture key response properties, (ii) explain the coupled structure-flow dynamics by an analysis of representative flow behavior (such as vortex shedding) and behavioral regimes of the phononic materials (such as propagating and stop bands), (iii) fabricate realistic phononic materials that respond at the relevant timescales determined valuable for flow control, with appropriate lengthscales of the targeted aerial vehicles.

3 Results summary

Row 1: A configuration was constructed and studied, enabling meaningfully designed reduced-order models of phononic materials to be integrated into canonical aerodynamic flows. We focused on a "grounded" phononic material (zoomed insert) to force the desired band gap resonance to be the first structural mode. The need to place this lower resonance mode in the band gap is a result of the near-constant component in the lift force, which preferentially excites the first mode of the structure. We discovered the need for a grounded phononic material to interact with aerodynamic flows, and published it at AIAA SciTech 2024.

Row 2: A key insight of the past year was to move away from "raw" structural parameters such as structural mass and stiffness parameters (left schematic and matrix), and instead synthesize non-dimensionalized parameters that allow for systematically tuning the structure based on the fluid-structure interaction (FSI) it induces. These parameters (right side of figures) are the frequency of the structural mode in the band gap, that mode's associated spatial decay rate, and the effective quasistatic stiffness of the structure.

Row 3: Ongoing studies are testing this set of synthesized structural parameters based on their effect on the FSI. High-fidelity FSI simulations were performed on different groups of raw structural parameters, each varied so that they feel within one of five groups of dimensionless parameters (left plot). The resulting mean lift varied by less than 5% of the average mean lift for that group, demonstrating that the overall dynamics are well captured by the proposed non-dimensionalization (right plot).

4 Future work

We are pioneering the use of meaningful dimensionless parameters that enable systematic tuning of the FSI. This effort is in its infancy, and must be further developed particularly as structural models become

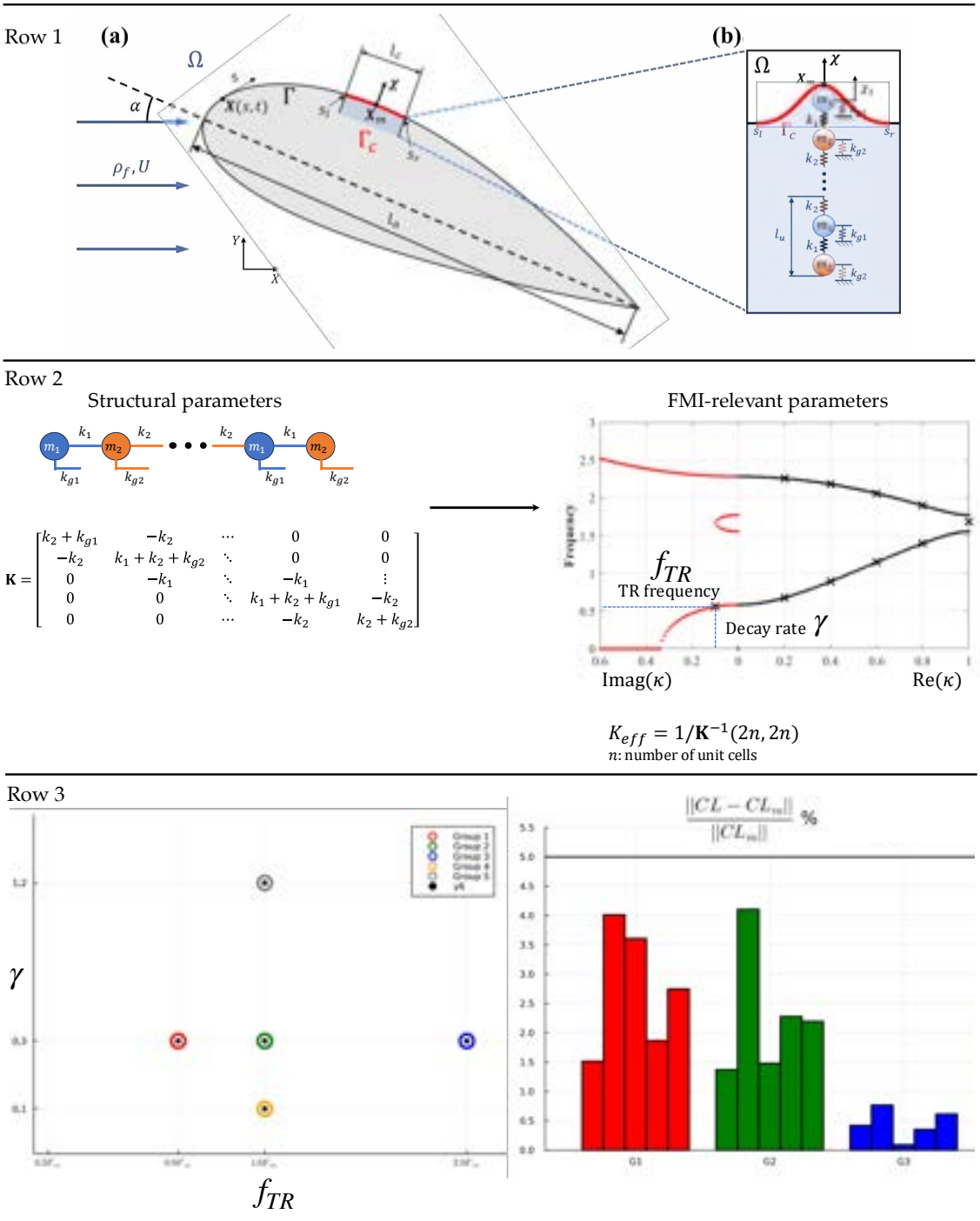

increasingly complex (e.g., continuum models or integrating structural nonlinearity). Future efforts could also continue to identify the most useful reduced-order structural models (e.g., incorporating canonical nonlinearity or considering defect-induced structures with grounding springs) that can be integrated into aerodynamic flows.

MURI: Fluid-Metamaterial-Interaction to Revolutionize Passive Control of Aerodynamic Flows
2024 Annual Summary for AFOSR FA9550-23-1-0299, PO Dr. Gregg Abate
PI Kathryn Matlack, University of Illinois

Abstract: This MURI program aims to establish the field of fluid-metamaterial interaction (FMI) that will discover new fluid-structure coupling between innovative materials and critical aerodynamic flows to enable passive control of transition delay, drag reduction, and separation. The program is driven by the underlying scientific question of how distinct classes of metamaterials interact with dynamics of dominant flow coherences in turbulent flows, and how these interactions are affected by porosity and surface texture. In 2023-2024, the FMI MURI program investigated five different highly collaborative and multi-disciplinary projects aligned with the program goals and objectives. The team made significant progress in developing experimental capabilities to probe FMI, designing, fabricating and testing initial metamaterials for FMI, experimentally probed multi-stable metamaterial interactions for turbulent boundary layer drag reduction and separation control, experimentally analyzed modal instabilities interacting with wall oscillations to learn bounds for FMI parameters, explored passive, adaptive separation control via flow-induced surface morphing, and developed computational capabilities for FMI and immersed boundary (IB) methods in turbulent flows. Below is an overview of representative results from the team's collaborative efforts.

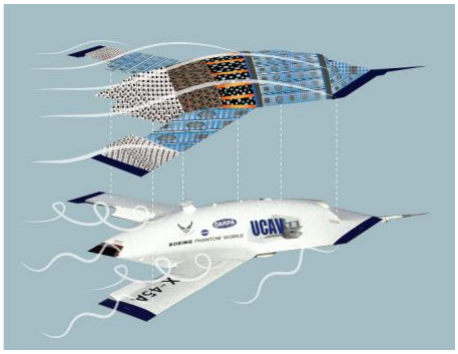

Coupling of Wake Vortex and Wall Vibration Modes: A canonical experiment was developed to investigate the interaction between prominent narrow-band flow features and prescribed vibration of local wall surfaces. The von Karman vortex street (KVS) produced in the wake of a cylinder was used to introduce vortex structures of known frequency scales, which was configured to interact with a nearby wall surface configured with an integrated shaker system for direct excitation. Measurements were compared with and without direct excitation, at different speeds and KVS frequencies. These experiments provided a basic understanding of relevant frequency scales and amplitudes required for interaction between the fluid-metamaterial surfaces for the design and integration of passive phononic subsurfaces.

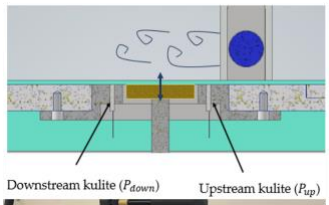

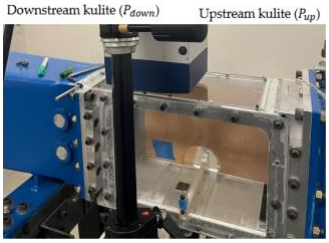

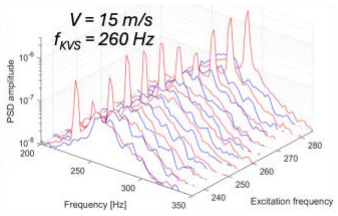

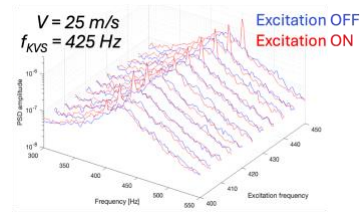

Multi-stable metamaterial interactions for turbulent boundary layer (TBL) drag reduction and separation control: Based on prior successful separation control, we designed and prototyped multi-configuration metamaterials for passive control of a TBL separating over a bump in a low-speed wind tunnel. Surface porosity that could be flipped open and closed and vortex generators that could be deployed and stowed were chosen as multi-configuration, passive control surface structures. To trigger the deployment of these structures, surface force signatures robustly associated with separation of a TBL over a bump were estimated from

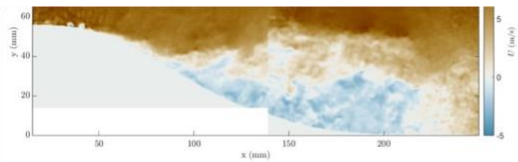

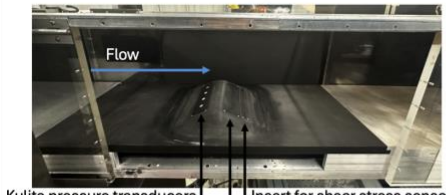

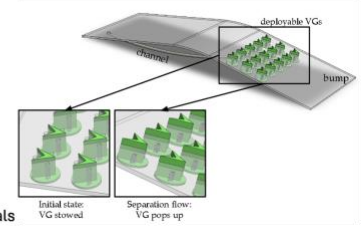

literature and computational data. Two robust separation signatures were identified that could trigger the configuration change: the pressure difference between the upstream and downstream surfaces of the bump, and the skin friction on the downstream surface of the bump. The multi-configuration metamaterials were designed to respond to these signatures, deploying vortex generators or opening porosity when the separation force signature was felt by the structure and returning to a stowed configuration under the force of the attached force signature. The structures were prototyped and tested outside the wind tunnel to characterize their force response and deployment. A flat plate - bump configuration was designed to enable multiple surface sensor measurements and the installation of multi-configuration metamaterials. The bump was manufactured and installed in the TBL facility at UIUC. Measurements of the surface pressure and skin friction of a TBL passing over the bump at multiple Reynolds numbers are on-going. Final measurements will be used to finalize the design of the metamaterial structures for implementation in the wind tunnel.

Computational capabilities for IB method in turbulent flow: We derived an IB resolvent method for streamwise-spanwise-temporal homogeneous flows that extends the traditional resolvent method to include spatially varying surfaces. We incorporated an IB formalism within resolvent analysis commonly used to analyze and model turbulent wall-bounded flows, respecting homogeneous directions to facilitate fast transforms be taken where possible. The IB formulation was tested for walls with periodic variation in one direction but is agnostic to the specific wall motion. In addition to this reduced-order design framework, we are building a fully coupled, high-fidelity computation framework for FMI simulations. To this end, we implemented the IB projection method in an existing 3D turbulent flow solver, including new improvements that include significantly more robust computation of surface stresses that will be key to the FMI settings to be considered. Ongoing algorithmic improvements are further reducing the computational cost and robustness of the IB algorithm.

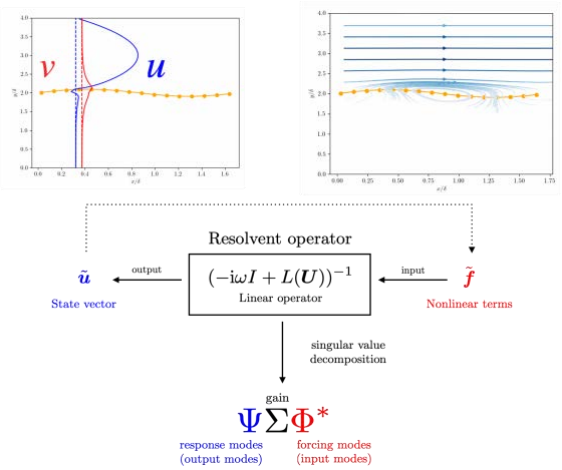

Interaction between resonant phononic materials and turbulent flows: We quantified the FMI of a turbulent channel flow with phononic subsurfaces with localized defect modes, which showed a possibility of up to 1% drag reduction. As a point of reference for the FMI studies, we first conducted a parametric computational study using a minimal flow unit to determine the length and time scales relevant for turbulent drag reduction, using harmonic blowing and suction boundary conditions. Based on these results, we designed, modeled, and analyzed band gap resonances in resonant phononic materials (RPMs) that aligned with the critical time scales from the blowing/suction cases. Then, we developed a loosely coupled solver that extracts pressure at the wall, imposes this as a forced boundary condition to simulations of the defect-mode-based RPM, from which the velocity response is extracted. This velocity response is used as a blowing and suction boundary condition back in the turbulent flow simulations. Initial simulations of a turbulent channel flow with this closed-loop control demonstrated a ~1% reduction in skin friction drag for certain RPM frequency parameters.

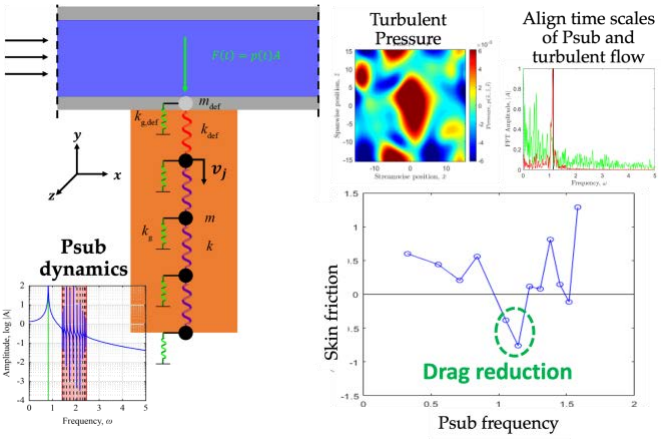

Understanding Vortex-Turbulent Boundary Layer Interactions to Mitigate Separation Using Textured Surfaces

(1-Aug-2023 – 31-Jul-2024)

Research Objectives

The overarching goal of the proposed research is to identify flow physics-based pathways to develop surface-texture-based strategies that mitigate turbulent boundary layer (TBL) separation over aerodynamic surfaces when subjected to an external perturbation. We propose coordinated and collaborative experiments that focus on two basic science aspects of flows over smooth- and textured-surfaces - (a) the structural response of a TBL subjected to a controlled pressure perturbation, led by PI Pathikonda at Arizona State University, and (b) the ensuing large-scale, unsteady aerodynamic response over an airfoil, led by Co-PI Raghav at Auburn University. Specifically, we consider a boundary layer interaction with an advecting vortex that can impose a temporally transient adverse pressure gradient on the boundary layer. For Year-1, we proposed: (1) development of a Convecting Rotating Cylinder (CRC) system where a rotating cylinder imposes a pressure-perturbation on a boundary layer developing over a flat-plate, and (2) development of Vortex Generator system that generates a line-vortex interacting with a stationary airfoil at high Angle of Attack (AoA). We aimed at examining the boundary layer response over both flat plate (at high Reynolds numbers) and of the airfoil using high-frequency wall-pressure measurements and PIV.

Outcomes of Research Activities in Year-1

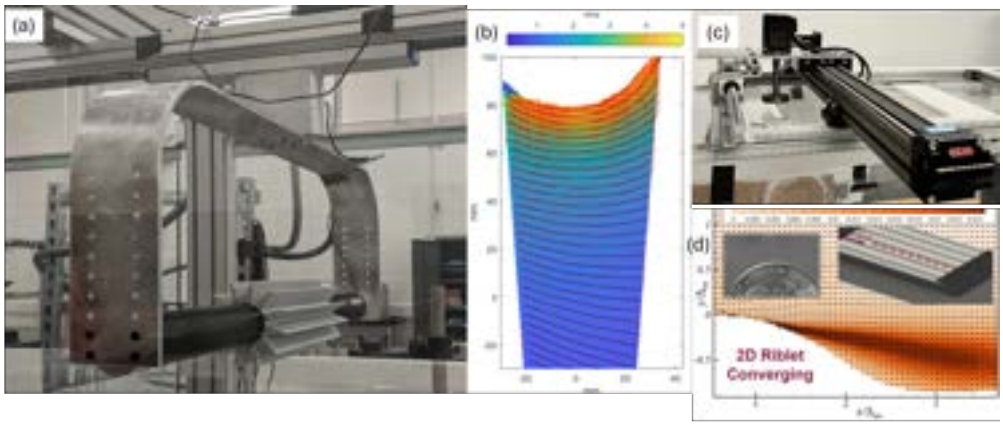

Figure 17: (a) CRC mechanism, (b) induced axisymmetric flow (small fins), (c) pitching-plunging vortex generator system and (d) separation shear-layer TKE over converging/LMP region.

Construction and Characterizing of CRC Mechanism: The main objective of the CRC is to create a controlled unsteady pressure pulse of travelling kind to represent vortex-wing interactions, in-ground effects (IGE), etc. This is performed using a rotating cylinder mounted on a fast-actuating linear-translation system driven by a servo motor, as shown. As part of Year-1 activities, we designed, constructed and installed the system inside the wind-tunnel test section to test the imposed pressure and flow perturbations under stationary conditions. The primary goals of characterization were to maximize the pressure perturbation on the wall, while minimizing the turbulence induced in the free-stream flow. Wall-pressure and planar PIV measurements were performed to this end, at varying distances from the wall, h/D (where D is the cylinder diameter), rotation speeds (RPMs) and cylinder fin-geometries. After

iterating over multiple fin configurations, it was concluded that the small-fin configuration (fin height 0.12 in) produced the most axisymmetric velocity field and minimal disturbance to the flow away from the cylinder, while also inducing strong azimuthal velocities.

Design and construction of vortex generator: The objective of this task was to generate well-characterized line vortices that advect downstream and impose a pressure perturbation on a high-AoA test airfoil. The vortex generator was based on a pitching-plunging airfoil mechanism that are controlled via independent servo motors. This system was designed, constructed and the ensuing vortex-flow was characterized in a wind-tunnel in this activity. Flow visualization experiments identified that, while the mechanism generated large votices of desired orientation, the high pitching-rate required to achieve the tightly-rolled vortex necessary for the research objectives could not be reliably achieved using the servos. For this reason, PIV experiments in a water-tunnel facility using the system are currently being planned, without altering the flow parameters.

Unsteady pressure measurement capabilities: The goal of this outcome was to develop unsteady pressure measurement capabilities to characterize both the imposed pressure perturbation, $\tilde{p}(t)$ and the unsteady response of the boundary layer over the airfoil. The efficacy of using surface pressure taps to measure unsteady pressure fluctuations on the airfoil was analyzed using a flat-plate setup. Unsteady pressure fluctuations were generated by a propeller assembly placed upstream of the flat plate such that the pressure ports on the flat plate aligned with the tip of the propeller blades. For the range of velocities and perturbation frequencies studied, we found that the pressure fluctuations of interest ($\sim \mathcal{O}(\delta/U_\infty)$) underwent consistent frequency-dependent attenuation and phase-lag which can be corrected for. We are currently building a system that can provide a repeatable impulse pressure pulse to the port, using which we can compute the transfer function.

Preliminary characterization of CD riblets and separation: We performed preliminary characterization of converging-diverging riblets and the role of boundary layer 3-dimensionality in altering the separation behavior. The primary goal of this activity was to ensure that the riblets can be manufactured reliably, and to confirm our hypothesized behavior of the boundary layer separation – that the differential stability of the boundary layers will result in drastically different separation behaviors. This was reinforced and quantified in this study, where the separation over the converging/low-momentum regions and the diverging/high-momentum regions show a significant difference in the separation behavior. Despite being only $\delta/2$ apart in spanwise direction, they exhibited $> 30\%$ in the turbulence kinetic energy in the separated shear-layer. This demonstrated that the boundary layer separation significantly amplifies the boundary layer three-dimensionality.

Plans for Year-2

The characterization of the CRC mechanism (with translation and relative velocity between the cylinder and the incident stream) and of the vortex generator will be completed. While the small-fin CRC configuration induced small pressures when stationary, we expect this to be amplified with relative velocity between incident stream and the cylinder, owing to the strong azimuthal flow and circulation induced by the rotating cylinder. The vortex generator translation to water-channel is currently underway, and will be finished in Q1 of Year-2. This is followed by identifying the smooth-wall boundary layer response and separation tendencies when subjected to the perturbations over both flat-plate and over an airfoil.

AFOSR FA9550-23-1-0762: Separation Control using Resonant Metamaterials
FY 2023-2024 progress summary

PI: Yulia Peet (Arizona State University)
Collaborators: Lorenzo Valdevit (UC, Irvine) and Kenneth Breuer (Brown University)

First year objectives:

1. Establish a computational model and initiate experimental investigations of a turbulent flow over a backward-facing step.
2. Identify the optimum responses (phases and gains) for metamaterial subsurfaces to interact successfully with fluid flows.
3. Develop a numerical framework for design of metamaterials to interact with fluid flows.

Work performed towards achieving the first-year objectives:

1. Computations and experiments of flow over a backward-facing step.

Computational investigations**:**

1) A computational model based on Direct Numerical Simulations (DNS) with a Spectral Element code (Nek5000) has been established to compute a turbulent flow over a backward facing step (BFS).
2) The model was executed successfully in a regime of a laminar boundary layer inflow (a parabolic inlet velocity profile) at a step Reynolds number of Re_h=3000 (corresponding to a reference paper by *Shäfer, Breuer & Durst JFM 2009*) and results are in good agreement with this paper.
3) However, to establish a more realistic benchmark case and to conform to experimental conditions, a turbulent boundary layer inflow is desired. The work is currently being done to establish a turbulent boundary layer inflow condition in a numerical model. This will likely be achieved via an overlapping grid methodology developed previously by PI Peet in Nek5000, where an auxiliary turbulent channel flow computation will feed into a BFS domain in a multidomain simulation setting.
4) The benchmark case for validation of the DNS data and the conforming experiments for a backward facing step has been selected (Re_h=5100, based on the paper by *Le, Moin & Kim JFM 1997*). The numerical and experimental results will be compared to each other and to the reference paper prior to augmenting the setup with fluid-structure interaction and cyber-physical models of interaction of the BFS flow with metamaterials.

Experimental investigations**:**

The experimental rig for characterizing the baseline (uncontrolled) flow has been designed and fabricated. It can be installed into the Brown University water tunnel and is compatible with the PIV system already installed there. It allows for us to replicate the

baseline flow (Re ~ 5000) and to measure the turbulent flow and reattachment characteristics. Experiments to characterize the flow will commence in September. The conceptual design of the cyber-physical surface has been started, although the detailed requirements and implementation are still tasks for the coming year.

2. **Identification of the optimum responses (phases and gains) to be used by adaptive surfaces to interact successfully with fluid flows.**

1) A Ph.D. student at Arizona State University, A. Subedi, has been investigating potential approaches for a successful intervention with fluid flows based on surface responses to the time-dependent fluid forces acting on such surfaces (pressure and shear stresses).
2) A DNS computational model has been established to evaluate such “optimum” responses in a turbulent channel flow (with the objective of drag reduction).
3) In our preliminary model, frequency-selected approaches have not yet been considered (a feedback law based on a fixed gain with respect to a measured shear stress was applied at every time instance). Future work will focus on selection of the optimum frequencies (an abstract submitted to AIAA SciTech 2025, see a dissemination section of this document).
4) Similar approaches will be extended to a flow separation control in the Year 2 of the project.

3. **Development of a numerical framework for design of metamaterials to interact with fluid flows.**

1) At UC Irvine, a postdoctoral researcher, Priyambada Nayak, has initiated a development of a computational model to design metamaterials to interact with fluid flows.
2) A model is based on a finite-element method and will allow us to investigate both the unit cell and the finite system configurations.
3) This task will interact closely with Task 2 to fine-tune metamaterial design based on the gains and frequencies identified as beneficial for flow control via DNS simulations.

Dissemination:

A. Subedi and Y. Peet, ``Turbulent Flow Control using Wall Sensing", AIAA paper 2024-3868, AIAA Aviation and Aeronautics Forum and Exposition, Las Vegas, NV, July 2024

A. Subedi and Y. Peet, ``Frequency-Tuned Approaches to Wall Transpiration Control", AIAA SciTech Forum and Exposition, Orlando, FL, January 2025, submitted

Project title: Stochastic modeling and analysis of random surface roughness

Progress report: 03/15/2023 - 03/14/2024

PI: Armin, Zare, Department of Mechanical Engineering, University of Texas at Dallas

In the first year of the project, effort has been placed on maturing pre-existing methods in the analysis of spatially periodic surface modulations on turbulent flows. In particular, we explored the efficacy of capturing the dynamics of velocity fluctuations over rough surfaces in the generalized curvilinear coordinate system that allows for an accurate representation of the roughness geometry, especially in scenarios where the immersed boundary method may be challenged. The immersed boundary method, which we had used in our earlier work on reduced-order modeling of riblets [1], offers a computationally efficient alternative to the use of stretched meshes, but its successful implementation often requires ad hoc parametric tuning and it ultimately results in approximate solutions that may not strictly adhere to no penetration boundary conditions, especially over sharp-tipped roughness (e.g., semi-circular riblets). Furthermore, its utility is challenged when modeling near-surface dynamics of thin boundary layers associated with high-speed flow regimes of interest to the Air Force. Our work is enabled by a transformation of the coordinate system given by

$$x \;=\; \tilde{x}, \quad y \;=\; F(\tilde{y},\tilde{z}) \;:=\; \frac{2\tilde{y}-f(\tilde{z})}{2-f(\tilde{z})}, \quad z \;=\; \tilde{z}$$

to map the wall-normal dimension $\tilde{y} \in [-1+f(\tilde{z}), 1]$ to $y \in [-1, 1]$. This transformation allows for an accurate representation without the need for a stretched mesh or excessive parametric tuning of the immersed boundary. Nevertheless, it reflects the spatial periodicity of the boundary conditions onto the differential operators and thereby convolutes the structure of the linearized dynamics by virtue of the chain rule. To further reduce the computational complexity of our simulation-free framework, which uses Lyapunov theory for linear systems to bypass the need for stochastic simulations, we have employed a perturbation analysis in the height of riblets (α) to arrive at a sequence of computationally efficient equations that can be solved to capture the flow physics. To the best of our knowledge, a perturbation analysis, which opens the door to higher resolution flow analysis, has not been offered examining the effect of riblets prior to our work.

To demonstrate the ability of our methodology in predicting drag-reduction trends in accordance with prior experimental [2] and numerical studies [3], we focus on the more challenging case of turbulent channel flow with $Re_\tau = 186$ over semi-circular riblets with height to spacing ratios of $\alpha/s = 0.55 \sim 1.2$ and different spatial frequencies. The riblets' height is restricted to $\alpha \leq 0.1$ to ensure the validity of our perturbation analysis. We show that all drag reduction trends obtained from our Lyapunov-based simulation-free analysis of the reduced-order model fall within the envelope of prior experimental and numerical studies and uncover a consistent parameterization for the "optimal" roughness geometry. We also capture up to 10% suppression in the kinetic energy of the flow for optimally spaced riblets [4]. Small riblets, i.e., those with small groove cross-sectional area, have been shown to induce drag reduction; see, e.g., Ref. [3]. However, for sizes beyond a generally agreed-upon optimal, drag reducing properties decrease. While there is little consensus on the cause for this reversal in drag reducing capabilities, prior studies have contributed it to one of two physical mechanisms: (i) the appearance of long spanwise rollers induced by the Kelvin-Helmholtz instability [3]; or (ii) the downward lodging of streamwise vortices into riblet grooves, which would increase the drag by adding to the overall wetted area [5, 6]. Below, we summarize the capability of our reduced-order models in uncovering such underlying flow mechanisms in the flow over larger riblets.

The presence of the Kelvin-Helmholtz instability can be identified by inspecting the spectral content of the turbulent flow. For larger riblets, highly amplified regions appear for $\lambda_x^+ \approx 175$

and $\lambda_z^+ \gtrsim 100$ in the energy spectra corresponding to all velocity components, in addition to the streamwise-wall-normal shear stress, which signify very wide flow structures reminiscent of the spanwise rollers that are triggered by the Kelvin-Helmholtz instability. On the other hand, the absence of such regions of pronounced amplification from the energy spectra of flow over small- and optimally sized riblets leads us to believe that in those cases, the Kelvin-Helmholtz instability does not prevail the flow dynamics. Finally, by examining the one-dimensional energy spectrum, we observe the wall-normal extent of the very wide spanwise structures to reside within the viscous sublayer and their dominant streamwise wavelengths to become slightly longer for progressively larger riblets, which is also in agreement with prior studies [7, 8].

We also investigated the effects of large semi-circular riblets on various features of the near-wall regeneration cycle. To this end, we focused on the length-scales associated with the near-wall cycle, and extracted the different velocity components from the dominant eigenmode of the steady-state covariance matrix of our reduced-order model. From the visualization of these modes, we first recognize that the streamwise and spanwise velocity components tilt away from the wall, which gives rise to quasi-streamwise vortices [9]. We observe that the presence of large sharp riblets can skew regions of high and low streamwise velocity within the viscous sublayer. As prior studies have also pointed out [10, 11], this is due to the interaction of near-wall turbulence with the spanwise periodic surface corrugation, which results in secondary flow contributions in enhancing cross-flow fluctuations in the roughness sublayer. On the other hand, for small riblets, we observe that the spanwise movements of near-wall streamwise vortices are restricted by interactions with their tips. In agreement with other studies, we found this to be especially prevalent when the spanwise spacing of riblets is less than the width of these vortices [6]. This phenomenon, which weakens the quasi-streamwise vortices, is itself known to result in drag reduction [9]. When the width of the streamwise vortices is smaller than the riblet spacing, these structures are allowed to lodge into the riblet valleys and directly interact with the surface.

Our ongoing effort is focused on obtaining a diagnostic model relating the geometric parameters of riblets to a drag coefficient. A data-driven method will be employed to extract such a model from results already obtained throughout our project and those available on the roughness database (http://roughnessdatabase.org/). Our model will be compared against existing models proposed for random roughness distributions. As an alternative approach to reduced-order modeling of roughness, we are also engaged in the direct characterization of roughness effects on the mean flow and thereby linearized dynamics.

As a byproduct of the theoretical work on input-output analysis of stochastic base flow uncertainty [12–14], which constituents another essential element in the analysis of random surface roughness, we have studied the effects of base flow velocity and temperature variations in a transitional high-speed compressible flow configuration [15]. Specifically, we have investigated the stability of laminar flows near leading edges and nose tips that have been shown to undergo an early transition to turbulence at supersonic and hypersonic free-stream speeds both in flight and wind tunnel conditions. Our analysis reveals that small amplitude near-wall perturbations of the base flow velocity can compromise the mean-square stability of the laminar flow. We also provide insights into how changes in different physical parameters, such as the temperature of the wall and its curvature, influence the mean-square stability of the fluctuation dynamics. We show that increasing the leading edge radius and decreasing the wall temperature can significantly deteriorate the robustness of laminar flows in the presence of base flow variations. Our approach offers a systematic framework for quantifying the influence of base flow uncertainties that can appear from stochastic sources (e.g., surface roughness and background turbulence) and are unavoidable in experiments in transitional high-speed flows.

Bibliography

[1] W. Ran, A. Zare, and M. R. Jovanovic, "Model-based design of riblets for turbulent drag reduction," *J. Fluid Mech.*, vol. 906, p. A7 (38 pages), January 2021.

[2] D. W. Bechert, M. Bruse, W. Hage, J. G. T. V. der Hoeven, and G. Hoppe, "Experiments on drag-reducing surfaces and their optimization with an adjustable geometry," *J. Fluid Mech.*, vol. 338, pp. 59–87, 1997.

[3] R. García-Mayoral and J. Jiménez, "Hydrodynamic stability and breakdown of the viscous regime over riblets," *J. Fluid Mech.*, vol. 678, pp. 317–347, 2011.

[4] M. Naseri and A. Zare, "Modeling turbulent channel flow over riblets using change of coordinates," in *proceedings of the 2024 AIAA Aviation Forum and ASCEND*, 2024, p. 3715.

[5] D. Goldstein and T.-C. Tuan, "Secondary flow induced by riblets," *J. Fluid Mech.*, vol. 363, pp. 115–151, 1998.

[6] S. J. Lee and S.-H. Lee, "Flow field analysis of a turbulent boundary layer over a riblet surface," *Experiments in fluids*, vol. 30, no. 2, pp. 153–166, 2001.

[7] A. Chavarin and M. Luhar, "Resolvent analysis for turbulent channel flow with riblets," *AIAA Journal*, pp. 1–11, 2019.

[8] S. Endrikat, D. Modesti, R. García-Mayoral, N. Hutchins, and D.Chung, "Influence of riblet shapes on the occurrence of kelvin–helmholtz rollers," *J. Fluid Mech.*, vol. 913, p. A37, 2021.

[9] J. Jiménez and A. Pinelli, "The autonomous cycle of near-wall turbulence," *J. Fluid Mech.*, vol. 389, pp. 335–359, 1999.

[10] D. Goldstein, R. Handler, and L. Sirovich, "Direct numerical simulation of turbulent flow over a modelled riblet covered surface," *J. Fluid Mech.*, vol. 302, pp. 333–376, 1995.

[11] S. Endrikat, R. Newton, D. Modesti, R. García-Mayoral, N. Hutchins, and D. Chung, "Reorganisation of turbulence by large and spanwise-varying riblets," *J. Fluid Mech.*, vol. 952, p. A27, 2022.

[12] D. Hewawaduge, T. Summers, and A. Zare, "Robustness of variance suppression in channel flows with imperfect transverse wall oscillations," in *Proceedings of the 2021 American Control Conference*, New Orleans, LA, 2021, pp. 292–297.

[13] D. B. Hewawaduge and A. Zare, "The effect of base flow uncertainty on transitional channel flows," in *Proceedings of the 2022 American Control Conference*, 2022, pp. 5050–5055.

[14] D. B. Hewawaduge and A. Zare, "Input-output analysis of stochastic base flow uncertaintys," *Phys. Rev. Fluids*, vol. 7, no. 7, p. 073901 (32 pages), July 2022.

[15] A. Dwivedi, A. Zare, and M. R. Jovanović, "Effect of stochastic base flow uncertainty in transitional high speed compressible flows," in *Bulletin of the American Physical Society*, Washington, DC, November 2023.

Novel Approaches in Flow Control

Fabrication of Fast-Responding, Luminescence-Enhanced micro-Spheres for the Digital Luminescent Particle Tracking Barometry Thermometry and Velocimetry System

Novoselov & Dabiri, University of Washington

Project Motivation: Today's experimental studies of turbulence that use imaging methods are huge improvements over previous single-point measurement techniques. Newer two-dimensional methods, such as Particle Image Velocimetry (PIV), and Particle Tracking Velocimetry (PTV) allow for 2D/3D measurements of time-evolving velocity; however, there are no techniques that can simultaneously provide temperature, pressure and velocity measurements in 2D/3D. Such data would allow us to better investigate turbulent viscous flows such as wakes, jets, shear layers, and turbulent boundary layers under adverse pressure gradients, as well as convection in boundary layers towards better understanding of flow physics, and its use to develop new and accurate physics-based turbulence models. Should the resolution of our methodology permit, we also plan on extending this technique to allow for aeroacoustic studies.

Project Objectives: The overall objective is to fabricate a novel measurement technique capable of simultaneously measuring pressure & velocity, temperature & velocity, or pressure, temperature & velocity within turbulent flow. This will be obtained by achieving the following specific action items:

- Develop fast responding and bright pressure-sensitive nanospheres (PSnSpheres), temperature-sensitive nanospheres (TSnSpheres), and pressure/temperature-sensitive nanospheres (PTSnSpheres), that will be used as flow tracers and pressure/temperature sensors within the flow of interest.
- Using these nanospheres, develop next generation digital luminescent particle tracking barometry, thermometry, and velocimetry (DLPTBTV) measurement system, that would include all data/image acquisition hardware, as well as all post-processing algorithms.
- Perform proof-of-concept experiments by using DLPTBTV to collect data from turbulent wake behind both a heated and non-heated cylinder, and comparing results with data in previously published literature.

Results and achievements: MEL-PSP and preparation of the nSpheres

- We have successfully shown that metal-enhanced luminescence (MEL) can be used to enhance both the brightness and sensitivity of PSP. Our films show a photoluminescence enhancement factor (PLEF) of 2, and a high pressure sensitivity of 0.94 %/kPa for low-speed flow measurements. The camera image (Figure 1a) shows the significantly enhanced photoluminescence of PSP due to MEL. Figure 1b shows that our pressure sensitivity is twice that of the commercialized UniFIB.
- We have begun fabricating nSpheres from which we will construct the PSnSpheres, TSnSpheres, and PTSnSpheres (Figure 2a). This structure exhibits photoluminescence ~15 times stronger than a sol-gel film with the same dye concentration and 80 times stronger than simply adsorbing the dye onto SiO_2 nanospheres (Figure 2b).
- We have successfully set up a pressure chamber for pressure calibration, the shock tube for response time measurements, the image acquisition system about our low-Speed wind tunnel (0-80 mph), and written data processing algorithms.

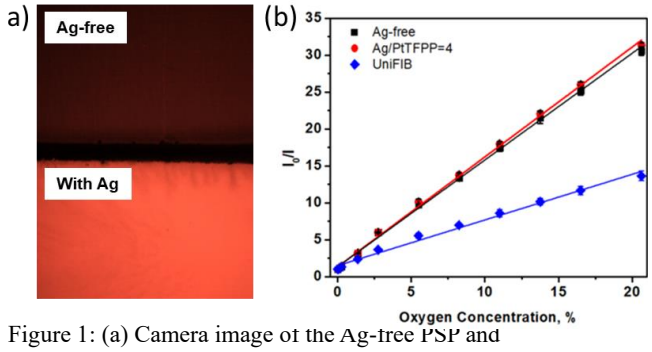

Figure 1: (a) Camera image of the Ag-free PSP and 95nmAg@5nmSiO2 incorporated MEL-PSP coated on an air foil

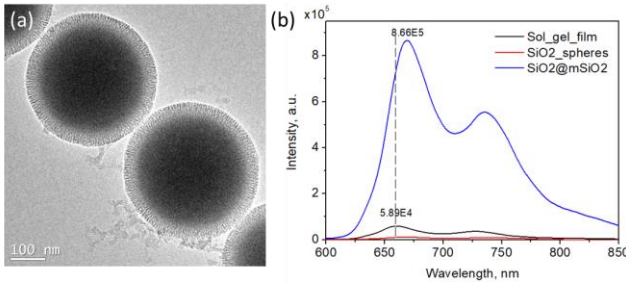

Figure 2: (a) TEM image of the SiO_2@mSiO_2. (b) PL spectra of PtTCPP in a sol-gel film, SiO_2 nanospheres, and SiO_2@mSiO_2.

Results and achievements: Application of MEL-PSP to low-speed flow measurements

In order to perform an interim test on our achievements thus far, we created two test articles to be tested in our low-speed wind tunnel, a flat plate and a NACA 0012 airfoil. For brevity, we will only show results as a measure of our success for flow over the forward section of a NACA 0012 airfoil at 5° angle of attack with an impinging free stream velocity of 60 mph.

- Figure 3 and Figure 4 show results for 60 mph flow over the airfoil at $\alpha = 5^{\circ}$. The surface pressure visualization of the conventional PSP for the forward portion of the airfoil appears noisy, with a variety of patches of pressure across the model not demonstrating any clear trend, as shown in Figure 4. The pressure visualization of the MEL-PSP, however, very clearly demonstrates a drop and rise in pressure, making the identification of the quarter chord a simple task. Since the pressure is expected to change along the chord, the standard deviation (SD) was calculated along the span. The SD of the conventional PSP is significantly higher than that of the MEL-PSP at 1.47 to 0.28 Torr, respectively, an 81% decrease. The pressure traces further confirm these observations as seen in Figure 4. The span-wise pressure trace demonstrates a significantly larger SD for the conventional PSP than that of the MEL-PSP at 3.12 compared with 0.67 Torr, respectively, a 78% decrease, as shown in Figure 4. While both chord-wise pressure traces demonstrate the drop in pressure about the quarter-chord, the decrease is much more noticeable for the MEL-PSP than for that of the conventional PSP.

Disseminated Results

- AIAA publication: Baxter, C.W., Feng, J. Dabiri D. 2024 *"Enhanced Luminescence of Pressure-Sensitive Paint using Metal-Enhanced Luminescence"*, Aviation, 7/29/2024-8/2/2024, Las Vegas, NV.
- Presentation: Baxter, C.W., Feng, J. Dabiri D. 2024 *"Enhanced Luminescence of Pressure-Sensitive Paint using Metal-Enhanced Luminescence"*, Aviation, 7/29/2024-8/2/2024, Las Vegas, NV.
- In preparation: *"Pressure Sensitive Paints with Ag@SiO_2 Metal Enhanced Luminescence and High Pressure Sensitivity"*.

Ongoing and future research

Standardization of experimental setup and procedures

- Building a simultaneous pressure/temperature calibration chamber with their respective controllers.
- Devise a procedure for performing simultaneous pressure/temperature calibrations of our nSpheres using this chamber.
- Devise an injection system for the nSpheres into our low-speed Jet Stream 500 wind tunnel (0-80 mph).
- Purchase a cartridge cylindrical heater and its temperature controller to be installed in this wind tunnel. We will measure the pressure, temperature and velocity field behind this heated cylinder.
- Collect pressure, temperature and velocity field behind a heated cylinder, and compare results with published literature.

Synthesis of TSnSpheres, PSnSpheres, & TPSnSpheres

- Continue fabricating nSpheres by loading dye molecules onto the Ag@SiO_2 NPs and assembling them into microspheres. Two dye-loading routes will be tested: mesoporous coating with EDC/NHS coupling; layer-by-layer assembly.
- Measure brightness, sensitivity and response time of the nSpheres.
- Devise a methodology to mass produce these nSpheres for wind tunnel use.

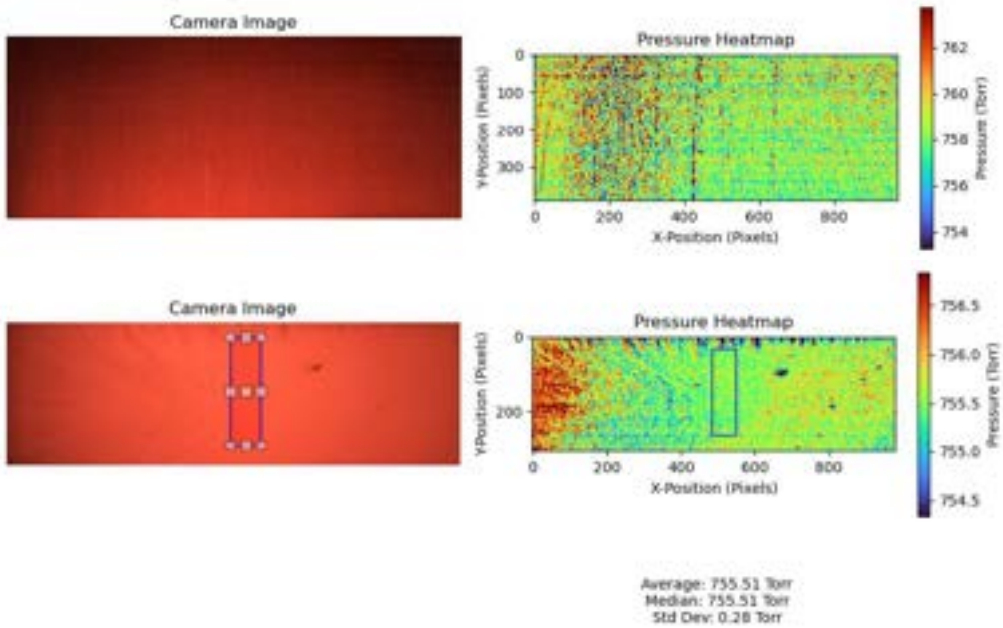

Figure 3: Forward Section of Flat Plate, 60 mph, $\alpha = 5^{\circ}$, Pressure Visualization. Top: conventional PSP; Bottom: MEL-PSP

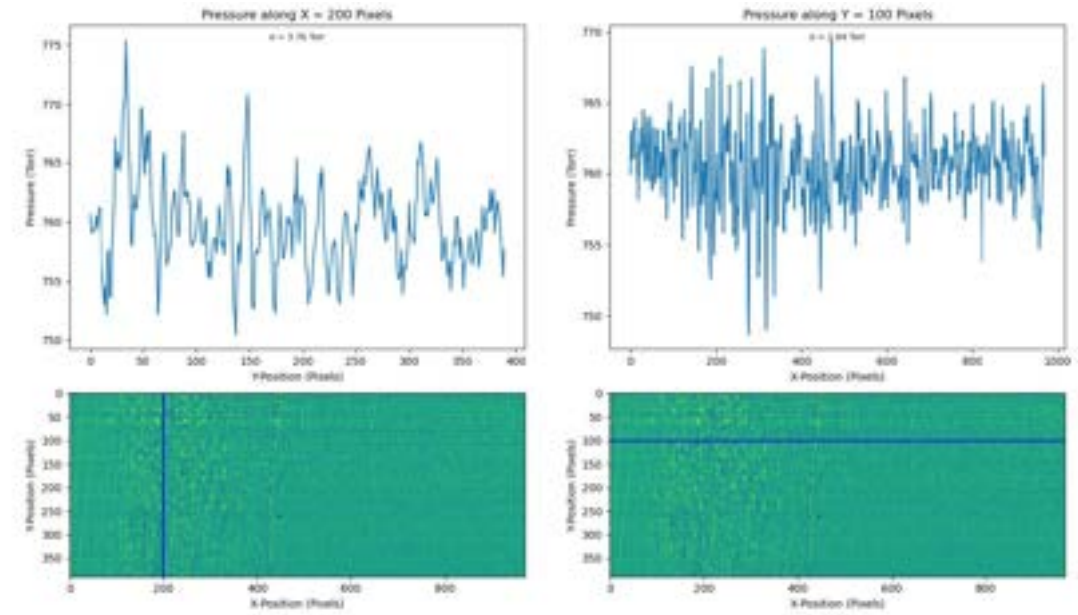

(Top) Conventional PSP

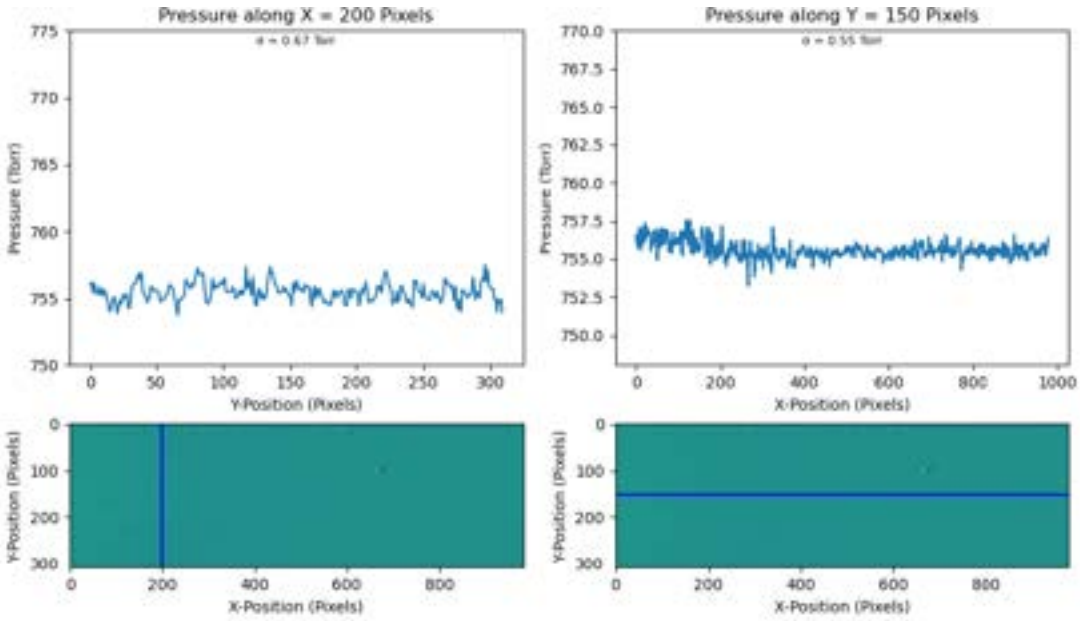

(Bottom) MEL-PSP

Figure 4: Forward Section of Airfoil, 60 mph, $\alpha = 5^{\circ}$, Pressure Trace of Span and Chord. Top: conventional PSP; Bottom: MEL-PSP

Evaluation of Event Cameras for 2D2C Velocimetry

Research Progress for 2023 – 2024
Sidaard Gunasekaran

Objective: The primary objective of this research is to advance the understanding and application of event-based camera technology in fluid flow analysis. This research aims to compare and evaluate the efficacy of three different event-based algorithms from the literature, along with one in-house developed algorithm employed for event-based velocimetry. The results from event-based velocimetry will be compared against the well-established traditional Particle Image Velocimetry (PIV) methods for validation.

Research Progress: The following tasks were completed in the past year to satisfy the objective:

1. Clear SD7003 Wing Fabrication: Several iterations of a transparent SD7003 wing were performed to obtain optical access to the upper and lower surfaces of the wing. In-house resin printing and several resin types from Xometry were used. The final design was printed from Accura ClearVue in high resolution, allowing for clear optical access around the wing. A picture of the clear wing is shown in Figure 1a.

2. Design and Construction of Simultaneous Traditional and Event Camera PIV Test Setup: Proper validation of event-based PIV and traditional PIV requires simultaneous imaging of the same flowfield by a traditional camera and an event camera. As such, a new test setup was designed and constructed in the University of Dayton Water Tunnel that can capture the same field of view using a PCO Dimax and a Prophesee EVK4 event camera, as shown in Figure 1b. A 45° mirror was placed underneath the test section, followed by a 50/50 beamsplitter that splits the intensity of the illuminated FOV in half and directs the light to the PCO and the event camera placed orthogonal to each other. The spatial resolution of the PCO Dimax was 10,000 pix/m, and the event camera was 7,400 pix/m. These spatial resolutions were obtained through dot-plate calibration. Since the event camera operates asynchronously, traditional dot-plate calibration algorithms couldn't be used. A novel dot-plate calibration algorithm was developed for the event camera, and a sample result is shown in Figure 1c.

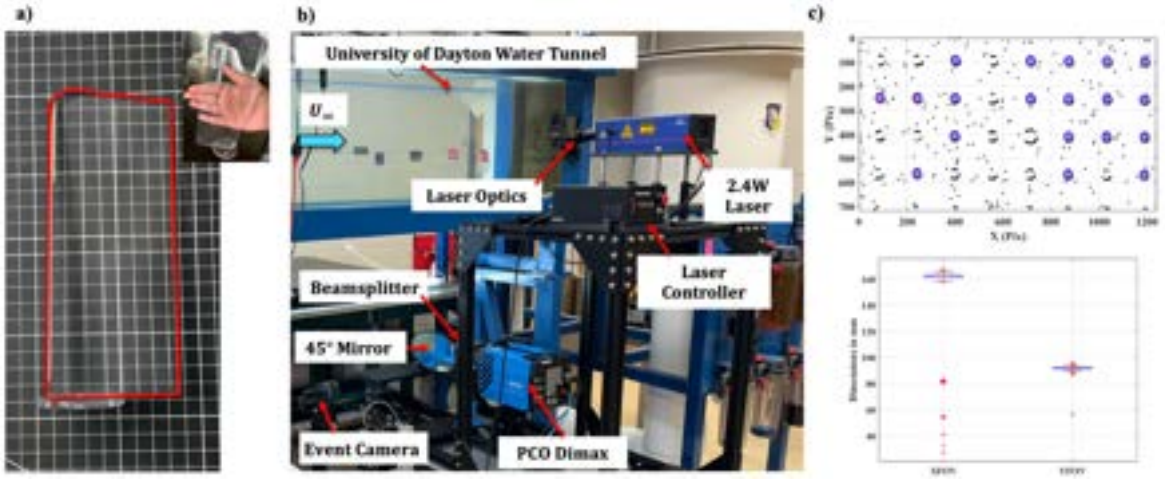

Figure 1 a) Transparent SD7003 wing, b) Simultaneous event-based and traditional PIV test setup, c) Results from dot-plate calibration of event-camera to obtain field of view

3. Development of Event-Camera Processing Codes from Literature: Three different event-camera processing algorithms were developed from the literature.

1. **Motion Capture Algorithm:** Willert, Christian E., and Joachim Klinner. "Event-based imaging velocimetry: an assessment of event-based cameras for the measurement of fluid flows." Experiments in Fluids 63, no. 6 (2022): 101.
2. **Particle Tracking Algorithm:** Drazen, David, Patrick Lichtsteiner, Philipp Häfliger, Tobi Delbrück, and Atle Jensen. "Toward real-time particle tracking using an event-based dynamic vision sensor." Experiments in Fluids 51, no. 5 (2011): 1465-1469.

3. **Particle Tracking Algorithm:** Wang, Yuanhao, Ramzi Idoughi, and Wolfgang Heidrich. "Stereo event-based particle tracking velocimetry for 3d fluid flow reconstruction." In European Conference on Computer Vision, pp. 36-53. Springer, Cham, 2020.

The source codes for these algorithms were not available. Therefore, they were developed based on the information provided in the above-mentioned publications. These algorithms were developed as part of a parallel study to validate the algorithms for synthetic images. The results were published in the following literature:

1. AlSattam, Osama A., Michael P. Mongin, Andrew Killian, Sidaard Gunasekaran, and Keigo Hirakawa. "Toward Event-Based Noise-Robust High Density Particle Velocimetry." In AIAA SCITECH 2024 Forum, p. 2663. 2024.

4. Simultaneous Data Acquisition of Traditional and Event-Based PIV: Simultaneous PIV was captured from traditional and event-based cameras for freestream-only cases at 0.2, 0.3, and 0.37 m/s, and for the SD7003 wing from 0° to 10° in 2° increments at the three different freestream velocities mentioned above. A sample comparative analysis of normalized streamwise velocity between the event camera results and the traditional PIV results is shown in Figure 2 for the SD7003 wing at a 10° angle of attack. The in-house developed algorithm was used to process the event camera data shown in Figure 2. The results from the event camera offer very similar insights as the traditional PIV at a fraction of the cost and computational time. The comparative analysis for other angle of attack cases and the mean square error between the traditional and event-based PIV results obtained from four different processing algorithms will be presented at SCITECH 2025.

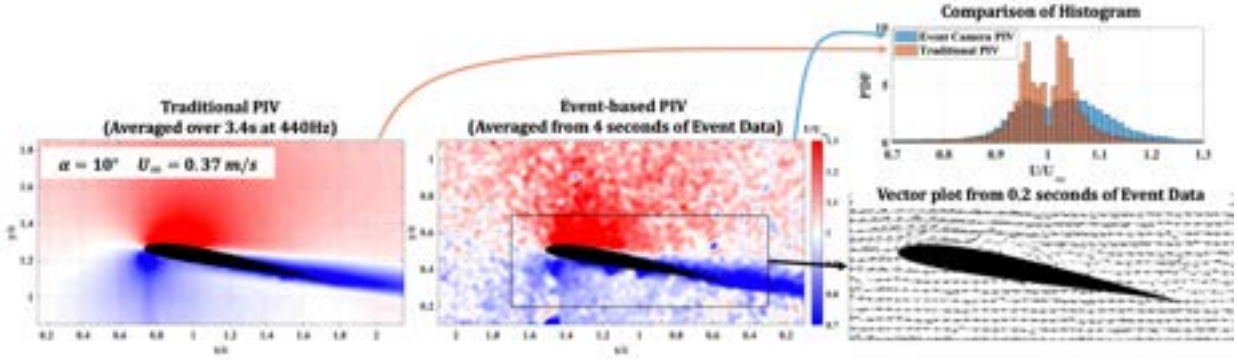

Figure 2 Sample comparative analysis of normalized streamwise velocity from traditional PIV and event-based PIV

5. Sensitivity Study on Event-Based PIV Results: While several rules of thumb exist for performing and processing traditional PIV, no such rules exist for event-based PIV. The results from the event camera and its processing time were found to be sensitive to the duration of analysis in each time segment (δt), the percentage of data analyzed, the value of the high pass filter (HPF) bias setting used in the event camera during data acquisition, and the type of algorithm used to process the results. Sample sensitivity results are shown in Figure 3 for the freestream velocity of 0.37 m/s. The first row in Figure 3 represents the raw data obtained from the event camera at three different HPF values for the same flowfield. A high bias setting in the camera can reduce ambient noise but also risks removing relatively slow-moving particle tracks. The bottom row represents the computed normalized mean streamwise velocity as a function of the percentage of data and the duration of the time segment used in the analysis. One hundred percent data represents four seconds of data collection. More than a 5% change in the mean normalized velocity is observed, and the results are dependent on the type of flowfield considered. Performing this sensitivity study was integral to determine the validity of the results obtained from the event camera, and an in-depth analysis of the results from the sensitivity study will be presented at SCITECH 2025.

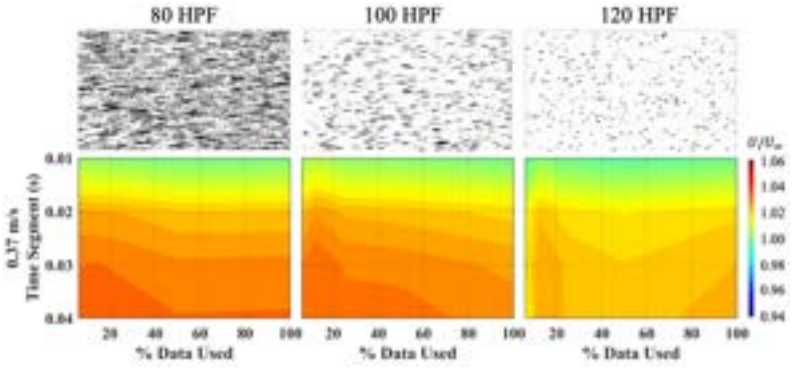

Figure 3 Normalized mean velocity results as a function of HPF, percentage data used, and duration of each time segment

A Variational Theory of Aerodynamics

Background:

Fluid mechanics is a branch of mechanics just as solid mechanics is also a branch of mechanics. The mother branch of mechanics has two main approaches: Newtonian mechanics and Lagrangian/Variational mechanics. The former can be succinctly summarized as writing Newton's law $F = m\,a$ for the system at hand (Navier-Stokes' equation for fluids), while the latter asserts that there is a fundamental quantity that Nature minimizes in every motion. Although the two approaches are equally fundamental, there is a severe asymmetry in fluid mechanics teaching and research in the favor of the Newtonian approach. This research is one of the few efforts that aim to revive the Lagrangian/variational approach in the fluids community by showing its value in presenting new insights and solving problems that have been hitherto elusive using the Newtonian approach.

For example, one of the most fundamental problems in aeronautics that remained open for a century is: how to compute lift over a two-dimensional object? The Newtonian approach was not successful in this problem because we cannot solve the Navier-Stokes equation analytically or numerically at a very high Reynolds numbers relevant to aviation. Without a rigorous academic resolution, industry engineers had to rely on an averaged form of Navier Stokes' equation: Reynolds Averaged Navier-Stokes (RANS). However, the RANS equation is not closed, invoking a model for the unknown Reynolds stress terms that arose because of averaging the Navier-Stokes. Unfortunately, RANS models are usually ad-hoc; a reasonable model in one application/flight condition may be inaccurate in another. However, it is typically a reasonable approach for analysis of classical problems such as attached flow over traditional airfoils at small angles of attack.

On the other hand, the lift theory, currently taught in all aeronautical engineering schools throughout the world, relies on the assumption that viscosity may be neglected in lift computation. So, the focus is on solving Euler's equation for an ideal fluid instead of Navier-Stokes'. However, Euler's equation admit infinitely many solutions. So, the question is: what solution does Nature select? This question could be answered only in the special case of a sharp-edged airfoil where all solutions are singular at the edge except one. Kutta's brilliant contribution in 1910 was to select the unique solution which eliminates this singularity.

Although Kutta's theory is the dominant theory of flight, it is quite fragile. For example, what happens if we have a smooth shape that is void of sharp edges (i.e., no singularities to remove)? **The century-old theory of lift suddenly collapses**; there is no theoretical model that can predict lift over smooth shapes without sharp edges. Simply put, **there are no alternatives!**

Research:

Approaching fluid mechanics via the variational branch of mechanics, the essential question is: What is the fundamental quantity that Nature minimizes in every incompressible flow? Interestingly, we discovered that it is the total pressure force over the domain. We proved that the magnitude of the pressure gradient over the field is minimum at every instant! We call it the ***Principle of Minimum Pressure Gradient*** (PMPG). We proved that the Navier-Stokes equation is the necessary condition for minimizing the pressure gradient subject to the continuity constraint. That is, a candidate solution that minimizes the *cost function* (i.e., total pressure force) is guaranteed to naturally satisfy the Navier-Stokes equation. Hence, the PMPG turns a fluid mechanics problem into a minimization one where fluid mechanicians need not to apply Navier-Stokes' equations, but merely need to minimize the cost function. The principle is deeply rooted in classical mechanics via the less well-known *Gauss' principle of least constraint*. Interestingly, for an ideal fluid, the cost reduces to curvature (see Taha et al. 2023, PoF).

Using the PMPG, we managed to solve two classical problems that have been hitherto elusive using the Newtonian approach (Navier-Stokes and Euler): the flow over a generic two-dimensional wing profile (not necessarily with a sharp edge), and the flow over a rotating cylinder. That is, among the infinitely-many solutions allowed by Euler's equation, Nature selects the solution with minimum total curvature in the domain. This theory reduces to the Kutta condition in the special case of a sharp-edged airfoil. However, unlike Kutta's, this new theory is derived from first principles in mechanics (Gauss' principle), and hence is applicable to arbitrary shapes (not necessarily sharp-edged airfoils). This work is published in the prestigious journal of JFM (Gonzalez and Taha 2022), which resolved a chronic century-old problem in aerodynamics, made a splash in the community. Our team made this short video to explain the idea to a broad audience. We continuously receive overwhelming comments about this new theory from professors throughout the world. Prof. Steven Collicott at Purdue wrote*: "Professor Taha, I am in the process of updating my undergraduate aerodynamics text book and am including a summary of your "Variational Theory of Flight" paper with Gonzalez…. Your article takes me back to my own undergrad and grad years in the 1980s, and that lingering, persistent, awkward question… I recall the disappointment in grad school that even after sweating through hours of conformal mapping pencil pushing day after day, this question fundamentally was never answered. So this question stuck with me through the decades…. I found your and Gonzalez's paper quite enlightening indeed – I found it through a publicity article that was written about it. Your paper of course answers the question that nobody ever discussed in classes and textbooks. We all waved our hands decade after decade. It has certainly bothered me that decades later as a Professor I couldn't do better for my students than was done for me. Thanks to you two, now I can do better*." Aerospace America interviewed Dr. Taha and Dr. Paul Bevilaqua (former chief engineer at Lockheed Martin Skunk Works who played the leading role in developing the F35) to discuss lift in the wake of the new theory: "*So you think you know lift? Better read this.*" It is expected that this new theory will replace (or taught side by side to) the classical theory in aeronautical engineering schools as well as applied math and physics departments throughout the world.

Relevance to DoD:

Current airplane technology has been stagnant for decades; almost all airplanes look the same. To help designers think out of the box, low-fidelity computational tools are needed—computational models that are (i) rich enough to capture the main physics of the flow dynamics and (ii) efficient and compact enough to be suitable for preliminary design phases where millions of design alternatives are being investigated (if a leap in design were to happen, it would have to happen in the preliminary design phase).

Currently, even the most powerful supercomputer of the time cannot perform a single simulation of Navier-Stokes' equations on a realistic airplane configuration. So, there is an acute need for novel computational algorithms that can result in accurate fluid simulations at very high Reynolds numbers, relevant to aviation. Interestingly, the recent advances of mathematical analysis of Navier-Stokes revealed a very important finding: That is, the lift and "*drag on the body in the infinite Reynolds limit can be computed entirely from the limiting Euler solution without the need to resolve small viscous lengths at the wall*." However, a selection criterion is needed to pick a unique solution from Euler's family that matches the limit of Navier-Stokes' solutions as $Re \to \infty$. Such a selection criterion will offer an unprecedented saving in computational cost of high Reynolds-number turbulent flows because one would simply simulate the cheap Euler's equation to obtain all possible solutions and use this selection criterion to pick the realistic representative. The PMPG is expected to provide such a selection criterion; i.e., the limiting solution from Euler's family is the one that minimizes the pressure gradient cost.

In conclusion, the current research is an essential step towards creating unconventional designs for next generation aerodynamic systems by providing both (i) low fidelity models needed in the preliminary design phase and (ii) efficient high-fidelity computational tools for the detailed design phase.

2023-2024 Annual Report – FA9550-21-1-0178

Data-Driven Control of Unsteady Flows

PIs: Kunihiko Taira (UCLA) & Steven L. Brunton (University of Washington)

The objective of the proposed work is to develop techniques to control fluid flows with large-amplitude unsteadiness, for example, due to gust disturbances or large aggressive maneuvers. To achieve the goals outlined in this project, we will develop novel data-driven techniques to 1) extract dominant patterns from high-dimensional fluid flow data, 2) robustly sense and estimate the flow from limited measurements, 3) develop reduced-order models for the flows, and 4) design controllers to modify the behavior of the flow. During the third year of this award, the UCLA team has focused on developing 1) an autoencoder-based flow modeling, estimation, and control technique for unsteady flows, 2) phase-reduction-based analysis to identify appropriate actuation timing to achieve phase advancement or delay, 3) analyzing perturbation dynamics about unsteady base flows, 4) navigating in a violent unsteady flow environment with finite-horizon model predictive control (with UW). The UW team has focused on applying data-driven methods developed in prior performance periods to advanced fluid flow scenarios, which involves 1) flow estimation from limited measurements, 2) data-driven decompositions of spatial flows into regions that cluster by similar dynamics, and 3) developing benchmark fluid flows to test control algorithms. Below we provide some highlights from 2023-2024.

Approach and Summary of Achievements:

- **Autoencoder-Based Modeling and Control:** To achieve real-time control for unsteady flows with excessively large degrees of freedom, a reduced-order model is necessary. We use a nonlinear autoencoder to obtain low-order, compressed representations of unsteady flows from a collection of time-series snapshot data. A regular autoencoder is often black-box and provides non-unique latent representations, which hinders practical uses of the network for downstream tasks including sensor-based reconstruction and control. In response, our autoencoder incorporates physical observables and topological information such as persistent homology of given flow data into the manifold identification process. The current autoencoder greatly compresses unsteady fluid flow data into a few variables of $O(1)$, transforming high-dimensional fluid flows to a compact representation that can be characterized by the phase and amplitude variables.

- **Phased-Based Modeling and Control:** For dynamics expressed with phase and amplitude, we can consider optimal control strategies to quickly modify the frequency of given dynamics. With an example of unsteady aerodynamic flows with transient gust encounters, we have shown that the present phase-amplitude-based control approach founded on the autoencoder low-order subspace can significantly reduce the effect of disturbance, even when these effects evolve over a relatively fast time scale. We also found that the low-order representations can be estimated from sparse sensors by using nonlinear machine learning, providing the potential for real-time control for a range of unsteady flows.

- **Optimally Time-Dependent Mode Analysis:** While the modal and stability analysis techniques currently available mostly assume a time-invariant base flow, this assumption is not strictly valid when controlling unsteady flows as their baseline flows may vary due to the presence of actuation. Toward identifying optimal timing and locations of actuation to efficiently control unsteady flows even under time-varying base states, we have considered the optimally time-dependent mode analyses. This analysis allows us to examine how the approach of disturbances in a flow field affects the wake dynamics while giving insights into the underlying flow physics via time-varying modal structures.

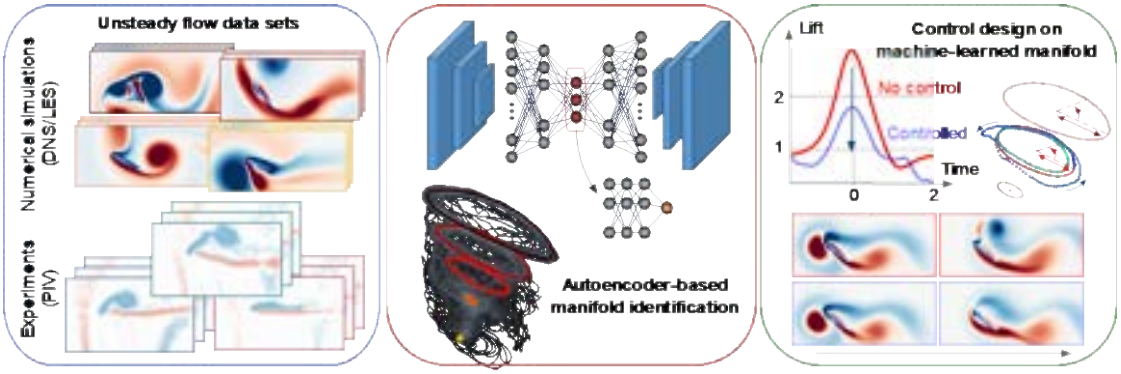

Data-driven control through machine-learning-based manifold identification for unsteady flows.

- **Trajectory Planning and Model Predictive Control:** We considered navigation and trajectory planning under unsteady flow scenarios. Facilitating a trajectory planning strategy is important in developing small- and medium-sized air vehicles that are tasked with flying in highly unsteady conditions such as turbulent wakes in urban environments, mountain ranges, and wakes behind large marine vehicles. We adopt model predictive control-based optimization to achieve efficient navigation in an unsteady wake. We find that leveraging the three-dimensionality of wakes helps in reaching the target faster with low actuation costs.

- **Flow Field Estimation:** We are leveraging Gaussian process regression (GPR) and sparse identification of nonlinear dynamics (SINDy) models to estimate flow fields from very sparse tracer information. Currently, the algorithm works for steady flows and is able to incorporate symmetries and constraints. Ongoing work will extend these algorithms to fully unsteady flows.

- **Dominant Balance Models:** Recent algorithms developed in the Brunton lab have made it possible to learn spatial decompositions of flows into clusters of regions that are governed by similar dynamics. These *dominant balance* regions are characterized by different subsets of the terms in the Navier-Stokes equation being active. We are now working with collaborators (PI Taira and others) to extend these methods to more complex and unsteady flows, such as three-dimensional unsteady flow around a wing and three-dimensional duct flow. Extending this algorithm involves improving noise robustness since it relies on computing high-order derivatives. We are currently implementing a *weak formulation* that leverages the variational integral formulation of the problem to improve noise robustness. This approach has been effective in extending SINDy to learn PDEs from noisy data.

- **Flow Control Benchmarks (*HydroGym*):** We are currently developing an open-source benchmark environment for flow control, where it will be possible to test various reinforcement learning (RL) control algorithms. This *HydroGym* environment uses the OpenAI Gym API, making it possible to leverage many existing (RL) algorithms. The current environments implemented include flow past a cylinder, the fluidic pinball, and cavity flow, as well as some simple one-dimensional flows. We have made the environment flexible, and future work will implement more sophisticated flows, including turbulent and three-dimensional configurations.

- **Path Planning and Control in Unsteady Flows:** This work has developed sparse sensor placement and path planning algorithms based on observability and Kalman filters for enhanced flow field reconstruction based on DMD models. These models work quite well for mobile sensing and path-planning algorithms. Similarly, we have studied how fluid coherent structures, identified with Lagrangian coherent structures, can be used for optimal drop locations for active sensing agents. This work has recently been published in IEEE Access, Sensors, and the CDC conference. Future work will apply these algorithms to more sophisticated three-dimensional flows with the Taira group.

Journal Publications

- Fukami, Nakao, and Taira, "Data-Driven Transient Lift Attenuation for Extreme Vortex Gust-Airfoil Interactions," *Journal of Fluid Mechanics*, accepted, 2024

- Yawata, Fukami, Taira, and Nakao, "Phase Autoencoder for Limit-Cycle Oscillators," *Chaos*, 34, 063111, 2024.

- Fukami, Goto, and Taira, "Data-Driven Nonlinear Turbulent Flow Scaling with Buckingham Pi Variables," *Journal of Fluid Mechanics*, 984, R4, 2024.

- Peitz, Stenner, Chidananda, Wallscheid, Brunton, and Taira, "Distributed Control of Partial Differential Equations Using Convolutional Reinforcement Learning," *Physica D: Nonlinear Phenomena*, 461, 134096, 2024.

- Smith, Fukami, Sedky, Jones, and Taira, "A Cyclic Perspective on Transient Gust Encounters Through the Lens of Persistent Homology," *Journal of Fluid Mechanics*, 980, A18, 2024.

- Chen, Kaiser, Hu, Rival, Fukami, and Taira, "Sparse Pressure-Based Machine Learning Approach for Aerodynamic Loads Estimation During Gust Encounters," *AIAA Journal*, 62(1), 275-290, 2024.

- Mai, Brunton, Kutz, "Mobile Sensor Path Planning for Kalman Filter Spatiotemporal Estimation," *Sensors*, 24(12), 2024.

- Godavarthi, Kawamura, and Taira, "Optimal Waveform for Fast Synchronization of Airfoil Wakes," *Journal of Fluid Mechanics*, 976, R1, 2023.

- Fukami and Taira, "Grasping Extreme Aerodynamics on a Low-Dimensional Manifold," *Nature Communications,* 14, 6480, 2023.

- Callaham, Loiseau, Brunton, "Multiscale Model Reduction for Incompressible Flows," *Journal of Fluid Mechanics*, 973(A3), 2023.

- Mai, Kutz, Brunton, "Observability-Based Energy-Efficient Path Planning with Background Flow via Deep Reinforcement Learning," *Conference on Decision and Control*, 2023.

- Krishna, Brunton, Song, "Finite Time Lyapunov Exponent Analysis of Model Predictive Control and Reinforcement Learning," *IEEE Access*, 11, 2023

In Review

- Godavarthi, Krishna, Brunton, and Taira, "Leveraging Three-Dimensionality for Navigation in Bluff-Body Wakes," in review, 2024.

- Zhong, Amiri-Margavi, Babaee, and Taira, "Optimally Time-Dependent Modes of Vortex Gust-Airfoil Interactions," in review, 2024.

- Linot, Schmid, and Taira, "On the Laminar Solutions and Stability of Accelerating and Decelerating Channel Flows," in review, 2023.

- Krishna, Nair, Krishnan, Brunton, Kaiser, "Control of Vortex Dynamics using Invariants," in review, 2023.

Extrapolative, progressive machine learning for turbulence modeling

PI: Xiang Yang, Pennsylvania State University

The recent validation and verification efforts have shown that most machine-learned turbulence models, despite their superior performance within the training dataset, perform poorly outside it [1–3]. This lack of generalizability renders machine-learned models unsuitable for practical engineering applications. This project aims to address this generalizability issue and develop more reliable machine learning models. By the end of the project, we hope to overcome, at least to some extent, long-standing challenges in turbulence modeling, including flow separation, high Mach numbers, non-equilibrium effects, and surface roughness.

In our previous 2023 report, we explained why existing machine-learned models do not generalize: the augmentations made by machine learning do not preserve the existing calibrations of the baseline model [4]. We proposed a new approach called the rubber-band approach [5]. Applying this approach to the Spalart-Allmaras model [6], we showed improved predictions for jet flows, separated flows, and airfoils at high angles of attack. To facilitate the dissemination of our work, we have also open-sourced our code on GitHub [7].

Earlier this year (FY24), we applied the rubber-band approach to two-equation models [6] and identified algebraic constraints for the basic calibrations in two-equation $k-\omega$ and $k-\epsilon$ models. Our efforts focused on enhancing the behavior of these models in the wall layer by incorporating the known compressible law of the wall as a basic calibration, while preserving the existing calibrations of the baseline model. In the following, we elaborate on these efforts.

In Ref. [8], we enhance the predictive capabilities of the Launder-Spalding $k-\epsilon$ model by integrating the law of the wall, including the viscous sublayer, buffer layer, and logarithmic layer into the model. Utilizing direct numerical simulation (DNS) data, we propose modifications to the unclosed dissipation terms in the k and ϵ equations specifically within the wall layer. This refined model accurately captures mean flow characteristics in both the buffer and logarithmic layers, resulting in robust predictions of skin friction for zero-pressure-gradient flat-plate boundary layers and plane channels. The model's effectiveness is further validated across various flow scenarios involving pressure gradients, showcasing highly favorable results. Additionally, although not the primary focus, the methodology proves beneficial for the $k-\omega$ model, improving predictions in the buffer layer.

In Ref. [9], we address the limitations of baseline two-equation Reynolds-averaged Navier-Stokes (RANS) models in predicting compressible flows, particularly at high Mach numbers. We critique existing log-layer compressibility corrections and develop viscous-layer compressibility corrections by modifying the dissipation terms in the RANS models to conform to semi-local scaling. This approach enhances the accuracy of mean velocity and temperature predictions in posteriori tests. Interestingly, the baseline one-equation Spalart-Allmaras model inherently produces results consistent with semi-local scaling without needing compressibility corrections.

In the coming fiscal year (FY25), we aim to build on these model augmentations and tackle the issue of pressure gradients—which arise due to surface curvature on airfoils among many other flow scenarios. We will demonstrate the compatibility of the rubber-band approach with symbolic regression. Additionally, we will expand our validation and verification efforts, providing more solid baselines for machine learning models.

References

[1] C. L. Rumsey, G. N. Coleman, and L. Wang, "In search of data-driven improvements to RANS models applied to separated flows," in *AIAA SCITECH*, p. 0937, 2022.

[2] N. McGreivy and A. Hakim, "Weak baselines and reporting biases lead to overoptimism in machine learning for fluid-related partial differential equations," *arXiv preprint arXiv:2407.07218*, 2024.

[3] P. E. Chen, Y. Bin, X. I. Yang, Y. Shi, M. Abkar, and G. I. Park, "A priori screening of data-enabled turbulence models," *Physical Review Fluids*, vol. 8, no. 12, p. 124606, 2023.

[4] Y. Bin, L. Chen, G. Huang, and X. I. Yang, "Progressive, extrapolative machine learning for near-wall turbulence modeling," *Physical Review Fluids*, vol. 7, no. 8, p. 084610, 2022.

[5] Y. Bin, G. Huang, and X. I. Yang, "Data-enabled recalibration of the spalart–allmaras model," *AIAA Journal*, pp. 1–12, 2023.

[6] Y. Bin, G. Huang, R. Kunz, and X. I. Yang, "Constrained recalibration of reynolds-averaged navier–stokes models," *AIAA Journal*, vol. 62, no. 4, pp. 1434–1446, 2024.

[7] "Details and cases of SAM model," 2022.

[8] X. Hu, G. Huang, R. Kunz, and X. Yang, "Data-guided low-reynolds-number corrections for two-equation models," *Journal of Fluids Engineering*, 2024. under review.

[9] X. Hu, P. Durbin, G. Huang, and X. Yang, "A viscous-layer compressibility correction for two-equation reynolds-averaged navier-stokes models," *AIAA Journal*, 2024. under review.